Doctoral Dissertation

Advanced Hydrogel Materials from Quaternized Sulfated Polysaccharides to Zwitterionic and Microneedles Fabrication

Chamaiporn Supachettapun

Supervisor: Kazuaki Matsumura

Graduate School of Advanced Science and Technology

Japan Advanced Institute of Science and Technology

Materials Science

September 2024

Abstract

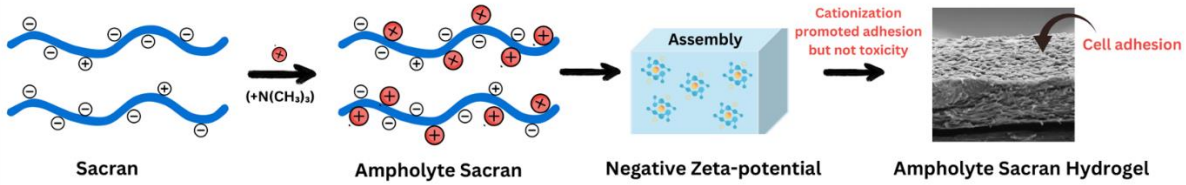

Graphical abstract

Sacran is a cyanobacterial supergiant polysaccharide with carboxylate and sulfate groups and shows anti-allergic and anti-inflammatory properties, while too high anionic functions restrict cell compatibility. Here quaternary ammonium groups were substituted to form sacran ampholytes and cell-compatibility of the cationized sacran hydrogels was evaluated. The cationized process involved using N-(3-chloro-2-hydroxypropyl) tri-methylammonium chloride reacting with the primary amine or hydroxyl group of sacran. The degree of cationization ranged from 32 % to 87 % for sugar residues. Hydrogels of sacran ampholyte were made by annealing their dried sheet by thermal cross-linking and exhibited anisotropic swelling properties. The water contact angle on the hydrogels decreased from 26.5° to 15.3° with an increase in cationization degree, enhancing the hydrophilicity. IC50 values of sacran ampholytes were reduced with an increased cationization degree to decrease cytotoxicity towards the L929 mouse fibroblast cell line, which is associated with an increased cell proliferation density after 3 days of incubation. SEM images show fibroblast intercellular connections. Thus, sacran ampholyte hydrogel showed increased hydrophilicity and cell compatibility, which can lead to various biomedical applications.

Keywords: Ampholyte Hydrogels, Sulfated Polysaccharide, Sacran, Anisotropic Hydrogels

Referee-in-chief: Professor Dr. Kazuaki Matsumura

Japan Advanced Institute of Science and Technology

Referees: Professor Dr. Masayuki Yamaguchi

Japan Advanced Institute of Science and Technology

Associate Professor Dr. Kosuke Okeyoshi

Japan Advanced Institute of Science and Technology

Associate Professor Dr. Eijiro Miyako

Japan Advanced Institute of Science and Technology

External referee: Professor Dr. Nongnuj Muangsin

Chulalongkorn University

Acknowledgements

This research was conducted at the School of Materials Sciences at the Japan Advanced Institute of Science and Technology (JAIST) in Japan. I am especially thankful for the Doctoral Dual Degree Program (JAIST-CU) for financial during my doctoral study.

I am deeply grateful to my supervisor, Professor Tatsuo Kaneko, and Professor Kazuaki Matsumura from JAIST, for his invaluable guidance, useful advice, and kind support throughout my time in Japan. My accomplishments during my studies would not have been achievable without his innovative thinking and enthusiastic mentorship.

I am deeply appreciative of Dr. Maiko Okajima for her kindness and care, which allowed me to complete my studies at JAIST smoothly, and Assistant Professor Kenji Takada for his suggestions and consistent support during my research there.

I would also my specially thank my second supervisor Associate Professor Toshiaki Taniike and the committee members my minor research advisor Professor Yamaguchi Masayuki, Associate Professor Kosuke Okeyoshi and Associate Professor Dr. Eijiro Miyako at JAIST, and Professor Nongnuj Muangsin from Chulalongkorn University, for their time and invaluable advice during the defense.

I am thankful for all of my Thai friends with whom I have shared difficult times and invaluable moments. My experience would not have been as enjoyable without them.

Chamaiporn Supachettapun

September 2024

Ishikawa, Japan

Contents

CHAPTER I

GENERAL INFORMATION

1.1 Natural Polysaccharides

Natural polysaccharides are complex carbohydrates found in nature (Figure 1.1), synthesized by various organisms including microorganisms, plants, algae, and animals. They offer numerous advantages such as non-toxicity, biocompatibility, biodegradability, good solubility, and stability (1). Polysaccharides extracted from microorganisms include alginate produced by *Azotobacter vinelandii*, bacterial cellulose generated from bacteria like *Salmonella, Acetobacter,* and *Agrobacterium*, hyaluronic acid from bacterial species such as *Streptococci, Pasteurella multocida,* and *Cryptococcus neoformans*, as well as dextran and xanthan (2-4) (Figure1.2). Polysaccharides extracted from plants (5) include starch, cellulose, pectin, and gums (Figure 1.3), while those extracted from animals include chitin and chitosan (6) (Figure 1.4). Polysaccharides from algae encompass agar, galactans (7), carrageenan (8), and sacran (9) (Figure 1.5). These polysaccharides play significant roles in various applications including food, pharmaceuticals, and cosmetics. Polysaccharides are the most common type of carbohydrate in nature. These polysaccharides have a molecular structure that consists of monosaccharides connected by glycosidic linkages or covalently attached to peptides, amino acids, and lipids(10). The main classification of natural polysaccharides includes homopolysaccharides (11), which consist of the same monosaccharides, and heteropolysaccharides (12), which contain heteroglycans made up of distinct types of monosaccharides can be classified based on their monosaccharide composition, chain lengths, and branching structures. Polysaccharides in nature can either store energy, like starch, or give

structural support, like cellulose, contributing to physical stability (13). Polysaccharides can be categorized according to their polyelectrolyte charges, including negatively charged polysaccharides such as alginate, hyaluronic acid, and pectin (14) and positively charged polysaccharides such as chitin and chitosan (15).

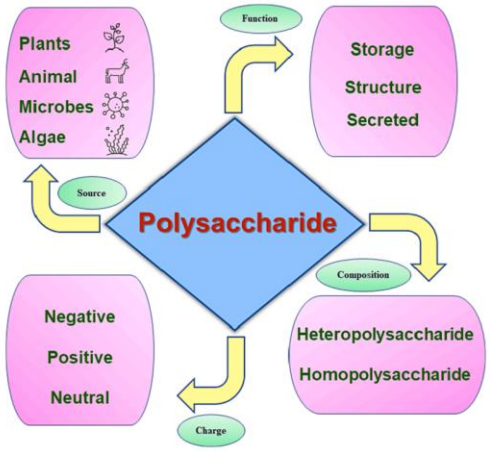

Figure 1.1 Different types of polysaccharides source and their classifications (16).

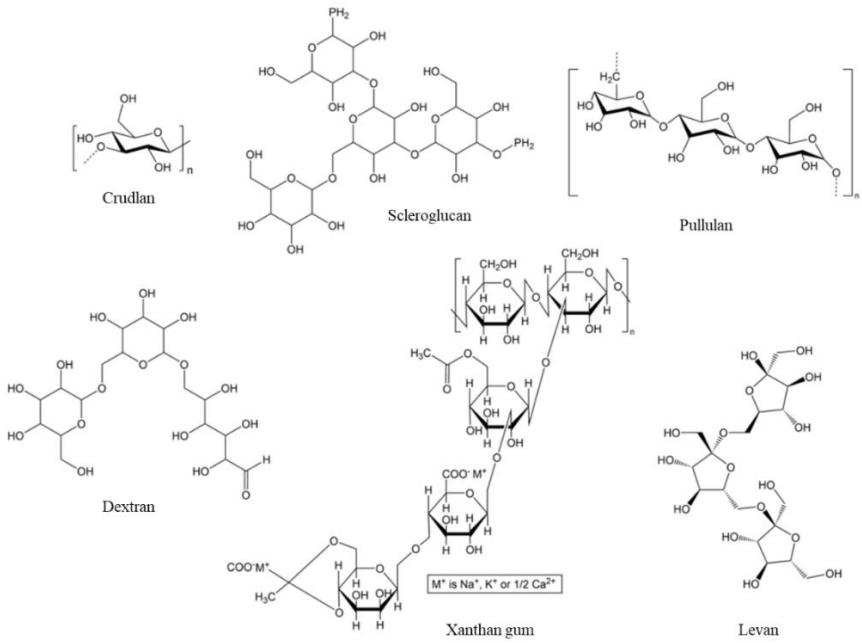

Figure 1.2 Chemical structures of natural polysaccharides from microbe source (17).

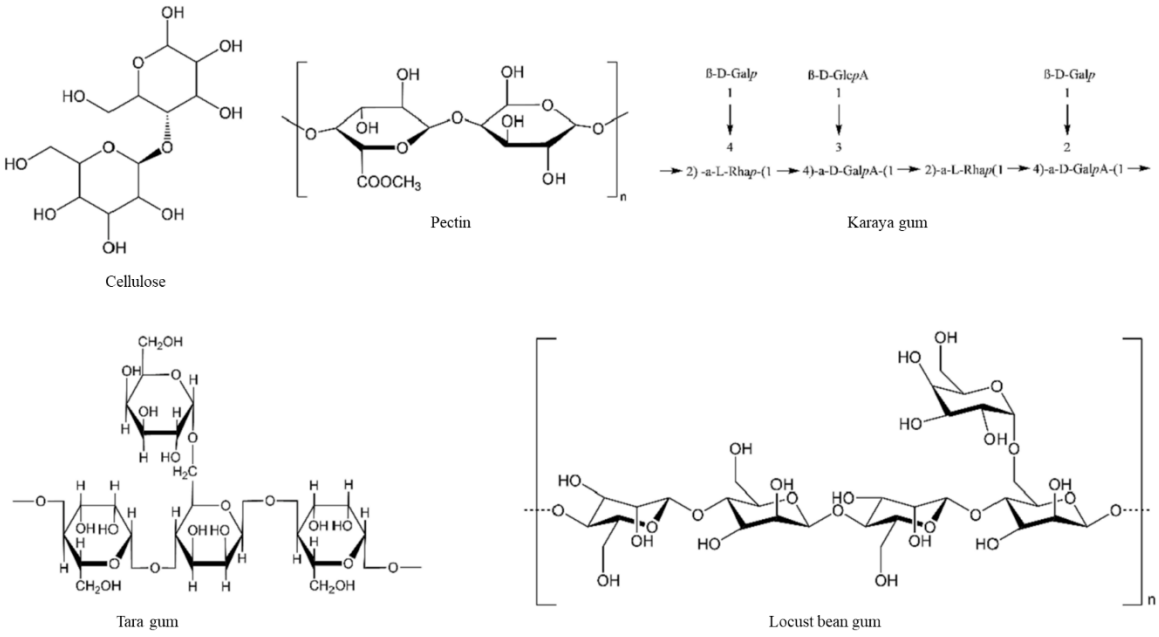

Figure 1.3 Chemical structures of natural polysaccharides from plant source (17).

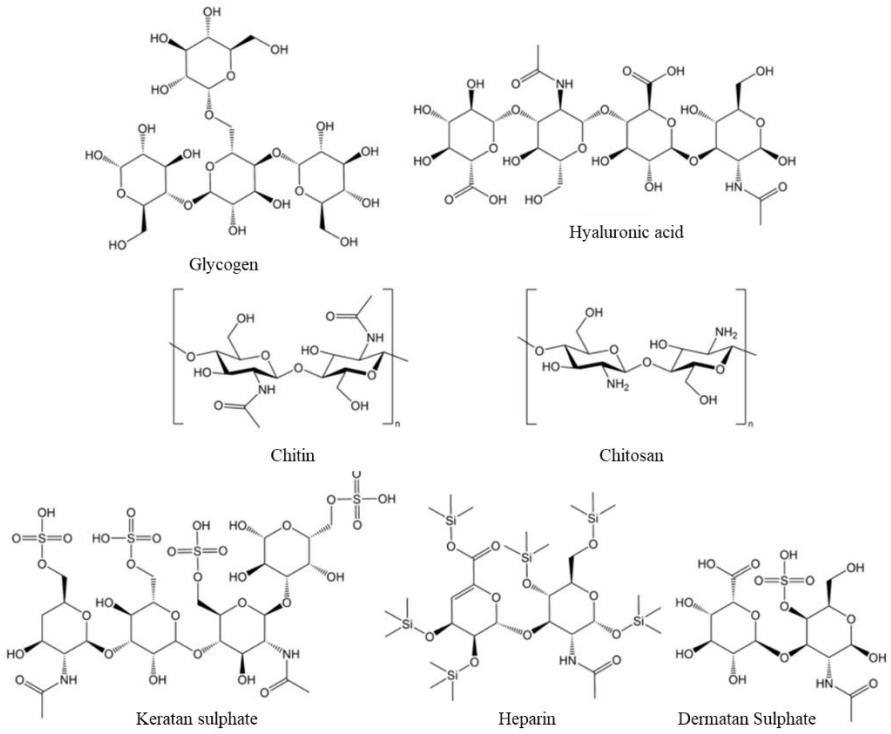

Figure 1.4 Chemical structures of natural polysaccharides from animal source (17).

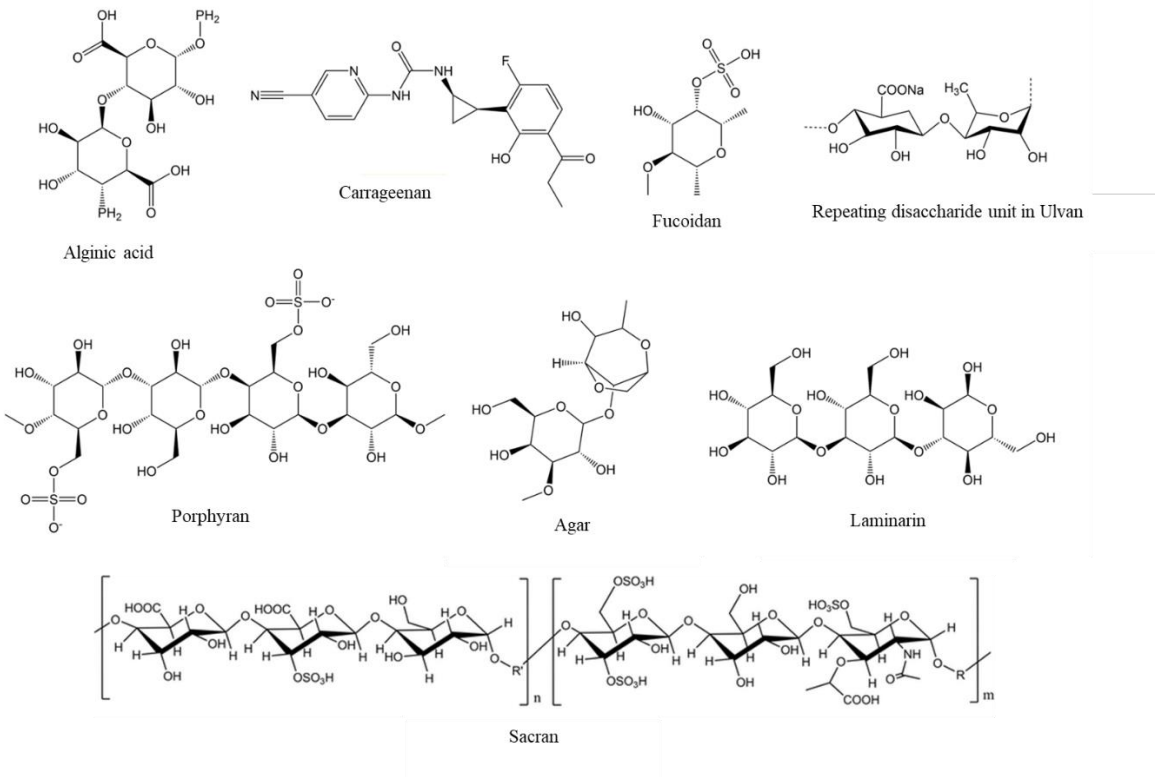

Figure 1.5 Chemical structures of natural polysaccharides from algae source (17, 18).

1.2 Hydrogel

Hydrogels are three-dimensional polymer networks that are hydrophilic (19). They can absorb and retain large amounts of water while maintaining their structure (20). These gels consist of hydrophilic polymer chains that form a network and are cross-linked to create a stable gel-like structure. The ability of hydrogels to absorb water is due to the presence of hydrophilic functional groups connected to the polymer backbone (21). The cross-links formed between the network chains are what give hydrogels their resistance to dissolution. Many substances, both natural and synthetic, meet the criteria to be classified as hydrogels. However, synthetic hydrogels have gradually replaced natural ones over the past two decades due to their increased durability, high water absorption capacity, and strong gel strength. Synthetic polymers have well-defined structures and can be easily modified to achieve the desired degradability and functionality. It is

also possible to create hydrogels using entirely synthetic components, which remain stable even under extreme temperature variations. Hydrogels can be categorized into two groups based on the type of cross-link junctions: chemically cross-linked networks have permanent junctions, (22). while physical networks have temporary junctions caused by entanglements of the polymer chains or physical interactions such as ionic contacts, hydrogen bonds, or hydrophobic interactions. Furthermore, hydrogels can be classified into four classes based on the presence or absence of an electrical charge on the crosslinked chains.

1.2.1 Methods to Preparation of Hydrogel

Chemical cross-linking

In hydrogels, chemical crosslinking is the process of forming covalent links between polymer chains to build a network that has the capacity to absorb and hold a lot of water. Because of the long-lasting bonds created by the crosslinking process, these hydrogels stand out for their stability and resilience. The functional groups, such as hydroxyl (-OH), carboxyl (-COOH), and amine ($-NH_2$) groups, are what define the majority of hydrophilic polymers. These functional groups are essential because, when paired with other cross-linking agents, they can take part in chemical cross-linking reactions. In order to turn individual polymer chains into the cohesive, three-dimensional network that constitutes a hydrogel, this cross-linking process is essential (Figure 1.6).

The Functions of Functional Groups in Cross-Linking.

- Hydroxyl Groups (-OH), These groups can generate ether or ester bonds by reacting with cross-linking agents such as diisocyanates or epoxides, which integrates the polymer chains into a network.

• Carboxyl Groups (-COOH): In the presence of amines, carboxyl groups can react with carbodiimides to produce amide bonds or engage in esterification reactions with alcohols. They are especially helpful for creating biodegradable connections in biomedical applications.

• Amine Groups (-NH_2): Amine groups are extremely reactive; they can combine with isocyanates to make urea linkages or with aldehydes to form covalent connections that result in Schiff bases. Because of the strength of the resultant bonds, these reactions are frequently utilized in the creation of hydrogels.

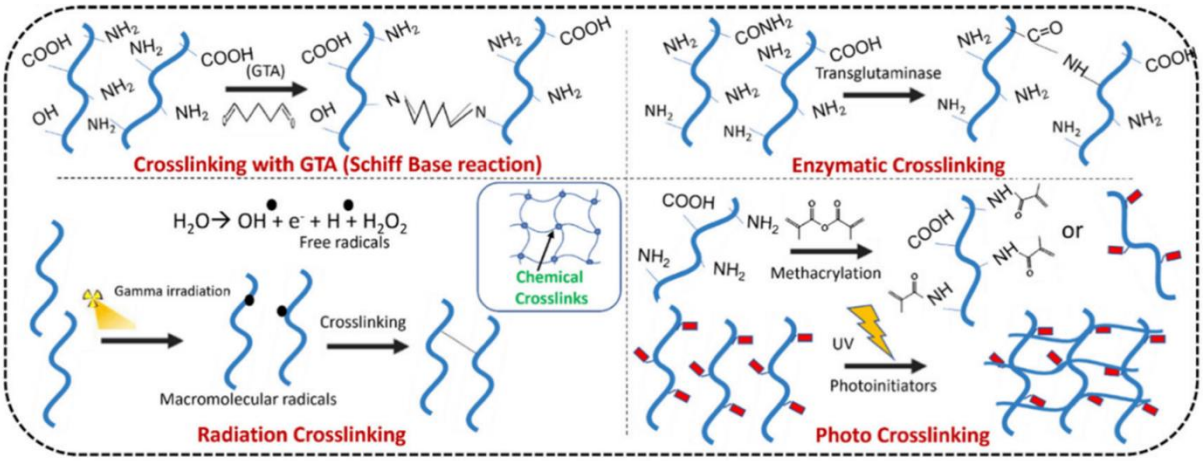

Figure 1.6 The chemical crosslinking mechanisms in gelation hydrogels (23).

Physical crosslinking

In hydrogel, Physical crosslinking of hydrogels occurs when non-covalent interactions, including hydrophobic, ionic, and hydrogen bonds, contribute to the formation of a three-dimensional polymer network. Physical crosslinking is typically conducted under milder conditions and does not necessitate the use of reactive agents, in contrast to chemical crosslinking that employs covalent bonds. Reversible environmental conditions, including temperature, pH, and ionic strength, are capable of inducing or reversing this crosslinking process (Figure 1.7).

Type of Physical crosslinking

- Hydrogen bonding is a form of crosslinking in which hydrogen atoms interact with electronegative atoms in the polymer chains, such as nitrogen or oxygen. Hydrogen bonds are frequently observed in polymers that contain amide (-CONH-) and hydroxyl (-OH) groups. In general, these bonds are more reversible and weaker than covalent bonds.
- Ionic crosslinking: This process occurs when multivalent counterions interact with charged polymer chains. For example, polymers that possess both positive and negative charges within the same molecular structure. These charges are typically balanced within the molecule, leading to unique interactions that can be exploited for hydrogel formation. Zwitterionic crosslinking capitalizes on the electrostatic interactions between the oppositely charged groups to form stable, water-soluble networks that exhibit minimal fouling, high biocompatibility, and unique response behaviors to environmental stimuli.
- Hydrophobic interactions can cause physical crosslinking in polymers comprising both hydrophilic and hydrophobic segments, as these interactions facilitate self-assembly in aqueous solutions. The sensitivity of this mechanism to temperature enables its application in the development of thermoresponsive hydrogels.

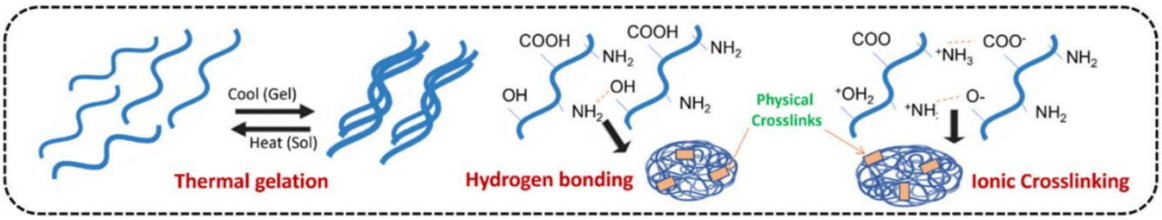

Figure 1.7 The physical crosslinking of hydrogels. (23)

1.2.2 Properties of Hydrogels

• Swelling Behavior

The swelling of hydrogels is mainly determined by the polymer network structure and the interactions between the polymer chains and the solvent, often water. When a dry hydrogel is exposed to water, the hydrophilic parts of the polymer attract water molecules through hydrogen bonding and other dipole interactions. The water molecules penetrate the network, leading to the expansion of the hydrogel as the polymer chains separate.

• Mechanical properties

The mechanical properties of hydrogels are influenced by their composition and structure. Fully swollen hydrogels, which have a high-water content, usually have low mechanical strengths. The mechanical properties of hydrogels are impacted by factors such as the composition of the monomers, the density of cross-linking, the conditions of polymerization, and the extent of swelling. In the swollen state, the mechanical strength of the hydrogel primarily comes from the cross-links, as physical entanglements are almost non-existent. Many researchers have extensively studied the relationship between mechanical properties and cross-link density. However, it is important to note that altering the cross-link density also affects properties other than strength. For instance, increasing the concentration of cross-linkers brings the polymer chains closer together, which reduces diffusivity, release and swelling rates, including the maximum degree of swelling. Consequently, these properties need to be re-evaluated whenever additional cross-links are introduced. The mechanical behavior of hydrogels can be best understood through theories of elasticity and viscoelasticity. These theories consider the time-independent and time-dependent recovery of chain orientation and structure, respectively. Elasticity theory assumes that when stress

is applied to a hydrogel, the strain response is instantaneous. However, this assumption does not hold true for many biomaterials, including hydrogels and tissues. For example, when a weight is suspended from a ligament specimen, the ligament continues to extend even though the load remains constant. Similarly, if the ligament is elongated to a fixed length, the load gradually decreases with time. This phenomenon is known as creep and stress relaxation, which results from viscous flow in the material. Despite exhibiting liquid-like behavior, hydrogels are functionally solids and are therefore considered to be perfectly elastic for the purpose of this study. The next section provides a brief introduction to the fundamentals of elastic theory.

1.3 Anisotropic Swelling of Hydrogel

Anisotropic gels, as a biomaterial, have been extensively studied in various applications, such as biomedical, optics or electronic materials. These anisotropic materials can be created through different methods, including self-assembly, directional freezing, magnetic field alignment, elongation, or the solvent casting method. Among these techniques, the solvent casting method stands out as the most straightforward approach for preparing films. In this method, oriented films are fixed through crosslinking and then rehydrated in solvents, resulting in the formation of oriented gels. In Figure 1.8 Okajima and coworker (24) reported The method to prepare anisotropic sacran hydrogel via solvent casting methods is described. The results show that when hydrogels are annealed at higher temperatures, they form smaller structures due to the ester bond formation between hydroxyl groups and carboxylate groups in their structure.

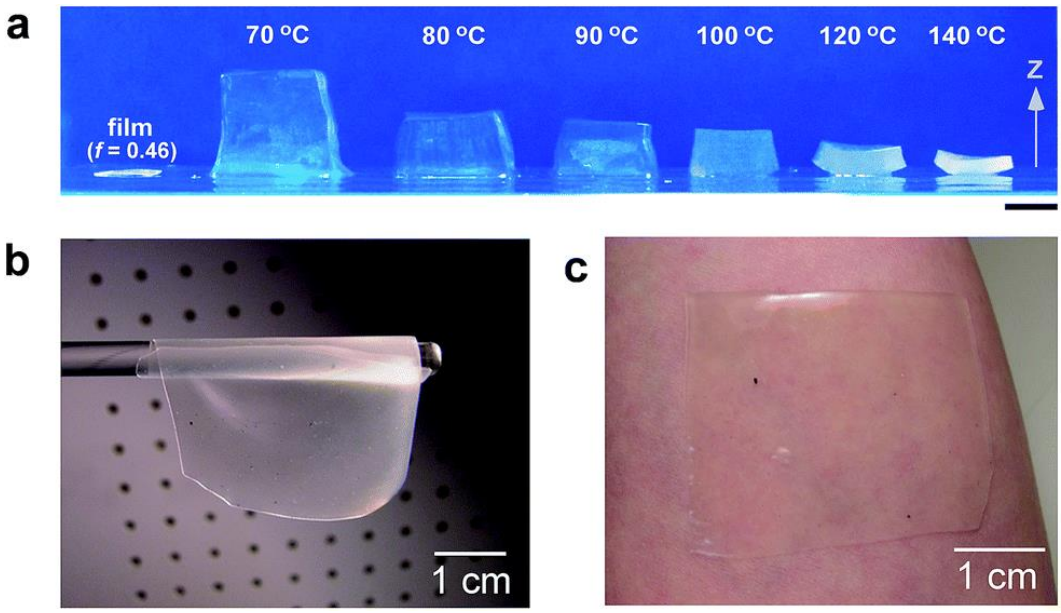

Figure 1.8 Photos of sacran film and hydrogels. (a) Sacran film (left) and hydrogels swelling in water after the film was annealed at various temperatures (right). Scale bar: 5 mm (b) hydrogel sheet is tough enough to deform and translucent enough to scatter the white light irradiated from right. (c) Hydrogel sheet put on the arm.

Dongdong Ye and coworkers (25) studied the formation of ACH with a highly ordered structure is demonstrated in this study. The process begins with the synthesis of LCG by reacting cellulose with a small amount of EPI in a LiOH/urea aqueous solution. The LCG-containing solvent (LiOH-urea) can be easily pre stretched under external force to create an oriented structure. Once the force is removed, the original shape of the LCG is immediately recovered, resulting in permanently oriented cellulose hydrogels (Figure 1.9).

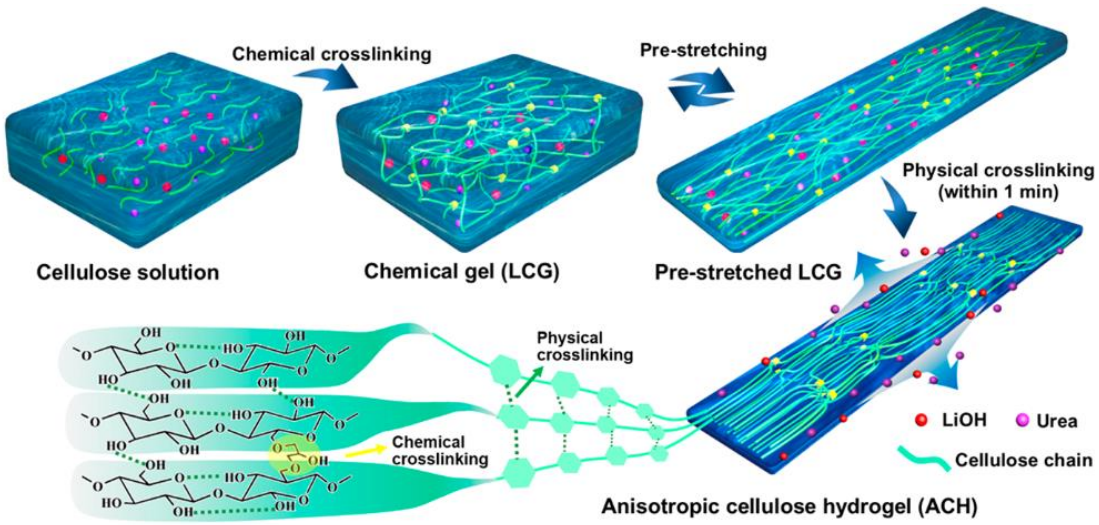

Figure 1.9 First, the loosely chemically cross-linked gel (LCG), fabricated from cellulose solution, was prestressed by external force and the hydrogel network aligned in the stretching direction to form a temporarily oriented structure. Then a relatively close-packed architecture including hybrid cross-linking networks formed in the acid solution driven by the strong self-aggregating force of the cellulose itself, leading to permanent locking of the orientation structure of the hydrogels (25).

1.4 Cyanobacterial Polysaccharide "Sacran"

Cyanobacteria, which are found in almost every water system on the planet, are well-known for producing toxins that endanger both aquatic life and humans. Recent investigations on cyanobacteria metabolites have revealed a major biological impact on human health. Notably, these microorganisms have the ability to manufacture and release polysaccharides containing varied functional groups, such as amino acids, phosphate, sulfate, and carboxylic acid, which is essential for adsorption processes (26). Among the myriad of cyanobacteria species, Aphanothece sacrum, also referred to as A. sacrum, stands out as a single-celled organism thriving in freshwater habitats Figure 1.10 This species is remarkable for its production of a

polysaccharide named sacran (27), characterized by its complexity. Sacran consists of various sugar residues including galactose, glucose, mannose, xylose, rhamnose, fucose, galacturonic acid, and glucuronic.

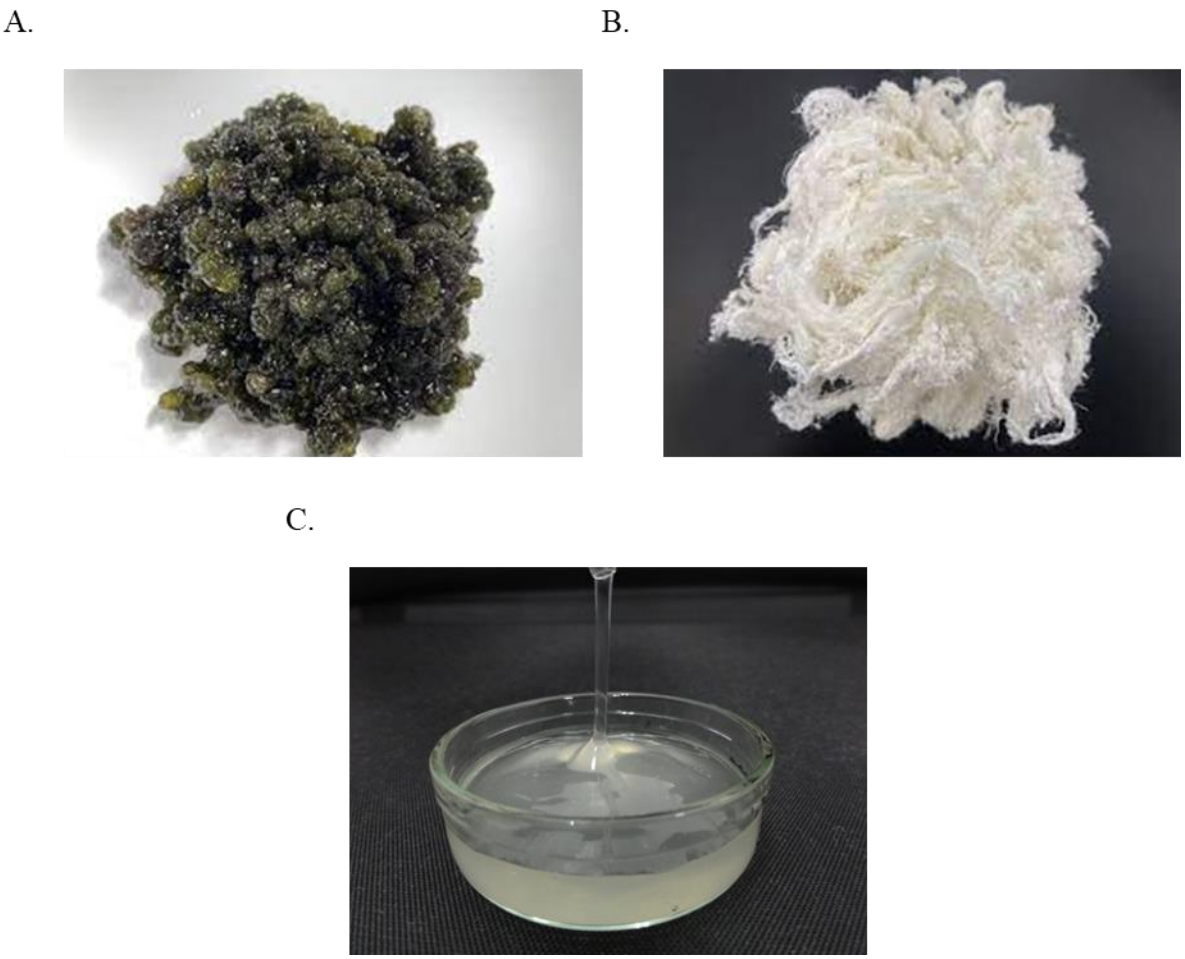

Figure 1.10 A) Suizenji Nori and B) Sacran™ and C) sacran in solution (27)

acid, with composition ratios of 25.9, 11.0, 10.0, 16.2, 10.2, 6.9, 4.0, and 4.2, respectively as shown in Figure 1.11 Additionally, this heteropolysaccharide is composed of at least six distinct types of sugar residues, Glucose (Glc), Galactose (Gal), Mannose (Man), Xylose (Xyl), Rhamnose (Rha), and Fucose (Fuc). Additionally, sacran contains approximately 20-25% uronic acids as anionic residues and trace amounts (around 1.0%) of aminosugar as cationic

residues. Besides sacran has sulfated sugar residues. As a result, sacran contains 22% carboxylates, 250% hydroxyls, and 11% sulfates groups, thereby exhibiting similarity to glycosaminoglycan (GAG)

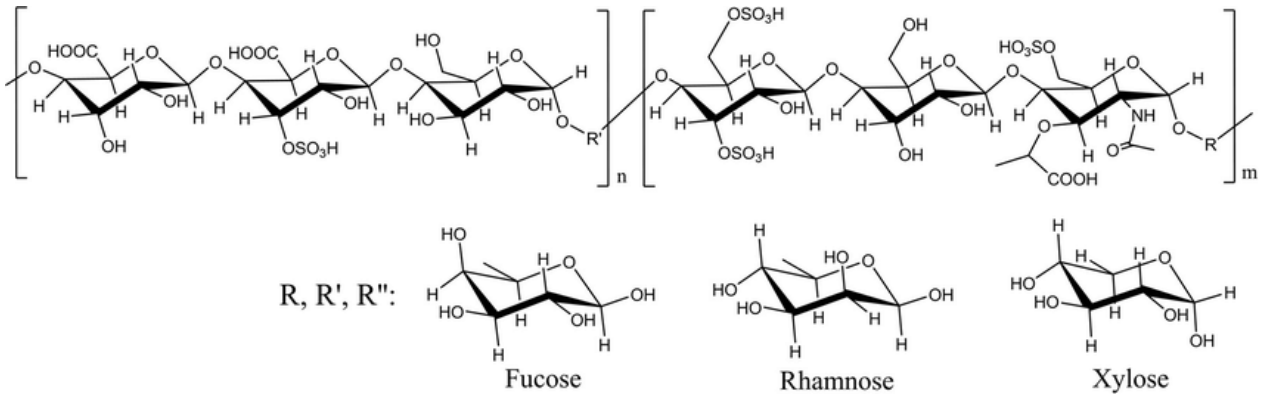

Figure 1.11 Main structure of sacran chains where the sequences in monosaccharide triads, pattern of glycoside linkages, steric conformations of hydroxyls or other substitutes are tentative(18).

Since sacran has a higher molecular weight (Mw), researchers have conducted investigations on its liquid crystalline properties (28). The study on dielectric relaxation has shown that sacran possesses various types of counterions, each with a different degree of interaction with the polyion. These counterions can be categorized as strongly bound or loosely bound. The concentration of entanglements and gelation affects the dielectric properties, such as relaxation duration and relaxation strength, but the concentration of overlap does not. The density of bound counterions, determined by the relaxation strength, suggests that the counterions are concentrated around the sacran chains (29). The reduction in the charge density of the sacran chains leads to a decrease in the repulsive force between the chains, resulting in the helix transformation or gelation behavior. The configuration of sacran molecules in pure water and the process of gelation are connected to the properties of liquid crystalline polyelectrolytes (18), as depicted in Figure 1.12

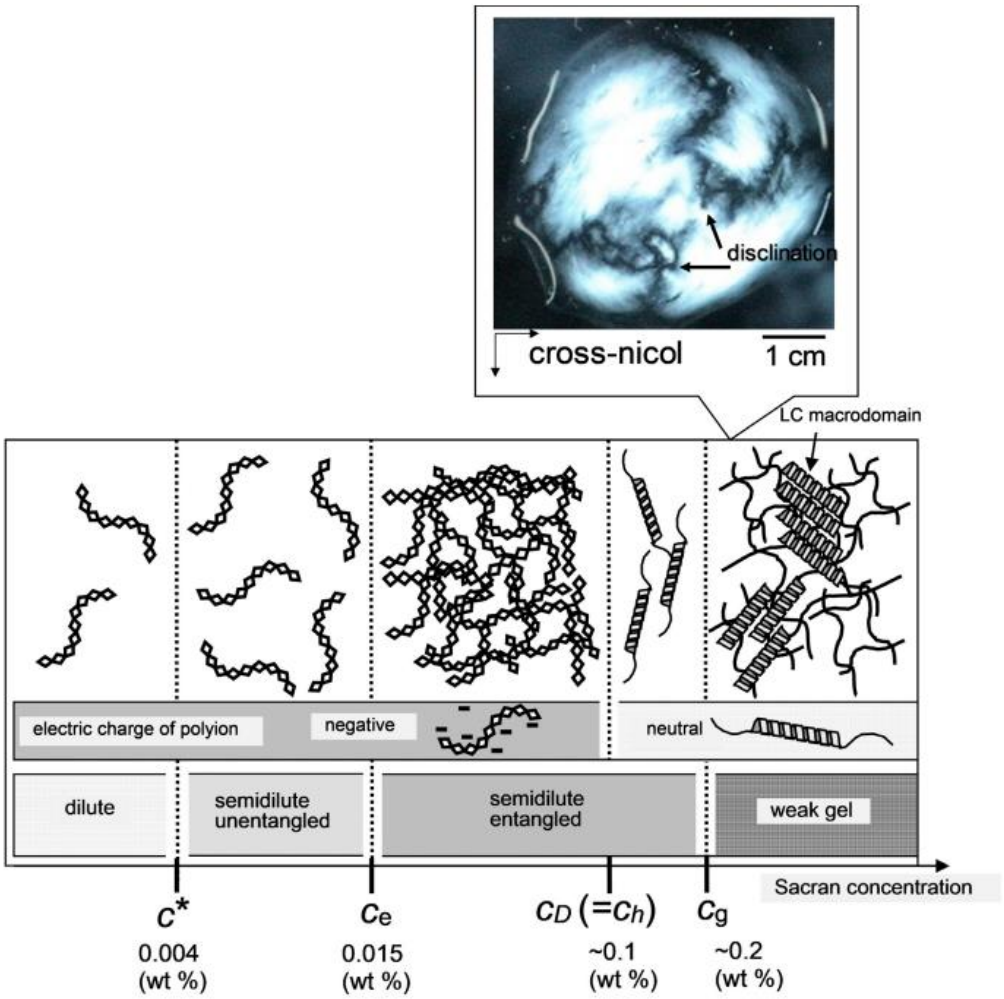

Figure 1.12 Schematic illustrations representing the chain conformation of sacran in salt-free solutions (c*: overlap concentration, c_e: entanglement concentration, c_D: critical polyelectrolyte solution, c_h: helix transition concentration, c_g: gelation concentration). The inset microscopic picture is Schlieren texture taken under cross-Nicol polarimetry in a concentration of 0.5 wt %.(18)

1.5 Quaternary Ammonium Compounds

Quaternary ammonium salts (QAC), which are known for their exceptional hydrophilic properties, are often used as components in polymers to increase their water solubility.

Quaternization is an essential method used to enhance polymer solubility. Under different experimental conditions, quaternary ammonium groups are chemically incorporated into or onto the polymer backbone through interactions with primary amino or hydroxyl groups. QAC is also preferred in many applications, including water solubility, pH sensitivity, biocompatibility, and biodegradability. (3-chloro-2-hydroxypropyl) trimethylammonium chloride, also known as Q188, is one of the most commonly used agents in the synthesis of cationic polysaccharides. It is favored due to its low toxicity and good solubility. When exposed to alkaline conditions, Q188 is converted into an epoxide. This quaternization process involves replacing the OH groups present in the polysaccharides. The degree of quaternization in the resulting product is influenced by factors such as the amount of quaternary ammonium added, reaction time, pH of the reaction, and reaction temperature. Increasing the content of Q188 and extending the reaction time gradually increases the degree of quaternization. QAC with high degree of quaternization which is suitable for drug transport, gene delivery and bacteriostat (Figure 1.13).

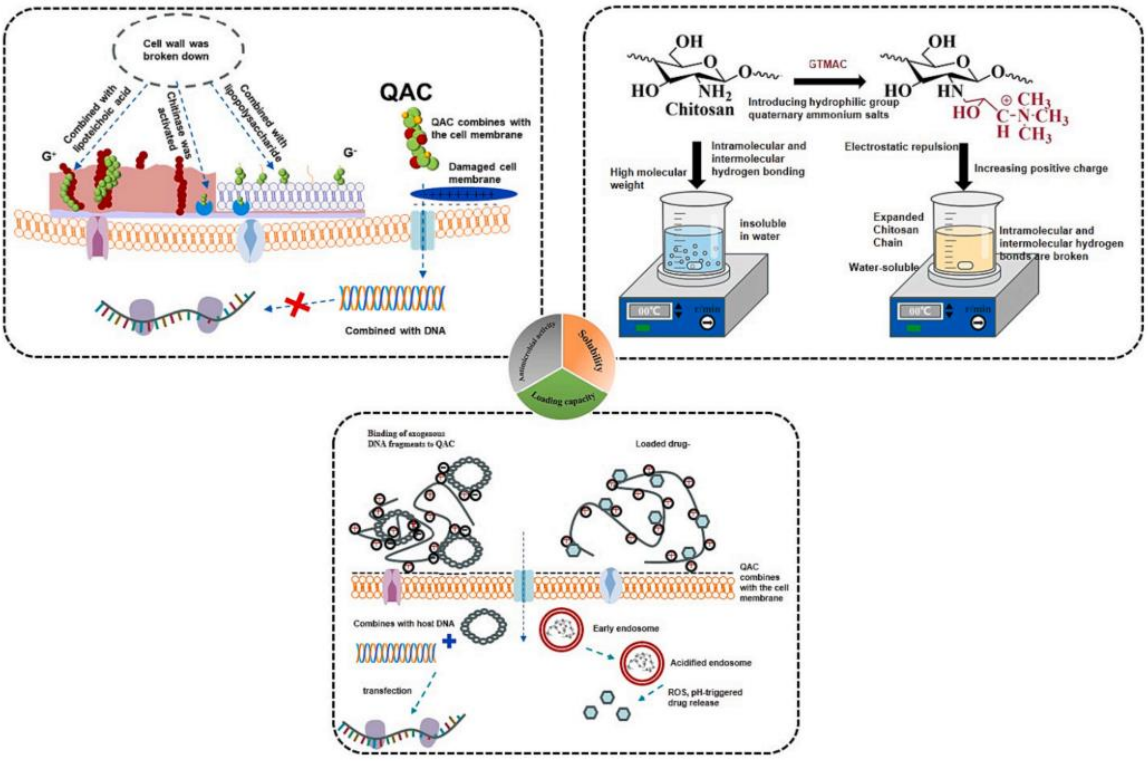

Figure 1.13 Functional mechanisms of QAC (30).

1.6 Ampholytic Polysaccharides

Ampholytic polysaccharides are complex polymers that contain both negatively charged (anionic) and positively charged (cationic) groups species on their polymer network in a single large structure (31). They combine the inherent benefits of polysaccharides, such as their ability to break down naturally, their compatibility with living organisms, and their lack of toxicity, with the functional properties of zwitterionic molecules. The polysaccharides possess a strong affinity for water molecules due to their dual charged groups, which enhance their hydrophilic character (32). This leads to the formation of a densely linked hydration layer. This feature not only gives the material excellent moisture retention qualities but also improves its fouling resistance (33), which is crucial for a wide range of applications. Moreover, the simultaneous presence of positive and negative charges within a single entity results in a distinct internal

charge balance. This balance modifies the interactions of the polysaccharides with other charged molecules, affecting numerous properties like solubility, binding tendency, and general stability. (34). The charge dynamics of ampholytic polysaccharides have a wider range of applications than traditional materials. They provide creative solutions in domains that need accurate molecular interactions. Previously work Yabin Zhang and coworker (35) report about the ampholytic hyaluronic acid-based hydrogel, a facile click reaction strategy is employed to form hydrogels in situ with cytocompatibility, biodegradability, self-healing property, and resistance to protein. The thiol-functionalized ampholytic carboxybetaine methacrylate copolymer, which takes part as a cross-linker in the "thiol-ene" click reaction with the methacrylate hyaluronic acid. The hydrogels are obtained under physiological conditions without the presence of any copper catalyst and UV light. The hydrogel consisting of ampholytic component shows an obvious reduction in protein adsorption and cell adhesion and avoids non-targeted factor interference in the biological experiments as shown in Figure 1.14.

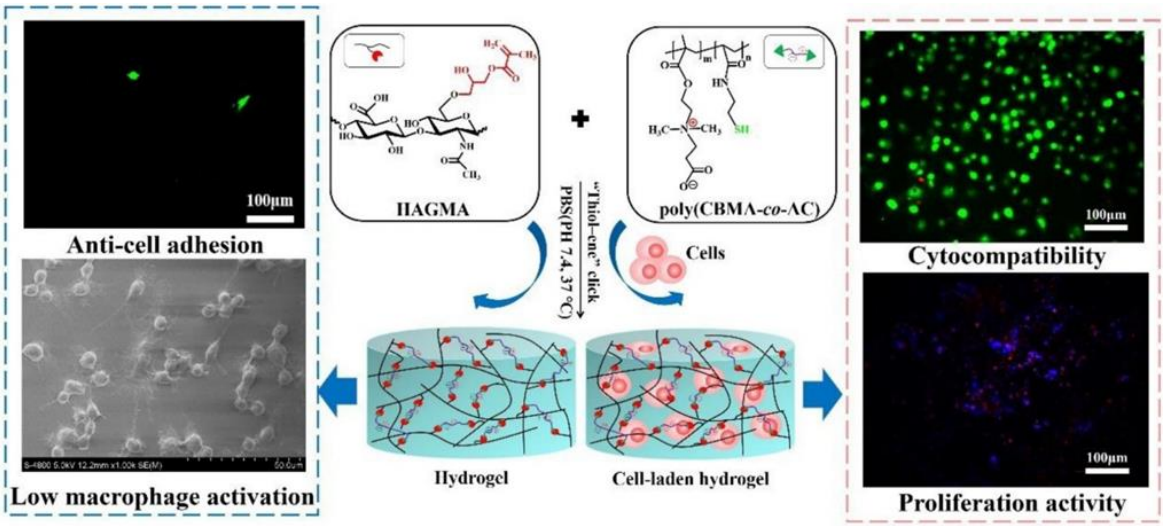

Figure 1.14 Hydrogels cross-linked via “thiol-ene” click reaction between HAGMA and poly (CBMA-co-AC) (35).

1.7 Microneedles

Microneedles represent a transformative approach in the field of drug delivery, offering a minimally invasive and efficient method for administering medications (36). This innovative technology consists of arrays of tiny needles, typically ranging from a few micrometers to a couple of millimeters in length, which can painlessly penetrate the outer layer of the skin (stratum corneum) to deliver therapeutic agents directly into the dermal tissue (37). The design and fabrication of microneedles leverage advances in microfabrication technology, enabling precise control over needle geometry and size. This precision allows for the delivery of a wide range of therapeutics including small molecule drugs, vaccines, and biologicals such as proteins and nucleic acids (38), directly to the systemic circulation or targeted dermal cells without passing through the gastrointestinal tract or undergoing hepatic first-pass metabolism. Microneedles are classified into several types based on their design, material composition, and the mechanism by which they deliver drugs. Here are the main types of microneedles commonly used in drug delivery Figure 1.15.

Solid Microneedles: These are used primarily to create microchannels in the skin. Once the skin is perforated, drug formulations applied topically can reach the dermis. Solid microneedles do not contain drug themselves; they merely facilitate its delivery (39).

Coated Microneedles: These have a thin layer of drug coated on their surface. When the needles penetrate the skin, the drug is dissolved and delivered into the interstitial fluid. The amount of drug that can be loaded onto coated microneedles is relatively limited (40).

Dissolving Microneedles: Made from water-soluble polymers and containing the drug within their structure, these microneedles dissolve upon insertion into the skin, releasing the drug directly into the tissue. This type allows for a higher drug load compared to coated microneedles (41).

Hollow Microneedles: Similar to traditional hypodermic needles but on a much smaller scale, these have a hollow center through which drugs can be injected once the needle penetrates the skin. This type is particularly useful for delivering liquid formulations and can be used for controlled drug release over time (42).

Hydrogel-Forming Microneedles: These microneedles are initially solid but absorb interstitial fluid upon insertion into the skin, forming a hydrogel that can slowly release the drug. They combine aspects of both solid and dissolving microneedles, providing a platform for sustained release (43).

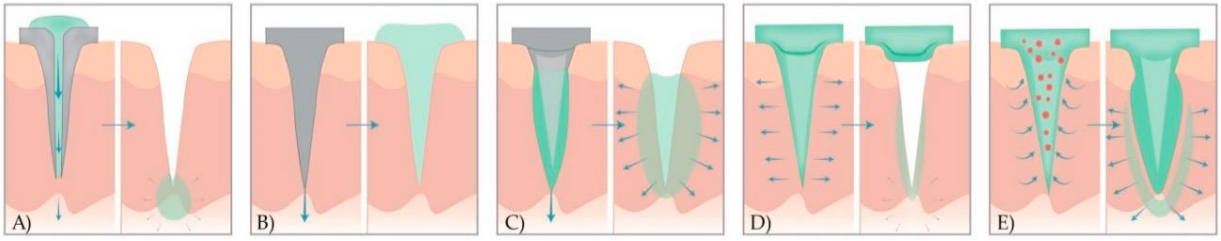

Figure 1.15 A schematic representation of drug release methods with five different types of MNs. (**A**) Hollow MNs pierce the skin (left) and provide the release of liquid drug formulation through the needle lumen (right). (**B**) Solid MNs pretreat the skin to create transient microchannels skin (left) and increase the permeability of the drug that is then, applied in the form of a transdermal patch, solution, cream, or gel (right). (**C**) Coated MNs with drug formulation (left) enable the fast dissolution of the coated drug in the skin (right). (**D**) Dissolving MNs are prepared from polymer and embedded drug in the MN matrix (left) to provide the bolus or controlled delivery of a drug

(right). (**E**) Hydrogel MNs poke the skin, uptake interstitial fluids (right), and induce diffusion of the drug from the patch through the swollen MNs (left) (44).

1.8 General Purpose

The main purpose of this study was to modify the sacran with Quat-188 to increase hydrophilicity, solubility, and cell-compatibility. After modification, the structure should be ampholytic, providing electrostatic interaction with water. Additionally, we aimed to apply the modified sacran in terms of hydrogel application. The interaction of -OH, -COOH from sacran structure and new functional groups ($+N(CH_3)_3$) from quaternary ammonium can bind together to make modified sacran showed more swelling hydrogel and hydrophilicity properties. Based on the aforementioned pieces of knowledge, we aim to utilize modified sacran in biological applications involving quaternary amines.

1.9 Reference

1. Yi Y, Xu W, Wang H-X, Huang F, Wang L-M. Natural polysaccharides experience physiochemical and functional changes during preparation: A review. Carbohydrate polymers. 2020;234:115896.

2. Liu Z-h, Niu F-j, Xie Y-x, Xie S-m, Liu Y-n, Yang Y-y, et al. A review: Natural polysaccharides from medicinal plants and microorganisms and their anti-herpetic mechanism. Biomedicine & Pharmacotherapy. 2020;129:110469.

3. Hasnain SM, Hasnain MS, Nayak AK. Natural polysaccharides: sources and extraction methodologies. Natural polysaccharides in drug delivery and biomedical applications: Elsevier; 2019. p. 1-14.

4. Ali M, Cybulska J, Frąc M, Zdunek A. Application of polysaccharides for the encapsulation of beneficial microorganisms for agricultural purposes: A review. International Journal of Biological Macromolecules. 2023:125366.

5. Ren Y, Bai Y, Zhang Z, Cai W, Del Rio Flores A. The preparation and structure analysis methods of natural polysaccharides of plants and fungi: A review of recent development. Molecules. 2019;24(17):3122.

6. Venkatesan J, Lowe B, Pallela R, Kim S-K. Chitosan-based polysaccharide biomaterials. Springer; 2014. p. 1837-50.

7. Feng Z, Lin Z, Tang H, Geng J, Hu Y, Mayo KH, et al. The model polysaccharide potato galactan is actually a mixture of different polysaccharides. Carbohydrate Polymers. 2023;313:120889.

8. Prajapati VD, Maheriya PM, Jani GK, Solanki HK. RETRACTED: Carrageenan: A natural seaweed polysaccharide and its applications. Carbohydrate polymers. 2014;105:97-112.

9. Doi M, Sagawa Y, Momose S, Tanaka T, Mizutani T, Okano Y, et al. Topical treatment with sacran, a sulfated polysaccharide from Aphanothece sacrum, improves corneocyte-derived parameters. The Journal of Dermatology. 2017;44(12):1360-7.

10. Chaudhary S, Jain VP, Jaiswar G. The composition of polysaccharides: monosaccharides and binding, group decorating, polysaccharides chains. Innovation in Nano-Polysaccharides for Eco-sustainability: Elsevier; 2022. p. 83-118.

11. Naseri-Nosar M, Ziora ZM. Wound dressings from naturally-occurring polymers: A review on homopolysaccharide-based composites. Carbohydrate polymers. 2018;189:379-98.

12. Ruthes AC, Smiderle FR, Iacomini M. Mushroom heteropolysaccharides: A review on their sources, structure and biological effects. Carbohydrate polymers. 2016;136:358-75.

13. Torres FG, Troncoso OP, Pisani A, Gatto F, Bardi G. Natural polysaccharide nanomaterials: an overview of their immunological properties. International journal of molecular sciences. 2019;20(20):5092.

14. Sabet S, Rashidinejad A, Melton LD, Zujovic Z, Akbarinejad A, Nieuwoudt M, et al. The interactions between the two negatively charged polysaccharides: Gum Arabic and alginate. Food Hydrocolloids. 2021;112:106343.

15. Fabiano A, Beconcini D, Migone C, Piras AM, Zambito Y. Quaternary ammonium chitosans: The importance of the positive fixed charge of the drug delivery systems. International Journal of Molecular Sciences. 2020;21(18):6617.

16. Hintze V, Schnabelrauch M, Rother S. Chemical modification of hyaluronan and their biomedical applications. Frontiers in chemistry. 2022;10:830671.

17. Tudu M, Samanta A. Natural polysaccharides: Chemical properties and application in pharmaceutical formulations. European Polymer Journal. 2023;184:111801.

18. Okajima MK, Sornkamnerd S, Kaneko T. Development of functional bionanocomposites using cyanobacterial polysaccharides. The Chemical Record. 2018;18(7-8):1167-77.

19. Khan SA, Shah LA, Shah M, Jamil I. Engineering of 3D polymer network hydrogels for biomedical applications: A review. Polymer Bulletin. 2022;79(4):2685-705.

20. Guo Y, Bae J, Fang Z, Li P, Zhao F, Yu G. Hydrogels and hydrogel-derived materials for energy and water sustainability. Chemical reviews. 2020;120(15):7642-707.

21. Rivero RE, Alustiza F, Rodriguez N, Bosch P, Miras MC, Rivarola CR, et al. Effect of functional groups on physicochemical and mechanical behavior of biocompatible macroporous hydrogels. Reactive and Functional Polymers. 2015;97:77-85.

22. Khandan A, Jazayeri H, Fahmy MD, Razavi M. Hydrogels: Types, structure, properties, and applications. Biomat Tiss Eng. 2017;4(27):143-69.

23. Song M, Wang J, He J, Kan D, Chen K, Lu J. Synthesis of hydrogels and their progress in environmental remediation and antimicrobial application. Gels. 2022;9(1):16.

24. Okajima MK, Mishima R, Amornwachirabodee K, Mitsumata T, Okeyoshi K, Kaneko T. Anisotropic swelling in hydrogels formed by cooperatively aligned megamolecules. RSC Advances. 2015;5(105):86723-9.

25. Ye D, Yang P, Lei X, Zhang D, Li L, Chang C, et al. Robust anisotropic cellulose hydrogels fabricated via strong self-aggregation forces for cardiomyocytes unidirectional growth. Chemistry of Materials. 2018;30(15):5175-83.

26. Qi X, Tong X, Pan W, Zeng Q, You S, Shen J. Recent advances in polysaccharide-based adsorbents for wastewater treatment. Journal of Cleaner Production. 2021;315:128221.

27. Okeyoshi K, Okajima MK, Kaneko T. The cyanobacterial polysaccharide sacran: characteristics, structures, and preparation of LC gels. Polymer Journal. 2021;53(1):81-91.

28. Kaneko T, Okajima MK. Super liquid crystalline polysaccharides produced by ultimately-ecological microreactors. Yakugaku Zasshi: Journal of the Pharmaceutical Society of Japan. 2018;138(4):489-96.

29. Amat Yusof FA, Yamaki M, Kawai M, Okajima MK, Kaneko T, Mitsumata T. Rheopectic behavior for aqueous solutions of megamolecular polysaccharide sacran. Biomolecules. 2020;10(1):155.

30. Qiu Y-L, Li Y, Zhang G-L, Hao H, Hou H-M, Bi J. Quaternary-ammonium chitosan, a promising packaging material in the food industry. Carbohydrate Polymers. 2023:121384.

31. Blackman LD, Gunatillake PA, Cass P, Locock KE. An introduction to zwitterionic polymer behavior and applications in solution and at surfaces. Chemical Society Reviews. 2019;48(3):757-70.

32. Li D, Wei Q, Wu C, Zhang X, Xue Q, Zheng T, et al. Superhydrophilicity and strong salt-affinity: Zwitterionic polymer grafted surfaces with significant potentials particularly in biological systems. Advances in Colloid and Interface Science. 2020;278:102141.

33. Chen Z. Surface hydration and antifouling activity of zwitterionic polymers. Langmuir. 2022;38(15):4483-9.

34. Lu M, Yu S, Wang Z, Xin Q, Sun T, Chen X, et al. Zwitterionic choline phosphate functionalized chitosan with antibacterial property and superior water solubility. European Polymer Journal. 2020;134:109821.

35. Zhang Y, Liu S, Li T, Zhang L, Azhar U, Ma J, et al. Cytocompatible and non-fouling zwitterionic hyaluronic acid-based hydrogels using thiol-ene “click” chemistry for cell encapsulation. Carbohydrate polymers. 2020;236:116021.

36. Ma G, Wu C. Microneedle, bio-microneedle and bio-inspired microneedle: A review. Journal of Controlled Release. 2017;251:11-23.

37. Phatale V, Vaiphei KK, Jha S, Patil D, Agrawal M, Alexander A. Overcoming skin barriers through advanced transdermal drug delivery approaches. Journal of controlled release. 2022;351:361-80.

38. Gupta J, Gupta R, Vanshita n. Microneedle technology: an insight into recent advancements and future trends in drug and vaccine delivery. Assay and drug development technologies. 2021;19(2):97-114.

39. Nagarkar R, Singh M, Nguyen HX, Jonnalagadda S. A review of recent advances in microneedle technology for transdermal drug delivery. Journal of Drug Delivery Science and Technology. 2020;59:101923.

40. Jeong H-R, Jun H, Cha H-R, Lee JM, Park J-H. Safe coated microneedles with reduced puncture occurrence after administration. Micromachines. 2020;11(8):710.

41. Sartawi Z, Blackshields C, Faisal W. Dissolving microneedles: Applications and growing therapeutic potential. Journal of Controlled Release. 2022;348:186-205.

42. Cárcamo-Martínez Á, Mallon B, Domínguez-Robles J, Vora LK, Anjani QK, Donnelly RF. Hollow microneedles: A perspective in biomedical applications. International journal of pharmaceutics. 2021;599:120455.

43. Hou X, Li J, Hong Y, Ruan H, Long M, Feng N, et al. Advances and Prospects for Hydrogel-Forming Microneedles in Transdermal Drug Delivery. Biomedicines. 2023;11(8):2119.

44. Tucak A, Sirbubalo M, Hindija L, Rahić O, Hadžiabdić J, Muhamedagić K, et al. Microneedles: Characteristics, materials, production methods and commercial development. Micromachines. 2020;11(11):961.

CHAPTER II

QUATERNIZED SULFATED POLYSACCHARIDES WITH SUPER HIGH MOLECULAR WEIGHT POLYMER

2.1 Introduction

Polysaccharides are large molecules composed of repeated monosaccharide units (45), which are produced by plants (46), animals (47), and certain microorganisms (48), including specific types of bacteria. These monosaccharide units are typically connected through glycosidic bonds, forming structures that can be either simple linear chains or more intricate branched configurations(10, 45). Sacran is a type of heteropolysaccharide made up of various sugar residues including galactose, glucose, mannose, xylose, rhamnose, fucose, galacturonic acid, and glucuronic acid (27, 49) . It also features minor amounts of alanine, galactosamine, uronic acid, and muramic acid. Notably, 11% of its monosaccharide components are sulfated, 22% contain carboxyl groups and 250 % hydroxyl groups. Natural polysaccharides offer multiple benefits for biological uses, including their derivation from renewable resources, their biocompatibility, and their non-toxic nature. However, the application of these biomaterials is limited in scope due to limitations imposed by their physicochemical and structural properties. Furthermore, specific polysaccharides obtained from natural organisms exhibit limited bioactivity, suggesting the necessity for further development. As a result, the development of methods to enhance the biological efficacy of polysaccharides is important. Numerous studies have demonstrated a variety of polysaccharide modification techniques and properties. Chemical modification has been found to significantly affect the biological activity of

polysaccharides(50-52). Chemical modification of polysaccharides involves altering their structure through chemical methods to produce polysaccharide derivatives that exhibit enhanced or novel biological activities. Chemical modification of polysaccharides can alter their biological functions by changing their functional groups. This process may also break down polysaccharides, adjust their molecular weights, improve solubility, and alter their biological effects (53-56).

Quaternization is a form of chemical modification in which a previous structure is modified by introducing a quaternary ammonium group (57). Frequently, to introduce ionic groups into polysaccharides, cationic agents are utilized. (3-chloro-2-hydroxypropyl) trimethylammonium chloride (Q-188) stands out as one of the most popular choices for creating cationic polysaccharides due to its affordability, low toxicity, and high stability (Figure 2.1). Under alkaline conditions, Q-188 is transformed into epoxide. One noted characteristic of quaternization is its ability to increase the qualities and commercial value of polysaccharides through modifications to their functionality while maintaining the majority of their residual characteristics unmodified (58).

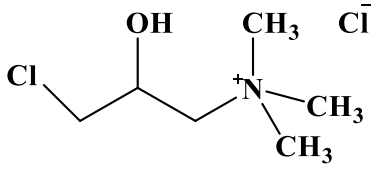

Figure 2.1 The structure of 3-chloro-2-hydroxypropyl) trimethylammonium chloride or Q-188.

3-Chloro-2-hydroxypropyl trimethyl ammonium chloride (Q-188) is favored among these agents due to its economical nature, low toxicity, improved stability, broad commercial

availability, and environmentally friendly nature. As a result, Q-188 is utilized extensively in the production procedure of quaternized ammonium polysaccharides (59, 60).

The Q-188 approach is utilized to modify sacran in order to create highly soluble ampholytic sacran for the production of ampholytic materials. This section primarily analyzes the modification ratio between sacran and agents, while also evaluating the characteristics of sacran and its derivatives.

2.2 Materials and Methods

2.2.1 Materials

Sacran, a polysaccharide was extracted from the frozen biomaterials of *Aphanothece sacrum*. Quat-188 (N-(3-chloro-2-hydroxypropyl)-trimethylammonium chloride) was purchased Tokyo Chemical Industry Co., Ltd. Sodium hydroxide (NaOH), hydrochloric acid (HCl), Sodium chloride (NaCl) and ethanol were purchased from Kanto Chemical, Japan. SnakeSkin ™ Dialysis Tubing, 10K MWCO, 35 mm dry I.D., 35 feet were purchased from thermos scientific, USA.

2.2.2 Extraction, Preparation of Sacran Polysaccharides.

The cyanobacteria sacran were collected from a river farm located on Kyushu Island, Japan. The sacran was subjected to freezing, followed by a soaking period of 2 days, and subsequently washed with distilled water to eliminate the aqueous pigment. Subsequently, the sacran was submerged and agitated in a 3% v/v solution of sodium hypochlorite. The cyanobacteria sacran had a color change from green to brown, followed by two rounds of filtration and washing with diluted water. Subsequently, a solution containing 4% v/v of hydrogen peroxide was agitated without applying heat. Next, include 4 grams of sodium hydroxide. Following a 2-hour heating

period at 60˚C using a mechanical motor stirrer, the polysaccharide should be fully dissolved. The polysaccharide solution was brought to a pH of 7 by adding 0.1 M hydrochloric acid. The solution was gradually immersed in pure isopropanol to cause the fibrous components to precipitate. The wet biomaterial polysaccharide was dried in an oven at a temperature of 60 ˚C for a duration of 2-3 minutes, resulting in the formation of fibrous materials.

2.2.3 Sonication Effect Study of Sacran

The process of ultrasonication was carried out using a vibra-cell ultrasonic liquid processor manufactured by Sonic and Materials, Inc. This processor operates at a frequency of 40 kHz. The ultrasonic energy was applied in a pulse with a 30-second duration of energy, followed by a 10-second cutoff. The amplitude of the energy was set at 40%. The 13-mm-diameter probe was placed in 50 mL of 0.5 wt% sacran solution. During the experiment, the sacran solution was placed on the ice bath through ultrasonication to prevent overheating.

2.2.4 Synthesis of Quaternary Ammonium Compounds-Sacran (Q-Sacran)

Sacran (0.5 g) was completely dissolved in 100 mL of Milli-Q water. Subsequently, a solution of sodium hydroxide was prepared by dissolving 5.0 g of the compound in 100 mL of DI water, resulting in a concentration of 5 wt%. followed this method 3 mL of 5 wt.% sodium hydroxide solution was introduced into the sacran solution, which was continuously stirred at an elevated temperature of 70 °C. Following a duration of 1 hour, Quat 188 (3.45 mmol) was carefully added to the sacran solution, the pH of solution decreased, and it was necessary to raise the pH to 12 using 5% weight of sodium hydroxide. The reaction proceeded continuously at a temperature of 70 ˚C for a duration of 24 hours. After the reaction was completed, the mixture was neutralized to around pH 7 using dilute hydrochloric acid aqueous and was reprecipitated over ethanol. The fibrous precipitates were re-dissolved in DI water and were dialyzed using a

dialysis membrane (Snakeskin dialysis membrane 10K MWCO, 35 mm; Thermo Scientific, USA) over DI water for 3 days to remove residual chemical constituents. The synthetic partway was shown in Figure 2.2. The resulting product, Q-Sacran, was collected and dried using a freeze-dryer. The higher amount of Quat 188 (6.90 mmol, 13.80 mmol, 20.73 mmol, and 27.64 mmol) was used to prepare the sacran having higher degrees of quaternization.

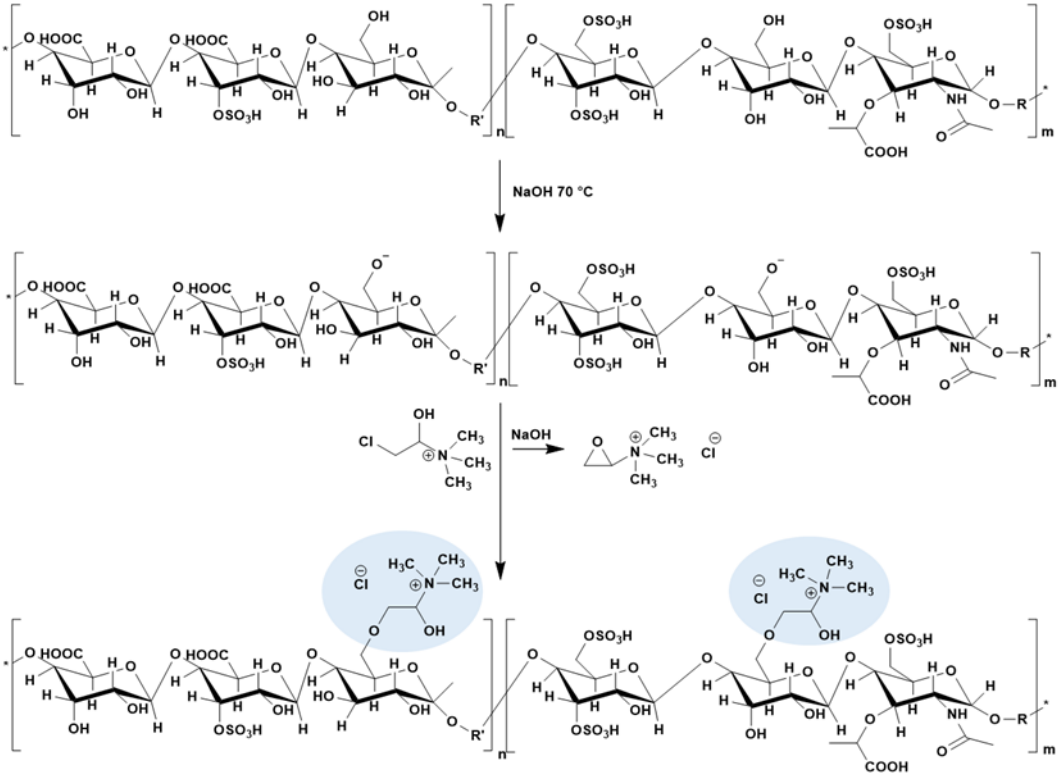

Figure 2.2 Synthetic partway of Q-sacran.

2.2.5 Characterization of Sacran Derivatives.

2.2.5.1 Nuclear Magnetic Resonance Spectroscopy (NMR)

The solid-state ^{13}C DD-MAS NMR spectra (125.8 MHz) of Sacran and its derivatives were acquired using a Bruker Avance III 500 spectrometer equipped with a 4 mm MAS probe head (4 mm VTN probe), The total recording time and recycle delay were measured to be 27 ms and

20 s, respectively. Notably, the spectra were carefully matched to the glycine carbonyl signal, which exhibited a chemical shift at 176.03 ppm (61).

2.2.5.2 Calculation of The Degree of Quaternization (%DQ)

The degree of quaternization was evaluated by ^{13}C NMR spectroscopy using equation (1)

$$\%DQ = \left[\frac{integral\ area\ of\ CH3\ of\ trimethylammonium\ (Quat)}{integral\ area\ of\ C1\ of\ sugar\ backbone}\ x\frac{1}{3}\right] x\ 100\% \quad (1)$$

Here, around 50 ppm represents the integral ^{13}C area of the trimethyl amino group of Quat, while that of a signal of the C_1 carbon for sugar residues around 100 ppm, as depicted in Figure 2.3 and Figure 2.4.

2.2.5.3 Calculation of Degree of Quat incorporation (DQ-incorporation)

To Calculate the degree of quaternary ammonium (Quat incorporation) or reaction degree relative to the initially fed quat amount in sacran, where the quat is positioned at the C_6 position and its cationic parts are assumed to form aggregates with their cationic parts on the top of surface to interact with inner anions.

- Calculate the molar amount of sacran

First determine the molar amount of sacran units available for substitution from this equation (2)

$$\text{Molar amount of sacran} = \left[\frac{weight\ of\ sacran}{Moalr\ mass\ of\ repeating\ unit}\right] \quad (2)$$

- Determine the theoretical molar amount of Quat for full substitution

To achieve a DQ of 100%, calculated the amount of Quat needed to fully substitute the available hydroxyl groups on sacran. (3)

Theoretical full substitution Quat amount = $\left[\frac{Molar\ amount\ of\ sacran}{Number\ of\ hydroxyl\ per\ sacran\ unit}\right]$ (3)

- Calculate the actual molar amount of quat incorporated (4)

Using the degree of quaternization from NMR to calculated

Actual Quat incorporated = Theoretical full substitution Quat amount x $\left[\frac{DQ}{100}\right]$ (4)

- Calculate the degree of Quat incorporation (5)

Finally, compare the actual molar amount of Quat incorporation to the molar amount of Quat initially added to calculate the degree of incorporation.

Degree of Quat incorporation = $\left[\frac{Actural\ of\ Quat\ incorporation}{Molar\ amount\ of\ Quat\ added}\right] x\ 100\%$ (5)

2.2.5.4 Attenuated Total Reflectance Fourier Transform Infrared Spectroscopy (ATR-FTIR)

The chemical structure of sacran and modified sacran, specifically the sulfate content, was characterized using chondroitin sulfate as an external standard through solid-state Attenuated Total Reflectance Fourier Transform Infrared Spectroscopy (ATR-FTIR). Analysis was performed using a Spectrum 100 FT-IR Spectrometer (Perkin Elmer). Spectra were recorded in transmittance mode across a range of 4000 to 400 cm^{-1}.

2.2.5.5 Thermal Gravimetric Analysis (TGA)

Thermogravimetric Analyses (TGA) of both Sacran and Q-sacran were conducted with a Rigaku TG 8121 instrument under a controlled nitrogen flow at a rate of 20 ml/min. Approximately 7 mg of the sample was placed in the platinum pan for analysis. Subsequently, the temperature parameters were programmed to increase at a rate of 20°C/min, ranging from an initial temperature of 50 °C to a final temperature of 850 °C. (62).

2.2.6 Molecular Weight Determination

The molecular weight of sacran was calculated using a size-exclusion chromatography multi-angle laser light scattering (SEC-MALLS) system equipped with a fused silica column. The column temperature was maintained at 40˚C. A 0.1 M sodium nitrate solution, flowing at a rate of 1 mL/min, was used as the eluent. Before measurement, the 100 mL sample solution, with a concentration of 0.01 wt%, was filtered using a 5 mm pore size filter. The light scattering measurements were performed using the DAWN Heleos multi-angle laser light scattering detector from Wyatt Technology, which operated at a wavelength of 665 nm. This detector was positioned between the SEC system and a precision refractive index (RI) detector, specifically the Wyatt Technology Optilab T-rEX, which has a laser wavelength of 658.0 nm. The refractive index increment (dn/dc) value for sacran was determined to be 0.185 mL/g (24).

2.2.7 Determination of Solubility and Salination Study

The solubilities of sacran and Q-sacran were investigated as follows. Sacran and Q-sacran were tried to dissolve in various solvents to see how well they dissolved. The samples were first mixed with a solvent at room temperature, and then the temperature was slowly raised until it reached 60 °C while being stirred until a clear solution formed. Moreover, we also investigated the impact of salination, aqueous mixes of sacran were prepared using 0.1 M solutions of NaCl in Milli-Q water.

2.2.8 The Dynamic Light Scattering (DLS)

Dynamic light scattering (DLS) technique is subsequently utilized to analyze and characterize the particle size, hydrodynamic diameter, or polymer coils suspended of the polysaccharide in solution. This analysis was conducted using a Zetasizer Nano ZS90 (Malvern Instruments Ltd.,

England). at a consistent temperature of 25 ˚C, the observed intensity of dispersed light is represented as the count rate of photons, measured in kilo counts per second (kcps). The sample container utilized in this study was a disposable folded capillary cell, namely the DTS 1070 model.(63),(64).

2.2.9 Steady-Shear Viscosity Measurement.

Viscoelastic measurements were conducted utilizing a rheometer (MCR 301; Anton Paar, Graz, Austria) which included a stainless-steel cone plate, which is the CP50 model manufactured by Anton Paar, having a diameter of 50 mm. The temperature during the viscoelastic measurement was recorded as 25.0 ± 0.5˚C using a Peltier plate. An experiment was conducted to measure the viscosity of a fluid under steady-shear flow conditions. The shear rate varied within the range of 0.001 to 1,000 s^{-1} (65).

2.3 Results and Discussion

2.3.1 Effect of Ultrasonication on Molecular Weight Reduction.

Ultrasonication is a technique that uses sound waves of high frequency to induce a mechanical force in a liquid medium. This technique is non-toxic and easy to provide lower polymer segment from large polymer segment. At the process, sacran solution concentration 0.5 wt.% was characterized by the molecular weight reduction with SEC as shown in Table 1.

Table 1. Ultrasonication effect to reduction of molecular weight of sacran chains.

Irradiation time (min)	*Mw* (g/mol)	PDI (*Mw*/*Mn*)
0	$3.07 \times 10^6 \pm 8.010\%$	2939.33±339
5	$2.89 \times 10^6 \pm 8.954\%$	807.70±65
10	$2.70 \times 10^6 \pm 12.418\%$	484.30±34
15	$2.46 \times 10^6 \pm 7.852\%$	103.72±21

2.3.2 Synthesis and Characterization of Modified-Sacran

2.3.2.1 ^{13}C-Nuclear Magnetic Resonance (^{13}C-NMR)

A quaternization reaction has three stages. The initial stage has the reaction between the sacran polysaccharide and sodium hydroxide, followed by the engagement of the epoxy ring from the quaternizing agent, and culminating in the reaction between the hydroxyl group of sacran polysaccharide and epoxide. This final step results in the formation of an ether bond within the structure. The reaction mechanism shown in Figure 2.3 illustrates the characterization, so confirming the structure of Sacran. The ^{13}C-DDMAS nuclear magnetic resonance (NMR) spectra showed signals at chemical shifts of 101.03 ppm (carbon atoms of C_1 and C2), 73.10 ppm (C3, C4, and C5), and 175.50 ppm (carboxyl group) were detected. Following the process of quaternization, Q-sacran exhibited a new signal corresponding to trimethyl ammonium ($+N(CH_3)_3$) within the chemical shift range of around 50–55 ppm. Furthermore, the degree of quaternizing was determined using equation 1**.** in the ^{13}C analysis. The findings demonstrate

that the quaternization degree (%DQ) of QAC-sacran is extensively reported in Table 2., in relation to the integral area of C_1 carbon inside the sugar backbone.

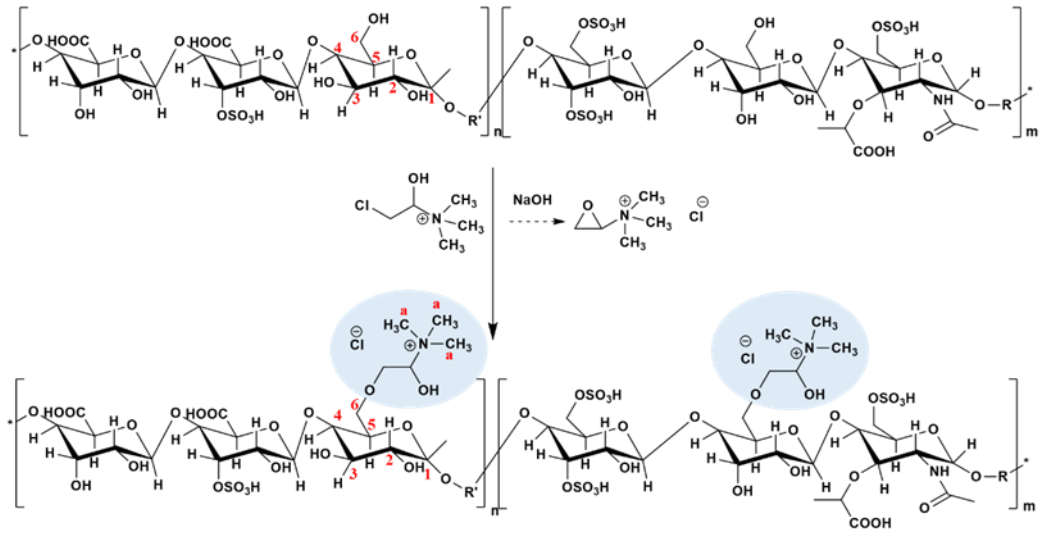

Figure 2.3 The structure showed the carbon atom of the main sugar ring of the sacran and modified sacran.

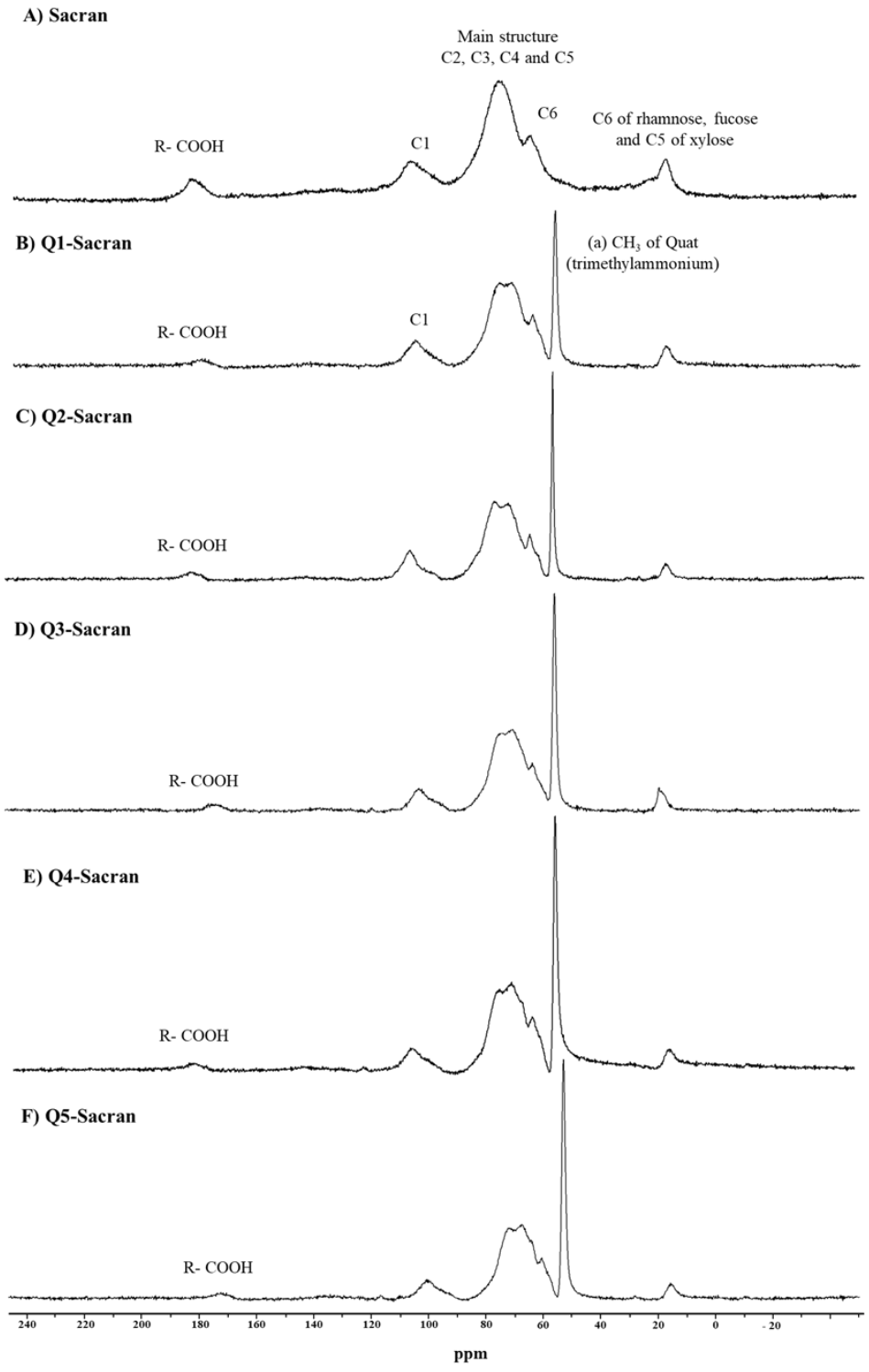

Figure 2.4 ^{13}C- NMR spectra of (A) sacran and (B-F) modified Sacran at difference amount of quaternary ammonium.

Table 2. Quaternization degree (%DQ) of Q-sacran prepared under different Quat amount added and Molecular weight of origin sacran and modification sacran.

Conditions	Amount of QAC (mmol)	Degree of Quaternization (%DQ)	Molecular weight (DA)
A. Sacran	-	-	$2.46x10^6$
B. Sacran with NaOH	-	-	$7.98x10^5$
C. Q1-Sacran	3.45	32±7	$7.41x10^5$
D. Q2-Sacran	6.90	33±1	$1.94x10^5$
E. Q3-Sacran	13.80	61±8	$2.23x10^4$
F. Q4-Sacran	20.73	79±6	$4.51x10^4$
G. Q5-Sacran	27.64	87±9	$4.18x10^4$

The modification of sacran has shown that it has a dual effect. The first effect, after being modified with a quaternizing agent, was transformed into an ampholytic polysaccharide that showed both anionic and cation charges. In addition, the second effect is the molecular effect of modification sacran, which will decrease due to the effect of alkaline hydrolysis, the result as shown in Table 2. The method of turning a hydroxyl group into ethers is a well-established reaction in the structure of several polysaccharides. In order to achieve the synthesis of sacran ethers, it is necessary to carefully control the reaction conditions within the pH range of around 13-14. This specific pH range is essential for facilitating the desired etherification reaction (16). Throughout this procedure, alkaline hydrolysis (OH^-) will be observed, wherein hydroxide ions act as nucleophiles and target the glycosidic connections within the sugar backbone. Sacran is a type of polysaccharide composed of a number of sugar rings. (66), The alkaline hydrolysis of modified sacran is shown in Figure 2.5

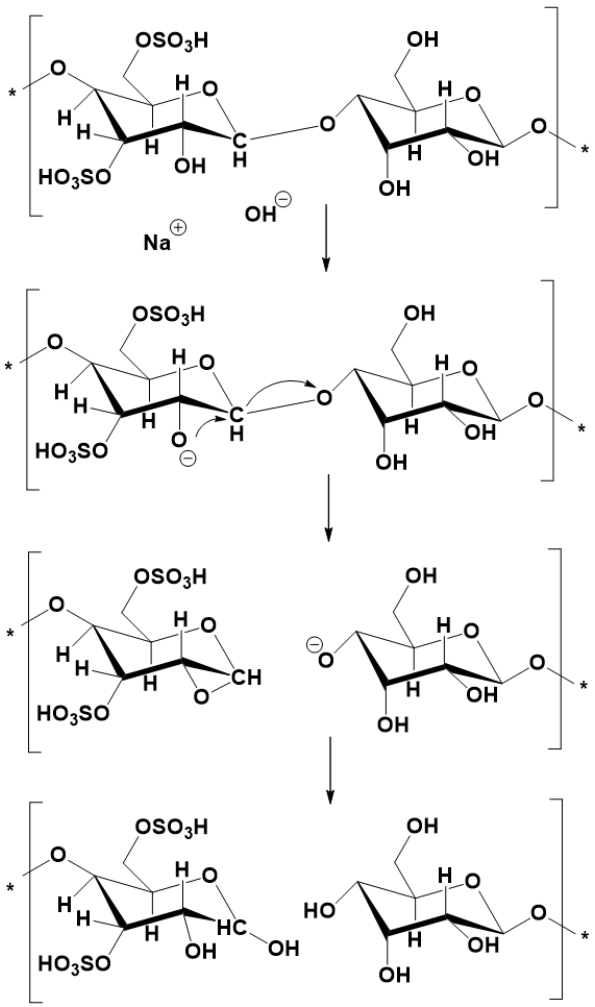

Figure 2.5 Alkaline hydrolysis of glycosidic linkages bond.

Hydroxide ion can be deprotonated hydroxyl group at the C2 of sugar ring on the structure, and then the sugar rings break down and the polymer molecular becomes smaller (67).

2.3.2.2. The Compositions of Carboxyl Groups and Sulfate Groups in Their Sacran Structure.

Sacran is a polysaccharide composed of anionic groups, including carboxylate and sulfonate, which constitute approximately 34% mol of the total sugar units. The degree of carboxylate incorporation in sacran and its modified forms is detailed in Table 3, showing similar levels of carboxylate group incorporation across all samples, ranging from 17-21%. These results suggest

that the quaternary ammonium (quat) groups interact with the hydroxyl groups at the C-6 position of the sugar rings.

Table 3. A summary incorporation of COOH in sacran and modified sacran.

Conditions	DQ Incorporation [a] (%)	COOH [b] (mol)	COOH incorporation [c] (%)
A. Sacran	-	$5.94x10^{-4}$	22
B. Q1-Sacran	67.95	$4.74x10^{-4}$	20
C. Q2-Sacran	35.65	$5.51x10^{-4}$	20
D. Q3-Sacran	32.54	$5.37x10^{-4}$	20
E. Q4-Sacran	28.19	$5.43x10^{-4}$	20
F. Q5-Sacran	23.30	$5.58x10^{-4}$	21

a) The incorporation valve of Q-188 has been incorporated into the sacran. b) mol of COOH refers to sacran, and c) %COOH incorporation of sacran and modified sacran.

In FTIR analysis, the purpose of this study is to estimate the number of sulfate groups present in sacran. The well-defined sulfate absorption peaks of chondroitin sulfate for FTIR spectroscopy were used as an external reference. Quantifying the sample amount directly in the FTIR analysis was not feasible; consequently, a ratiometric approximation was employed to measure the change in the intensity of absorption bands. This is a relative method for comparing band intensities, providing clues about changes in the composition or structure of the sample (68). The normalized spectra for both the reference standard and sacran are identical and correspond under ideal conditions. Comparative analysis of the peak heights for sacran and chondroitin sulfate is presented in **Figure 2.6**. In the chondroitin spectrum, a strong S=O absorbance band at 1226 cm^{-1} indicates the presence of sulfate groups, constituting approximately 50% mol of chondroitin sulfate. The peak at 1033 cm^{-1} is attributed to the C-O-C bonds of aliphatic ethers and sulfate

groups in polysaccharides, with polysaccharides having 200% ether per sugar residue. In the sacran spectrum, the specific S=O band appears at 1226 cm^{-1}, and the peak corresponding to the ether and sulfate in polysaccharides is observed at 1037 cm^{-1}. **Table 4.** summarizes the FTIR normalized peak height ratios for specific peaks. The results indicate that the ratio of peak heights at 1226/1033 cm^{-1} for chondroitin and 1226/1037 cm^{-1} for sacran corresponds to a sulfate composition of approximately 13% mol per sugar residue.

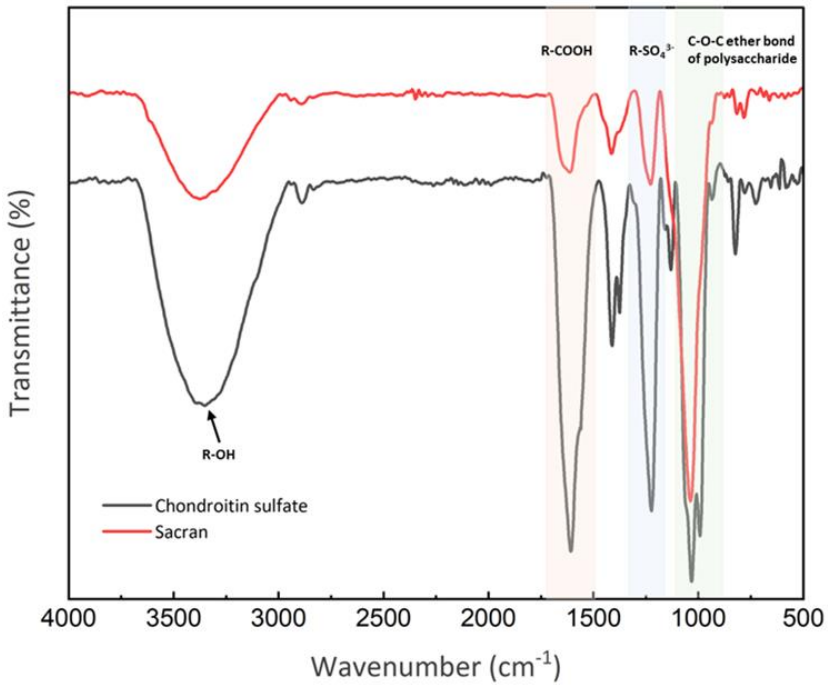

Figure 2.6 The FTIR spectrum of chondroitin sulfate has 50%mol sulfate to sugar residues and sacran polysaccharide.

Table 4. A summary of the FTIR peak height ratio from chondroitin sulfate as an external standard comparing with sacran.

Compound	Peak (cm^{-1})	Intensity Ratio (1226/1033 or 1226/1037)	Sulfate Composition (% mol)
Chondroitin Sulfate	1226/1033	0.83	50
Sacran	1226/1037	0.21	13

2.3.2.3 Thermogravimetric Analysis (TGA)

The thermal characteristics of sacran and Q-sacran were evaluated by TGA. Derivative TGA analyses (DTG) were also made. Figure 2.7 illustrates TGA of sacran and various Q-sacran specimens. The TGA of sacran profile showed weight loss observed in the temperature range of 25-130˚C was approximately 10 %. This can be attributed to moisture vaporization from the specimens. Subsequently, the second and third stages of mass-loss were observed. The large mass-drops down to around 50 % were identified in the range of 250-300˚C and DTG peak of sacran were observed at a temperature of 282 ˚C as shown in Figure 2.7B**,** which should be assigned thermal degradation due to the breakdown of the sacran backbone. The profiles of TGA and DTG of sacran with NaOH and without Quat also showed weight loss due to moisture vaporization from specimens around 13.45% at the same temperature as sacran. Furthermore, the second state of the TGA thermogram of the sample showed a weight loss due to the structure decomposition of around 28.70% at a temperature range of 170–230 ˚C. The DTG were observed at a temperature of around 222 ˚C. To compare the DTG peak of sacran and sacran with NaOH, the temperature was shifted to a lower temperature after hydrolysis due to the

hydrolysis reaction breaking the glycosidic bonds, leading to the cleavage of polysaccharide (1). TGA and DTG analyses of Q-sacran at various concentrations (Figures 2.7A and 2.7B) demonstrated a moisture content spanning from 10-12 % at 25-130 ˚C. The mass reduction attributed to thermal degradation varied between 45% and 60%. When comparing the DTG peaks of sacran with NaOH and Q-sacran, a slight decrease in temperature was observed from 222 ˚C to approximately 280 ˚C. The results of this study suggest that the temperature degradation was accelerated by the etherification reaction between quaternary ammonium and sacran. The DTG peak temperature difference Q-sacran, however, was not significantly impacted by quaternization.

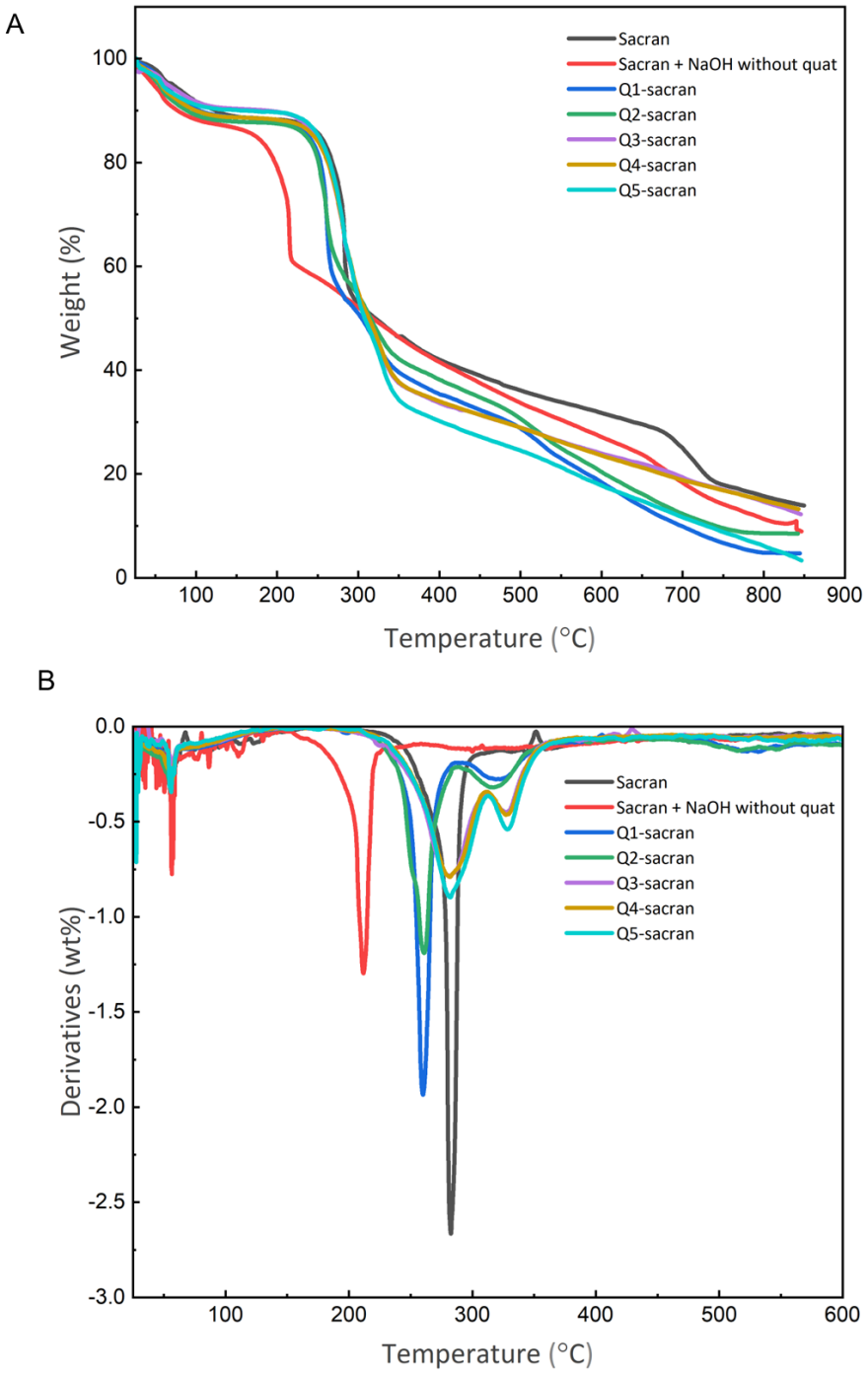

Figure 2.7 A) Presents the thermogram obtained from the thermogravimetric analysis (TGA) of sacran and Q-sacran derivatives under six different settings and B) displays the temperature composition obtained from the derivative thermogravimetry (DTG) analysis.

2.3.3 Hydrodynamic Radius and Zeta Potential of Modified Sacran

The dynamic light scattering (DLS) was used to measure the hydrodynamic radius and zeta potential of Q-sacran in aqueous solutions at a temperature of 25 ˚C (Table 5). The hydrodynamic radius, R_h, of sacran as particles in water was evaluated at approximately 4700 ± 1300 nm. R_h values of Q-sacran with degrees of 32 %, 33 %, 61 %, 79 %, and 87 % were estimated as 1600 ±220 nm, 950 ± 80 nm, 950 ± 80 nm, 1100 ± 120 nm, and 990 ± 30 nm, respectively, indicating that cationization of sacran reduced R_h. Sacran intrinsically formed supercoiled assembles in spite of densely substituted anionic groups, presumably based on hydrogen bonding and hydrophobic interactions. (69) As the composition of cations increased, the ion pair number of quaternary ammonium groups with original anions of sacran increased. These interactions have two effects 1) on interfering the assemble formation by the bulky Q-group, 2) on tightening the assemble form by ionic interaction of incorporated cations with original anions. These effects resulted in the reduction of R_h.

Table 5. Characterization the hydrodynamic radius (R_h) results for original sacran and sacran with Q-composition in DI-water and DMSO of sample in aqueous solution

Conditions	In water	In DMSO
	Hydrodynamic radius (nm)	Hydrodynamic radius (nm)
A. Sacran	4700±1300	517±160
B. Sacran with NaOH	1790±120	597±30
C. Q1-Sacran	1600±220	982±65
D. Q2-Sacran	950±80	658±70
E. Q3-Sacran	950+80	2405±105
F. Q4-Sacran	1100±120	3217±977
G. Q5-Sacran	990±30	4724±892

In DMSO, as the number of cations in Q-sacran increased, the ion pair number of modified QAC groups with the original anions of sacran also increased. These interactions caused the polymer chains to aggregate, resulting in a decrease in their solubility. Based on the interchain interaction, the modification with QAC enhanced the resulting aggregation, leading to an increase in particle size was shown in Figure 2.8.

Figure 2.8 Solubility in DMSO A) Sacran and from B-G are modified sacran B) Q1-Sacran C) Q2-Sacran D) Q3-acran E) Q4-Sacran and F) Q5-Sacran

The R_h and zeta-potential of Q-sacran were evaluated in a saline solution (Table 6), showing that R_h decreases and zeta potential increases as the cationization degree increases by NaCl addition. This phenomenon can be explained by the interplay between electrostatic interactions among the charged groups of Q-sacran and ions from the saline solution. Upon the addition of NaCl, Na^+ and Cl^- ions can connect with Q-sacran assembles to dissociate and to reduce R_h values.

Table 6. The zeta potential of original sacran and the modification sacran as a difference Q-composition in NaCl 0.1 M.

Conditions	In NaCl 0.1 M	
	Hydrodynamic radius (nm)	Zeta Potential (mV)
A. Sacran	1100±260	-18.9±0.2
B. Q1-Sacran	820±120	-17.2±0.6
C. Q2-Sacran	700±40	-15.9±0.6
D. Q3-Sacran	640+80	-14.0±0.5
E. Q4-Sacran	560±20	-10.0±0.2
F. Q5-Sacran	520±60	-9.2±0.5

2.3.4 Screening Effect of Sacran and Modified Sacran

The value of the zeta potential of original sacran was approximately -59.2 mV, whereas those of Q-sacran had increased values from -54.8 to - 41.9 mV with increasing compositions of the quaternary ammonium group (Figure 2.9) This can be regarded as evidence of cationization. The increasing rate was estimated as 19 mV per cationization unit. It is noteworthy that the zeta-potential is negative even for samples with large cationization degrees. The assembled characteristics can be attributed to both positive charges ($-N(CH_3)_3^+$) and original negative charges ($-COO^-$ and $-SO_4^-$) of sacran, as well as their interactions with one another. The sacran chains were very efficiently assembled to form micro-scaled supercoils against electrostatic repulsion. Even in high cationization degrees, the supercoil assembles were formed in which not only anions but also incorporated cations were contained inside. Around the surface of assembles, it is speculated that the 6-substituted cation groups should be directed inside to interact with inner anions, and necessarily sulfated anions groups substituting at opposite 2- or 3-positions should be directed to the surface.

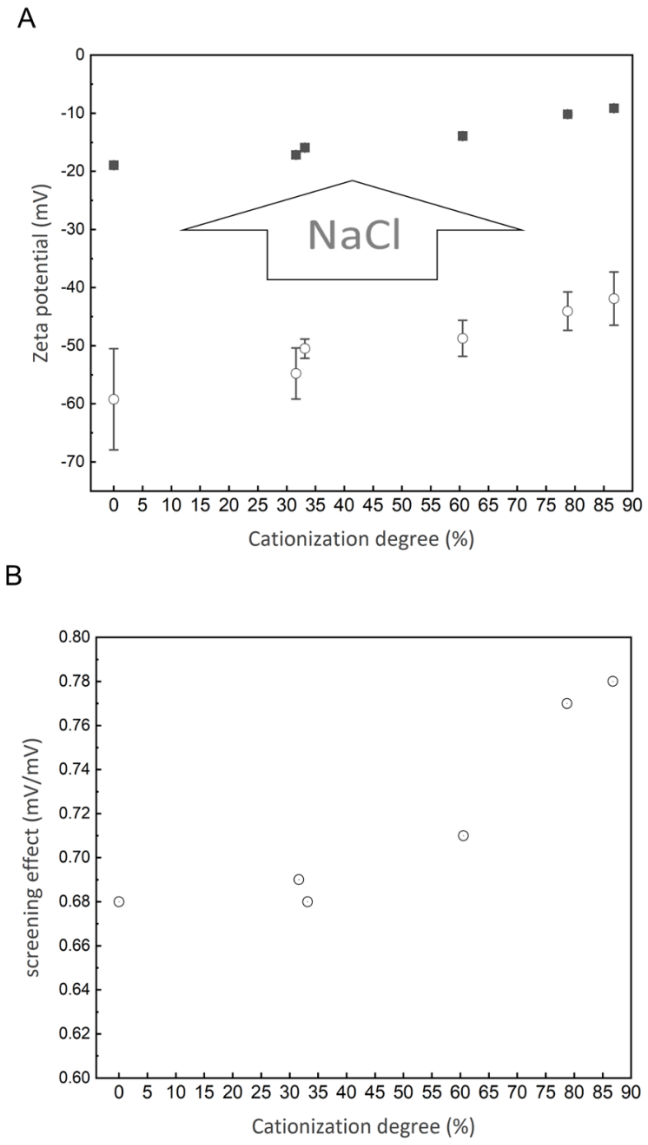

Figure 2.9 Zeta potential, ζ, of Q-sacran with various compositions. A) Open circle, ζ_0,: in water, Closed circle, ζ_{NaCl},: in NaCl solution (0.1M). B) Screening effects of NaCl addition to sacran Zeta potential estimated as $(\zeta_0-\zeta_{NaCl})/\ \zeta_0$.

2.3.5 Viscosity Properties of Sacran and Modified Sacran

The graph illustrates the dependence of apparent viscosity on shear rate for aqueous sacran solutions and modified sacran with varying quantities of quaternary ammonium compounds (QAC). Both the sacran and Q-sacran solutions in water exhibit characteristics of a non-Newtonian, shear-thinning fluid. When the viscosities of these solutions are compared, it is clear that all of the samples of modified sacran have lower viscosities than sacran at a concentration of 0.5 wt.%. In basic, at a lower concentration of $c<0.004$ wt%, the sacran solution exhibited a significantly reduced viscosity behavior at the given shear rate. When the concentration of sacran was increased to $0.015 < c < 0.20$ wt.%, the viscosity of sacran increased because the sacran chain became closer together and formed a semi dilute-entangled regime (70) For this reason, the sacran solution at 0.5 wt.% as shown in Figure 2.10 has a very high viscosity of more than 100 Pa·s at a shear rate of 0.1 s^{-1}, and the sacran chains, which can be close to each other, make the viscosity higher. Furthermore, the effect of difference concentration of quaternary ammonium on sacran. The results indicate that the viscosities of Q1 and Q2 are much lower. Moreover, as positively charged Q3, Q4, and Q5 are introduced, the viscosity further diminishes, reaching a minimum of 1 Pa·s at a shear rate of 0.1 s^{-1}. The primary cause of this phenomenon can be linked to variations in molecular weight and the secondary phenomenon of electrostatic repulsion between its segments. The repulsive forces between the polymer segments lead to their dispersion. On the other hand, the observed decrease in viscosity resulting from the introduction of sacran structures with positive charges can mostly be attributed to electrostatic interactions between the quaternary ammonium compounds with positive charges and the sacran with negative charges.

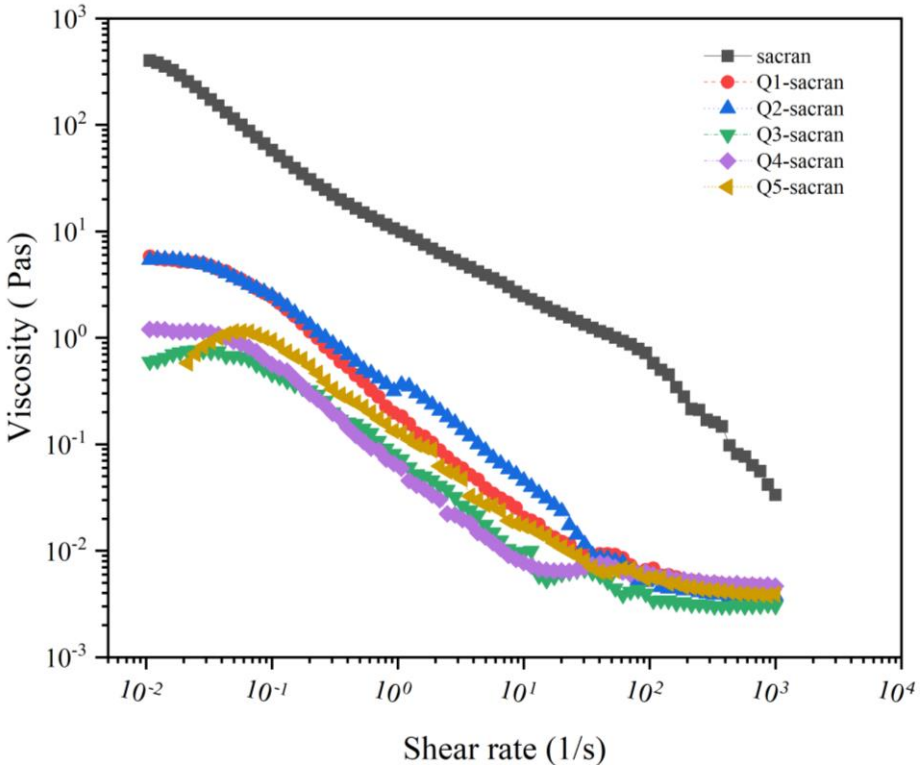

Figure 2.10 Shear-rate dependence of the apparent viscosity for sacran derivatives solution at 25°C with 0.5 %wt.

2.4 Conclusion

The sacran polysaccharide was synthesized and its properties were analyzed after modification. Quaternary ammonium was incorporated into the sacran structure through an etherification process. The quaternization level of the quaternary ammonium was measured using 13C NMR and ranged from 33% to 87% substitution. The modification of sacran resulted in two structural changes: 1) improved ampholytic properties, with well-balanced anionic and cationic charges, and 2) conversion of the hydroxyl groups into cationic entities to increase the charge density. Sacran consists of anionic groups, specifically carboxylate and sulfonate, which make up about 32% mol of the total sugar units. The extent of carboxylate integration in sacran and its modified variants is

detailed, showing consistent levels of carboxylate groups in all samples, ranging from 17-21%. These results demonstrate that the quaternary ammonium (Quat) groups interact with the hydroxyl groups at the C-6 position of the sugar rings and with a sulfate composition of approximately 13% mol per sugar residue. The hydrodynamic radius, Rh, of sacran particles in water was determined to be approximately 4700 ± 1300 nm. Rh values for Q-sacran with quaternization degrees of 32%, 33%, 61%, 79%, and 87% were found to be 1600 ± 220 nm, 950 ± 80 nm, 950 ± 80 nm, 1100 ± 120 nm, and 990 ± 30 nm, respectively. These findings suggest that cationization of sacran leads to a reduction in R_h. As the cation content increased, the number of ion pairs formed between the quaternary ammonium groups and the original anions of sacran also increased. These interactions influence the assembly in two ways: 1) by disrupting the assembly formation through the bulky Q-group, and 2) by tightening the assembly through ionic interactions between the incorporated cations and original anions, resulting in a reduction of R_h. The R_h and zeta potential of Q-sacran were assessed in saline solution, showing that R_h decreases and zeta potential increases with higher degrees of cationization due to the addition of NaCl. This behavior is attributed to the interplay of electrostatic interactions among the charged groups of Q-sacran and ions from the saline solution. When NaCl is added, Na^+ and Cl^- ions can associate with Q-sacran assemblies to dissociate and decrease R_h values. The rotational viscosities of Q-sacran in aqueous solutions displayed non-Newtonian and shear-thinning properties. All variants of Q-sacran exhibited lower viscosities compared to sacran across all shear rates, which can be explained by the interaction of sacran anions with the integrated cations leading to a more compact configuration in water, thus reducing viscosity along with a decrease in molecular weight.

2.5 Reference

45. Kabir SF, Rahman A, Yeasmin F, Sultana S, Masud RA, Kanak NA, et al. Occurrence, distribution, and structure of natural polysaccharides. Radiation-processed polysaccharides: Elsevier; 2022. p. 1-27.

46. Li C, Wu G, Zhao H, Dong N, Wu B, Chen Y, et al. Natural-derived polysaccharides from plants, mushrooms, and seaweeds for the treatment of inflammatory bowel disease. Frontiers in pharmacology. 2021;12:651813.

47. Aleid S, Wu M, Li R, Wang W, Zhang C, Zhang L, et al. Salting-in effect of zwitterionic polymer hydrogel facilitates atmospheric water harvesting. ACS Materials Letters. 2022;4(3):511-20.

48. Perfileva AI, Tsivileva OM, Nozhkina OA, Karepova MS, Graskova IA, Ganenko TV, et al. Effect of natural polysaccharide matrix-based selenium nanocomposites on Phytophthora cactorum and rhizospheric microorganisms. Nanomaterials. 2021;11(9):2274.

49. Sulastri E, Lesmana R, Zubair MS, Elamin KM, Wathoni N. A comprehensive review on ulvan based hydrogel and its biomedical applications. Chemical and Pharmaceutical Bulletin. 2021;69(5):432-43.

50. Xie L, Shen M, Hong Y, Ye H, Huang L, Xie J. Chemical modifications of polysaccharides and their anti-tumor activities. Carbohydrate Polymers. 2020;229:115436.

51. Luo M, Zhang X, Wu J, Zhao J. Modifications of polysaccharide-based biomaterials under structure-property relationship for biomedical applications. Carbohydrate Polymers. 2021;266:118097.

52. Rial-Hermida MI, Rey-Rico A, Blanco-Fernandez B, Carballo-Pedrares N, Byrne EM, Mano JF. Recent progress on polysaccharide-based hydrogels for controlled delivery of therapeutic biomolecules. ACS Biomaterials Science & Engineering. 2021;7(9):4102-27.

53. Cui R, Zhu F. Ultrasound modified polysaccharides: A review of structure, physicochemical properties, biological activities and food applications. Trends in Food Science & Technology. 2021;107:491-508.

54. Zhang B, Lan W, Xie J. Chemical modifications in the structure of marine polysaccharide as serviceable food processing and preservation assistant: A review. International Journal of Biological Macromolecules. 2022;223:1539-55.

55. Wang W, Xue C, Mao X. Chitosan: Structural modification, biological activity and application. International Journal of Biological Macromolecules. 2020;164:4532-46.

56. Riaz T, Iqbal MW, Jiang B, Chen J. A review of the enzymatic, physical, and chemical modification techniques of xanthan gum. International journal of biological macromolecules. 2021;186:472-89.

57. Zhou Z, Zhou S, Zhang X, Zeng S, Xu Y, Nie W, et al. Quaternary ammonium salts: Insights into synthesis and new directions in antibacterial applications. Bioconjugate Chemistry. 2023;34(2):302-25.

58. Yin X, Xie H, Li R, Yan S, Yin H. Regulating association strength between quaternary ammonium chitosan and sodium alginate via hydration. Carbohydrate Polymers. 2021;255:117390.

59. Mi Y, Zhang J, Zhang L, Li Q, Cheng Y, Guo Z. Synthesis, characterization, and evaluation of nanoparticles loading adriamycin based on 2-hydroxypropyltrimethyl ammonium chloride chitosan grafting folic acid. Polymers. 2021;13(14):2229.

60. Zhai S, Li Y, Dong W, Zhao H, Ma K, Zhang H, et al. Cationic cotton modified by 3-chloro-2-hydroxypropyl trimethyl ammonium chloride for salt-free dyeing with high levelling performance. Cellulose. 2022:1-14.

61. Okajima MK, Nguyen QTl, Tateyama S, Masuyama H, Tanaka T, Mitsumata T, et al. Photoshrinkage in polysaccharide gels with trivalent metal ions. Biomacromolecules. 2012;13(12):4158-63.

62. Okajima MK, Kumar A, Fujiwara A, Mitsumata T, Kaneko D, Ogawa T, et al. Anionic complexes of MWCNT with supergiant cyanobacterial polyanions. Biopolymers. 2013;99(1):1-9.

63. Okajima MK, Kaneko D, Mitsumata T, Kaneko T, Watanabe J. Cyanobacteria that produce megamolecules with efficient self-orientations. Macromolecules. 2009;42(8):3057-62.

64. Budpud K, Okeyoshi K, Kobayashi S, Okajima MK, Kaneko T. Super-Moisturizing Materials from Morphological Deformation of Suprapolysaccharides. Macromolecular Rapid Communications. 2022;43(11):2200163.

65. Joshi G, Okeyoshi K, Yusof FAA, Mitsumata T, Okajima MK, Kaneko T. Interfacial self-assembly of polysaccharide rods and platelets bridging over capillary lengths. Journal of Colloid and Interface Science. 2021;591:483-9.

66. Le Nguyen QT, Okajima M, Mitsumata T, Kan K, Tran HT, Kaneko T. Trivalent metal-mediated gelation of novel supergiant sulfated polysaccharides extracted from Aphanothece stagnina. Colloid and Polymer Science. 2012;290:163-72.

67. Berglund J, Azhar S, Lawoko M, Lindström M, Vilaplana F, Wohlert J, et al. The structure of galactoglucomannan impacts the degradation under alkaline conditions. Cellulose. 2019;26(3):2155-75.

68. Putri OD, Petchsuk A, Buchatip S, Supmak W, Kaewsaneha C, Thananukul K, et al. Preparation of Eumelanin-Encapsulated Stereocomplex Polylactide Nano/Microparticles for Degradable Biocompatible UV-Shielding Products. Nanomaterials and Nanotechnology. 2023;2023(1):9832904.

69. Budpud K, Okeyoshi K, Okajima MK, Kaneko T. Vapor-Sensitive Materials from Polysaccharide Fibers with Self-Assembling Twisted Microstructures. Small. 2020;16(29):2001993.

70. Mitsumata T, Miura T, Takahashi N, Kawai M, Okajima MK, Kaneko T. Ionic state and chain conformation for aqueous solutions of supergiant cyanobacterial polysaccharide. Physical Review E. 2013;87(4):042607.

CHAPTER III

PREPARATION OF ANISOTROPIC AMPHOLYTIC HYDROGEL MATERIALS

3.1 Introduction

Hydrogels are a type of material composed mainly of water that is contained within a network of polymer chains (71). These materials are characterized by their significant water content, generally exceeding 90% (72), resulting in their softness, flexibility, and compatibility with living organisms. Hydrogels possess a unique set of characteristics that make them extremely well-suited for a wide range of uses, especially in the field of biomedicine (73). Hydrogels possess specific characteristics that result from the physical or chemical connections between the polymer chains (74). The gel structure is kept stable by the cross-links even with its high-water content. The specific type of linkages in hydrogels allows for two classifications.: chemically cross-linked, which involves the formation of covalent bonds between polymer chains, and physically cross-linked, which relies on entanglements or non-covalent interactions like hydrogen bonds or ionic bonds to maintain the network structure (75, 76). Hydrogels are highly adaptable and find application in several fields such as drug delivery (77), wound dressings (78), tissue engineering scaffolds (79), and contact lenses (80). In drug delivery, hydrogels can be created to deliver therapeutic compounds with high specificity, in response to specific stimuli such as pH, temperature, or enzymes. Hydrogel ability to adapt to ambient conditions makes them well-suited for developing more precise and effective treatments with fewer adverse effects. Hydrogels can be synthesized using many techniques, such as polymerizing hydrophilic monomers (81), cross-linking pre-formed polymer chains (82), or utilizing natural sources like gelatin or alginate. The selection of synthesis technique and materials can be customized

to get specific qualities necessary for various applications, emphasizing the versatility of hydrogels in meeting a wide range of requirements.

Anisotropic structures are commonly found in organisms, giving them extraordinary physiological functions and properties that help them adapt to various environments. These structures have distinct mechanical, optical, and biological characteristics. For example, collagen molecules are tightly packed and precisely aligned bundles of elastic fibers found in skeletal muscles. The mechanical strength of this hierarchical fibrous arrangement is significant when viewed in the direction of the fibers. Specialized anisotropic functions, like load bearing, directional movement, and muscle contraction support, rely entirely on these properties. Anisotropic structures provide materials with directional physical properties and exceptional mechanical strength, as well as unique biological characteristics (Figure 3.1).

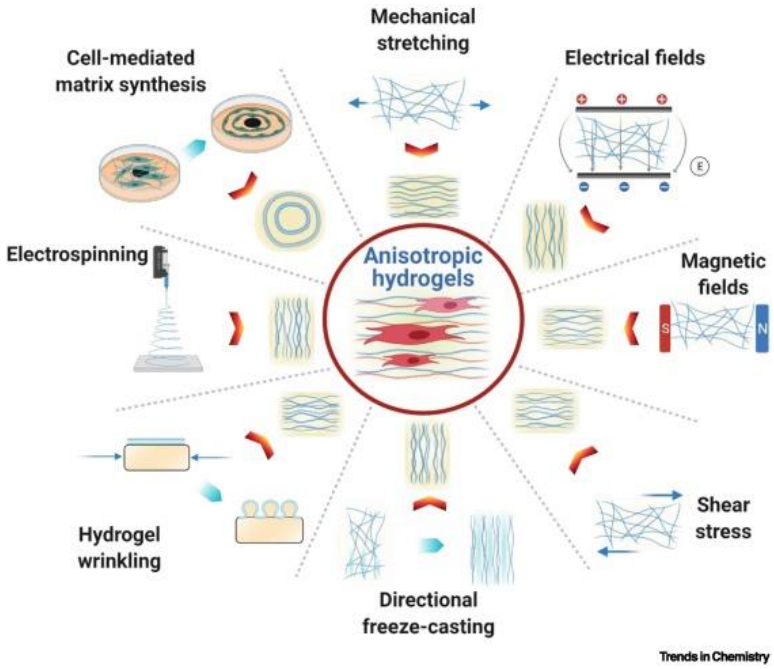

Figure 3.1 Structurally anisotropic hydrogels for tissue engineering (83).

Sacran, a megamolecular polysaccharide derived from the cyanobacterium Aphanothece sacrum, possesses unique anisotropic properties due to its highly organized molecular structure. This anisotropy allows for distinct and favorable material characteristics, particularly

in mechanical and biological applications. The anisotropic structure of sacran is a result of molecular alignment, which occurs in different orientations depending on the processing conditions. This alignment significantly affects its physical properties, such as viscosity, elasticity, and tensile strength, making it suitable for diverse applications requiring directional dependency. For instance, sacran can exhibit increased mechanical strength along one axis while maintaining flexibility or having varying properties along other axes. Moreover, the anisotropy of sacran contributes to its biological functions. In biomedical applications, the structure of sacran can be modified to mimic the natural extracellular matrix, thereby promoting cellular orientation and proliferation. This unique feature makes it an ideal material for scaffolding in tissue engineering, where guiding specific cell growth directions is crucial. Furthermore, the anisotropic nature of sacran allows it to respond to environmental stimuli like humidity and temperature, making it suitable for smart material applications. For example, it can be used in wound dressings that adjust their characteristics in response to changes in the wound environment. Additionally, it can be utilized in packaging materials that alter their permeability according to external conditions.

Recently, we modified sacran with quaternary ammonium (Q-188), the modified sacran become like an ampholytic polysaccharide containing both positive and negative charges. The increasing positive on the structure made the sacran have a low molecular weight and low viscosity. According to chapter 2, we were able to successfully prepare the ampholytic sacran.

3.2 Materials and Methods

3.2.1 Materials

Sacran, a polysaccharide was extracted from the frozen biomaterials of *Aphanothece sacrum*. Quat-188 (N-(3-chloro-2-hydroxypropyl)-trimethylammonium chloride) was purchased Tokyo Chemical Industry Co., Ltd. Sodium hydroxide (NaOH), hydrochloric acid (HCl), Sodium chloride (NaCl) and ethanol were purchased from Kanto Chemical, Japan. SnakeSkin ™ Dialysis Tubing, 10K MWCO, 35 mm dry I.D., 35 feet were purchased from thermos scientific, USA. 3-(4,5-dimethylthiazol-2-yl)-2,5-diphenyltetrazolium bromide (MTT) dye were obtained from Sigma-Aldrich, USA. DMEM; sigma-Aldrich, St. Louis, MO, USA containing 10% fetal bovine serum (FBS).

3.2.2 Hydrogel and Anisotropic Swelling

Sacran and modified sacran were fabricated using the solvent casting process. In brief, a 0.5 w/v% solution of sacran and Q-sacran was cast onto a polypropylene case (2 cm x 2 cm x 1.5 cm) and dried in an oven at 60 °C for 24 hours to form a dry film. The dried film has a thickness of around 0.02-0.04 mm, and the film was cut into 5 mm x 5 mm squares using a surgical knife. These square films were then thermally annealed at 140 °C for 4 hours to crosslink the sacran chains in the dry film. Subsequently, the square films were immersed in deionized (DI) water at room temperature and left for 24 hours, causing the dry film to transform into a hydrogel. Excess water on the hydrogel was removed by using tissue paper. Afterward, the swelling degree (q), defined as the weight ratio of the hydrogel to the dry film, was calculated using the following equation (1).

$$\text{Swelling degree (q)} = W_{gel} / W_{film} \qquad (1)$$

In the given expressions, where W_{gel} represents the weight of the hydrogel, and W_{film} denotes the weight of dry films, the degree of anisotropy in swelling was clarified. The

modified sacran exhibited anisotropic swelling in water, whereby the swelling degree along both the width (x-axis and y-axis) remained nearly constant, while the swelling along the thickness (z-axis) increased. The degree of anisotropy in swelling ratio was computed using the following equation. (2)

$$\text{The degree of anisotropy in swelling} = \alpha T/\alpha\omega \quad (2)$$

The linear swelling ratios, denoted as αT for the thickness along the z-axis and αw for the thickness along the x-axis or y-axis, were determined using the following equation (4)

$$\text{The linear swelling ration} = (l_1 - l_0)/\, l_0 \quad (3)$$

Here, where l_1 represents the thickness after swelling, and l_0 denotes the thickness before swelling.

3.2.3 Wettability and The Contact Angle (Θ)

The procedure involved the painstaking preparation of solutions containing sacran and its modified derivatives at a hydrogel film, The static contact angle of the samples was measured using a contact angle goniometer (Model DN-501 AC100-240V 50/60Hz, Kyowa Interface Science Co. Ltd.). During this process, the interval of time taken for the water droplets of 1.5 μL to spread on the hydrogel film was measure. The contact angle was determined using software based on the analysis of the droplet images. A series of five measurements were performed on a sample film, and the resulting contact angles were recorded and averaged (26).

3.2.4 Cytotoxicity

The cytotoxicity of different quantities of each Q-sacran has been evaluated using the 3-(4,5-dimethylthiazol-2-yl)-2,5-diphenyl tetrazolium bromide (MTT) method. Briefly, fibroblast cell lines (L-929) were introduced into a 96-well plate, with each well containing

0.1 mL of media and a cell concentration of 1.0 X 10^4 cells/mL. Following a 72-hour incubation period at 37 ˚C, the cells were subjected to the addition of 0.1 mL of medium containing varying concentrations of Q-sacran solution. Following that, the cells were incubated for a further 24 hours. Subsequently, the medium was put away, and the cells were subjected to three rinses using 0.2 mL of phosphate-buffered saline (PBS). Later, a volume of 0.1 mL of MTT solution with a concentration of 100 μg/mL was introduced. This MTT stock solution was made by dissolving 10 mg of MTT dye in DMEM, resulting in a final volume of 10 mL. Then, 2 mL of the stock MTT dye solution was mixed with 18 mL of DMEM without fetal bovine serum (FBS). The resulting mixture was added to the experimental, which was then subjected to incubation at a temperature of 37 ˚C for a duration of 4 hours. The insoluble formazan crystals generated by the reduction of MTT were dissolved in 0.1 mL of dimethyl sulfoxide (DMSO), and their absorbance at 540 nm was measured using a microplate reader (Versa Max, Molecular Device Japan K.K., Tokyo, Japan) (27).

3.2.5 Cell Culture

A mouse fibroblast-like cell line (L929) was chosen for all biological assays to assess the biocompatibility and cell adhesion properties of the ampholytic sacran hydrogel. L929 cells (American Type Culture Collection, Manassas, VA,USA) were cultured in DMEM (Sigma Aldrich) supplemented with 10% fetal bovine serum (FBS, Biochrom AG, Germany). incubated at 37 °C in a humidified atmosphere with 5% CO_2.

3.2.6 Cell Adhesion and Proliferation

The original sacran and modified sacran film hydrogels were shaped into circular forms to fit into a 24-well plate. Subsequently, the films underwent sterilization using a 70% ethanol solution and were allowed to air dry on a sterile 24-well plate within a biosafety cabinet.

Following this, the L929 fibroblast cell line was incubated in DMEM containing 10% FBS in a humidified atmosphere with 5% CO_2 at 37°C. After the designated incubation period, 1 mL of a 1.0 x 10^5 cells/mL suspension was seeded onto each hydrogel sample and cultured. After three days of culture, the samples were rinsed with sterile PBS buffer, and the number of adhered cells was subsequently counted. After being rinsed with PBS, each hydrogels sample was immersed in 0.1 mL of the growth medium supplemented with 10 µL of CCK-8 stock solution. The hydrogels sample were subsequently cultured for a duration of 3 hours at 37 °C in a humidified atmosphere consisting of 5% CO_2. An analysis was performed to measure the absorbance at a specific wavelength of 450 nm.

3.2.7 Cell Morphology

The morphology of adherent cells on both the original and modified sacran hydrogel was observed by SEM images. L-929 cells (1.0 x 10^5 cells /mL) were seeded onto the hydrogel and allowed to incubate for 72 hours. Following incubation, the cells were fixed using a 10% neutral buffered formalin solution (Wako, Japan) for 24 hours. Subsequently, the samples underwent a dehydration process by immersion in ethanol, transitioning from lower to higher concentrations (60% to 100% ethanol) to remove water from the samples. Following this, the samples were immersed in *t*-butanol twice for one hour each to further dehydrate them. The dehydrated samples were then air-dried at room temperature. Once dried, the hydrogel samples were sputter-coated with gold and subsequently examined using SEM to visualize the cellular morphology and interactions with the hydrogel substrate.

3.2.8 Live and Dead Cell Viability Assay

The viability of adherent cells on both the original and modified sacran hydrogel was evaluated through staining with calcein acetoxymethyl ester (Calcein AM) and ethidium homodimer-1 (EthD-1). To prepare the working solutions, a calcein AM 50 µM in DMSO

(Add 2 µL of calcein AM to 158 µL of DMSO) and make an EthD-1 2 mM in DMSO. L-929 cells (1.0 x 10^5 cells /mL) were seeded onto the hydrogel and incubated for 72 hours, followed by three rinses with PBS buffer. Subsequently, 2 µL of 50 µM calcein AM and 4 µL of 2 mM EthD-1 were added to each 1 mL of medium on the hydrogel, and the samples were thoroughly mixed. The cells were then incubated for 20 minutes in a humidified atmosphere with 5% CO_2 at 37 °C, protected from light. After the incubation period, the stained cells were examined using a fluorescence microscope (BZ-X810). The stained cells were categorized into two groups: live cells, which emit green fluorescence, and dead cells, which emit red fluorescence. The cell density was evaluated by using ImageJ software.

3.3 Results

3.3.1 Hydrogel Properties

Hydrogels represent intricate three-dimensional networks of hydrophilic polymers capable of absorbing and retaining water. A noteworthy bio-polysaccharide, sacran, exhibits distinctive hydrogel properties. The formation of sacran hydrogel can be achieved through either chemical means utilizing divinyl sulfone (DVS) or through physical crosslinking employing thermal crosslinking methods. In this work, original sacran and modified sacran with QACs were prepared into hydrogels via thermal crosslinking. For sacran, during the process of water evaporation heating, the sacran chains can create intermolecular interactions, including hydrogen bonding with other sacran chains, which leads to the formation of physical cross-links between the chains, as shown in Figure 3.2 Meanwhile, the modification of sacran also introduced hydrogen bonding to their structure, including

the electrostatic interaction between positive charges from quaternary amine and negative charges from carboxyl groups.

Figure 3.2 the intermolecular interaction with physical crosslinking between

During the swelling experiments, a dried film was immersed in a large quantity of deionized water for 24 h at room temperature. Subsequently, the hydrogel was carefully wiped and weighed in its swollen state, as determined by equation 2. The summarized results are

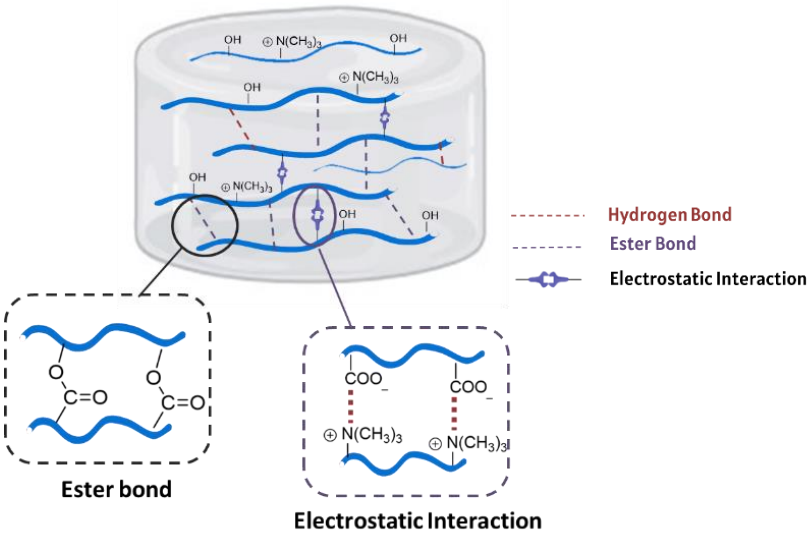

presented in Figure 3.3 Upon reaching equilibrium swelling, the hydrogel with a Q-composition of 87% exhibited a swelling ratio of 9.3. In contrast, the original sacran hydrogel displayed a swelling ratio of 7.1, while other hydrogels with Q-compositions ranging from 32% to 79% showcased varying swelling ratios of 5.9, 6.4, 7.3, and 8.0, respectively. The difference in hydrogel ratio can be ascribed to intermolecular interactions like double crosslinking facilitated by hydrogen bonding and ionic repulsion. Furthermore, it is noteworthy that the crosslinking density of hydrogels can impact their degree of swelling ratio.

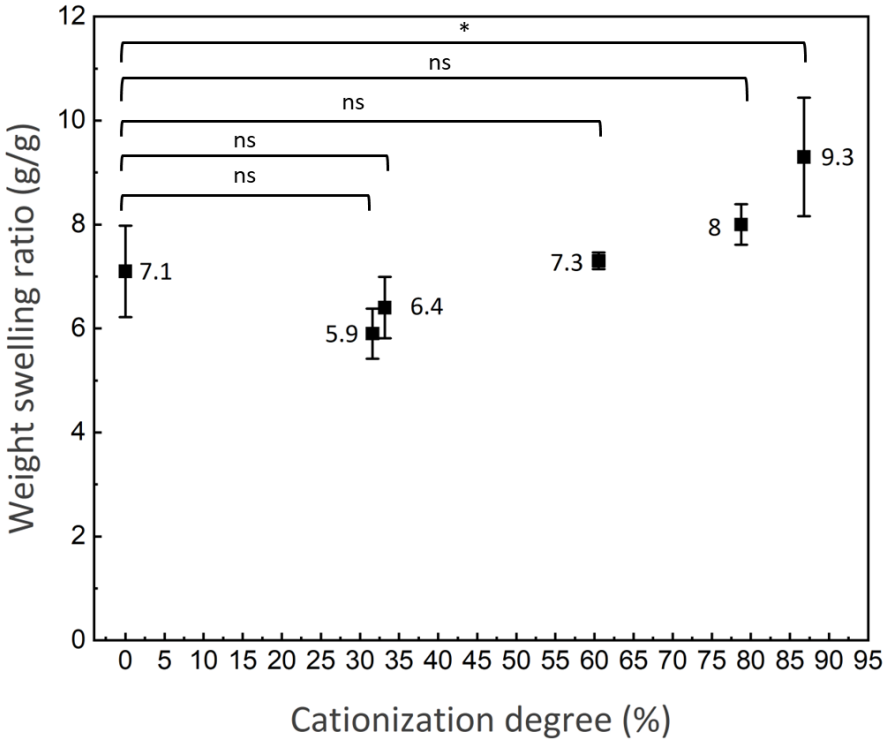

Figure 3.3 Swelling degrees of Q-sacran hydrogels with various cationization degrees. Data are shown as a mean ±s.d., (n=3), ****p<0.0001, ***p<0.001, and *p<0.05, determined by one-way ANOVA followed by Tukey's test.

3.3.2 Anisotropy Properties

The anisotropy in swelling, denoted by αT /αω, was determined by calculating αT for the thickness along the z-axis and αw for the thickness along the x-axis, as derived from equation 3. In Figure 3.4, the results depicted the variation in αT /αω values across physical crosslinked hydrogels produced through thermal crosslinking at 140 °C, ranging approximately from 62. the impact of physical crosslinking by modified sacran on αT as notable, particularly with the increase in Q-composition on sacran chains. As the Q-composition reached its highest,αT /αω exhibited a value range of 122. This value was approximately twice that of the original sacran. This phenomenon can be explained in terms of swelling behavior because of the modification sacran have a strong electrolyte function

group. Strong electrostatic interaction between the polymer sidechains of sacran hydrogel was observed.

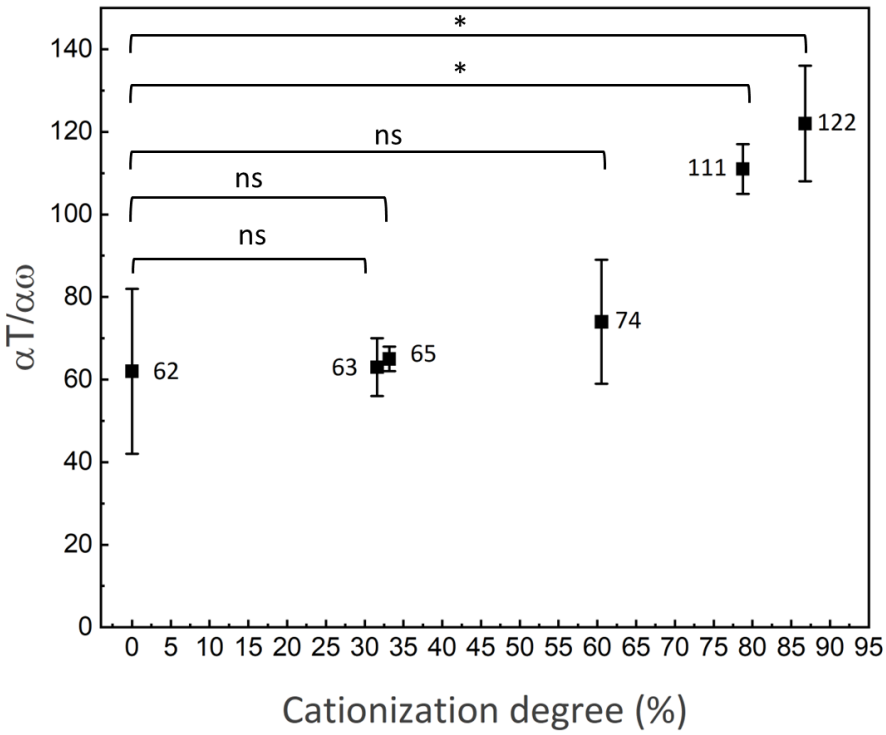

Figure 3.4 ratio of linear swelling degree of thickness to that of width. Data are shown as a mean ±s.d., (n=3), ****p<0.0001, ***p<0.001, and *p<0.05, determined by one-way ANOVA followed by Tukey's test.

As the swelling degree ratio increased, there was a corresponding spontaneous increase in anisotropy. The summarized results were shown in Figure 3.5. The anisotropy versus swelling degree of all hydrogels was increased from 4.9 to 8.6, respectively. These results can suggest that the diameter of the gel (thickness) rises but its length does not change as the gel expands (its volume increases).

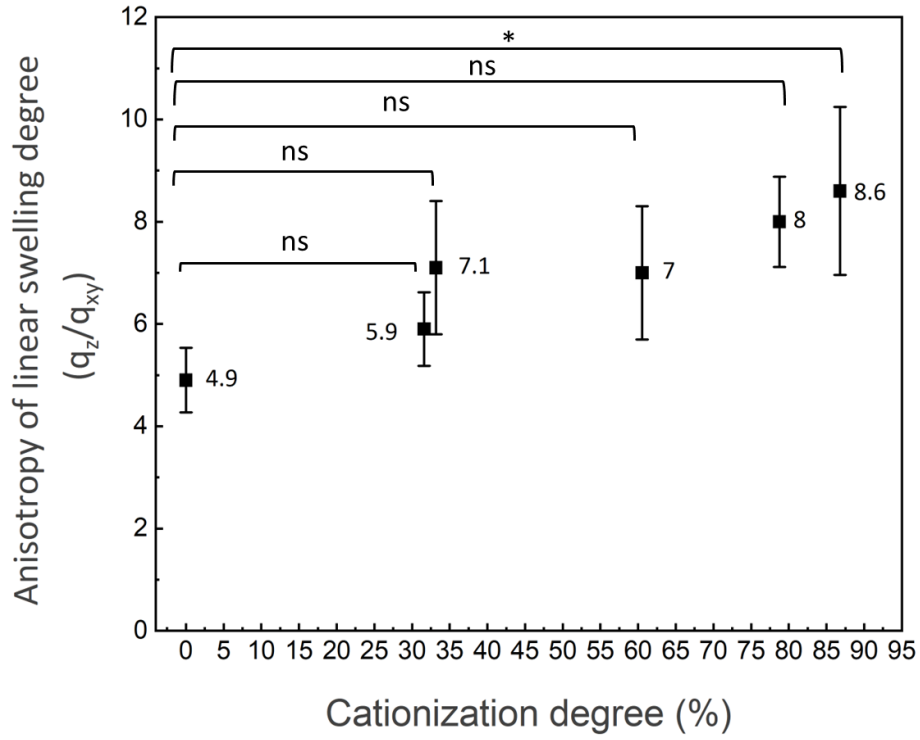

Figure 3.5 Normalized anisotropy by swelling degrees. Data are shown as a mean ±s.d., (n=3), ****p<0.0001, ***p<0.001, and *p<0.05, determined by one-way ANOVA followed by Tukey's test.

The water contact angle was a method utilized to quantify the extent of water droplet dispersion across a material surface. Fundamentally, the absorption characteristics of a surface can be classified as hydrophilic (10°<θ<90°), hydrophobic (90°<θ<150°), or superhydrophobic (150°<θ<180°) (84, 85). For the purpose of this study, is a measure of wettability and how water interacts with the surface of the materials. A total of six samples, including the origin sacran (0% Q-composition) and the quaternary ammonium modification of sacran as a various composition, were analyzed. The measurement of the sample angle was performed subsequent to the application of water onto the hydrogel polymer at an annealing temperature of 140 °C. Figure 3.6 The contact angle of sacran with water was observed to be approximately 26.5°. and gradually decreased down when the Q-composition increased, as the 87 % Q-composition the water contact angle was

approximately 15.3°. This phenomenon could be explained that a decrease in the water contact angle indicates an increase in hydrophilicity, the surface of the quaternary ammonium modification of sacran becomes more wettable and water-loving. The quaternary ammonium modification of sacran consist of both positive and negative charges within the same molecular structure this balanced charge distribution minimizes electrostatic repulsion between the hydrogel surface and water molecules, facilitating better wetting and a lower contact angle.

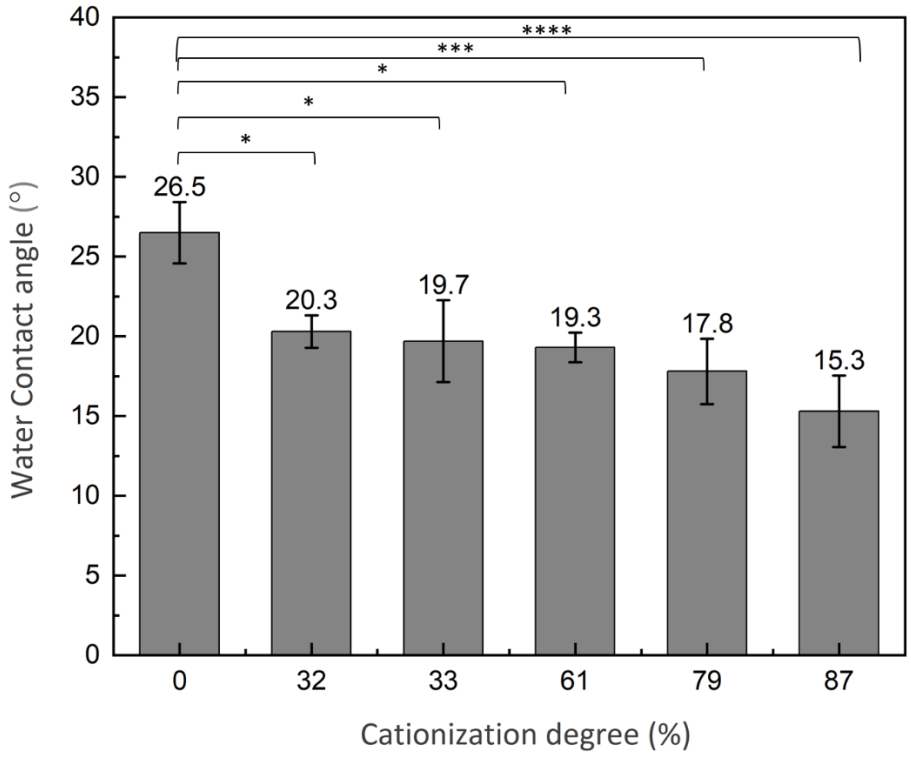

Figure 3.6 Water contact angle on Q-sacran with various cationization degree. Data are shown as a mean ±s.d., (n=3), ****p<0.0001, ***p<0.001, and *p<0.05, determined by one-way ANOVA followed by Tukey's test.

3.3.3 Cytotoxicity Evaluation of Fibroblast Cell Lines

To examine the safety of the quaternary ammonium modification sacran, the MTT assay was performed in fibroblast L-929 cell line. As seen in Figure 6. The cell viability of sacran

and Q-sacran was demonstrated. This MTT assay method should be noted that the cell viability was measured after incubated cell line for 24 h with sample at 37 °C. in addition the amount of sample was showed difference concentration, the highest concentration of sacran was found to be 0.5 wt.%, while the maximum concentration of Q-sacran was 5.0 wt.% In this experiment, the modified sacran with the highest concentration of quat was investigated. Figure 7A demonstrates that sacran exhibited the least cytotoxicity, with a viability of 55 % at a sacran dosage of 0.5%. In contrast, Figure 3.7 demonstrates that Q-sacran, at almost the same concentration of 0.625 wt.%, showed cytotoxicity with viability of 62% and 70 % for the quaternary ammonium modification sacran as 79 and 87 %, respectively. When the amount of all samples was increased to 5.0 wt.%, the cell viability suddenly decreased as the amount of sample increased, and the viscosity of the sample also increased, causing the cell to die. In summary, it could be concluded that sacran (86) and modified sacran did not show any cytotoxicity to fibroblast cell lines, suggesting that modified sacran can be applied in biological application.

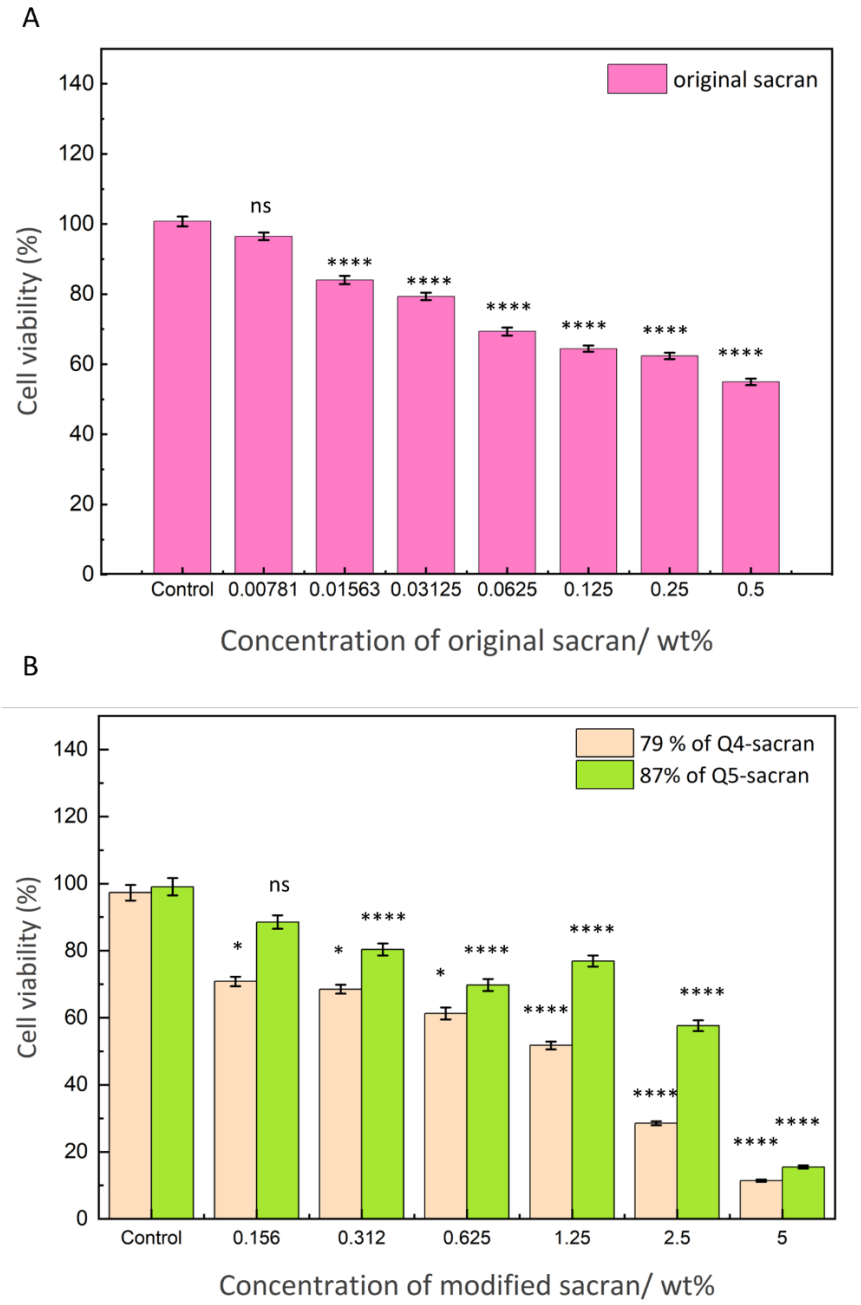

Figure 3.7 Cytotoxicity of various concentrations of A) sacran as highest concentration 0.5 wt.% and B) Q-sacran as a 79 and 87 % of cationization degree highest concentration 5.0 wt.% with fibroblast L-929 cells line. Data are shown as a mean ±s.d., (n=8), ****p<0.0001, ***p<0.001, *p<0.05 and ns = not significant compare with control of each sample, determined by one-way ANOVA followed by Tukey's test.

3.3.4 Cell Proliferation

We examined how varying the amount of quaternary ammonium added to sacran affected the properties of the resulting hydrogel and its impact on cell viability, as shown in **Figure 3.8.** It has been shown that significant differences in cell proliferation were observed between day 1 and day 3. According to the Q1-Q4 Sacran modifications, with cationization degrees ranging from 32% to 79%, do not show significant differences in cell proliferation compared to the original Sacran. This suggests that these levels of cationization do not sufficiently alter the molecular structure to significantly affect cellular interactions. The inherent biological properties of sacran might overshadow the effects of lower degrees of cationization. However, Cells exposed to Q5-sacran demonstrated the highest proliferation rate from day 1 through day 3, whereas cells exposed to original sacran exhibited the lowest proliferation rate during this period. This trend is likely attributed to the presence of trimethyl ammonium ($-N(CH_3)_3^+$) groups, which have been shown to enhance cell attachment and increase cell numbers on modified hydrogels promoting greater cell proliferation. Moreover, the hydrophilicity on surface the hydrogels, the wettability of cell adhesion surface can affect cell adhesion. cells are likely to adhere to hydrophilic surface. According to previous studies, the attachment of L929 cells largely depends on surface wettability-hydrophilic surfaces support better cell attachment (87). Cells often do not adhere well to hydrophobic surfaces and are relatively unchanged and remain round and non-spread. On the other hand, cells attach in significantly higher numbers and begin to spread on hydrophilic surfaces **(Figure 3.6**) suggesting a direct relationship between surface wettability and the extent of cell attachment.

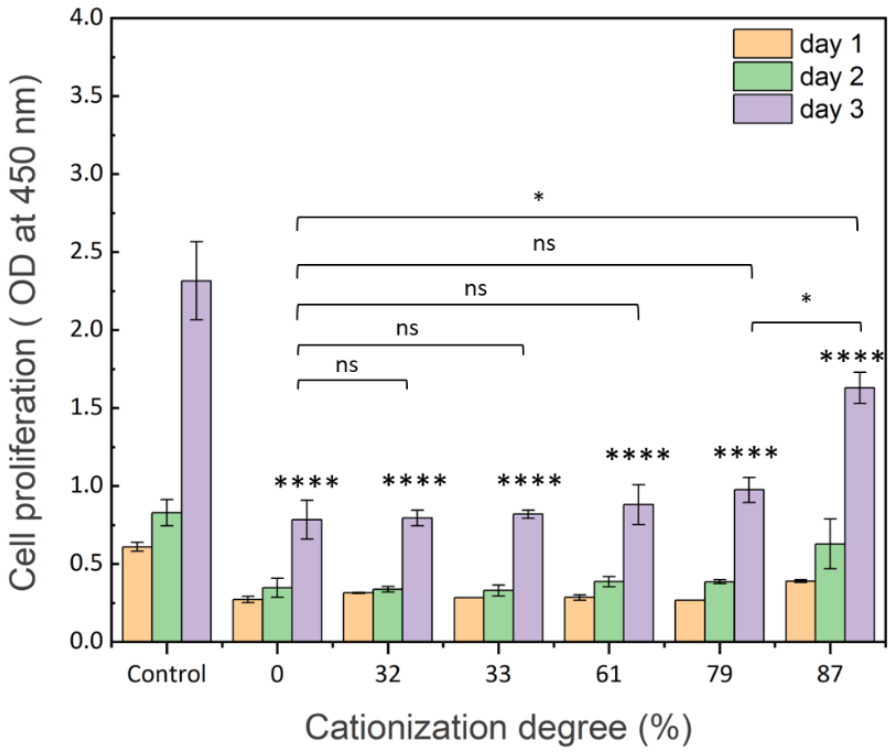

Figure 3.8 The viability of L929 cells cultured on Q-sacran at different concentrations of quaternary ammonium for 3 days was measured via CCK-8 assay. Data are shown as a mean ±s.d., (n=3), ****p<0.0001, ***p<0.001, *p<0.05 and ns = not significant compare with control and original sacran, determined by one-way ANOVA followed by Tukey's test.

3.3.5 Modification Sacran Increased Adhesion Of L-929 Cells Line.

SEM images were utilized to examine the surface structure and compare the adhesion of L-929 cell lines to hydrogels created from original sacran and Q-sacran after 3 days incubation period, as shown in **Figure 3.9**. The cells extruded on all hydrogel materials. The SEM images confirm the presence of intercellular connections on all six material compositions, but the number of cells adhered to the surface varies. The images showed an increased number of cells adhered to the surface of Q-sacran, indicating cell proliferation. SEM being qualitative, portrays the information about cell morphology as well as adhesion behavior (88). The original sacran surface is negatively charged, which matches the negative charge of the cell lines.

Despite this, certain cells can adhere to the sacran surface. On the other hand, Q-sacran develops a positive charge due to its potent hydrophilic characteristics and the presence of quaternary ammonium. Q-sacran appears to improve the adhesion of cell lines to the material surface.

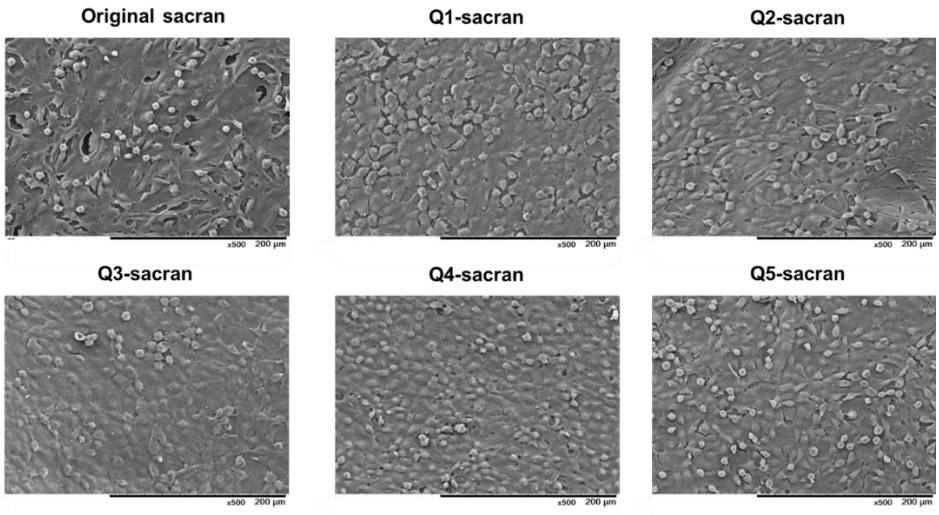

Figure 3.9 SEM images of L-929 cells line adhered to sacran and modified sacran after incubated 3 days.

3.3.6 Cells Live and Dead.

L-929 cells were cultured in Q-sacran hydrogels at a concentration of 1.0 x 10^5 cells/mL for 3 days. Fluorescence assays, which are quantitative, can reveal information related to cell viability and density. This was assessed within the hydrogels using Calcein AM and EthD-1 staining to distinguish between live and dead cells. The findings indicated a high level of cell viability in both types of hydrogels, with the majority of cells remaining viable (green) throughout the culture period, and only a minimal occurrence of dead cells (red) as shown in Figure 3.10A. The live cell count was reported in units of mm^2, with values of 210±20 for the original sacran. As the cationization degree in the sacran hydrogel increased, the number of cells increased to 420±30, 1000±20, 1040±300, 1060±100, and 1950±50, respectively. Consequently, the number of dead cells was 250±140, 50±10,

30±10, 50±30, 90±10, and 180±50, respectively, after 3 days of culture. These results suggest that increasing the amount of cation composition may be an effective strategy for promoting cell survival, as shown in Figure 3.10B.

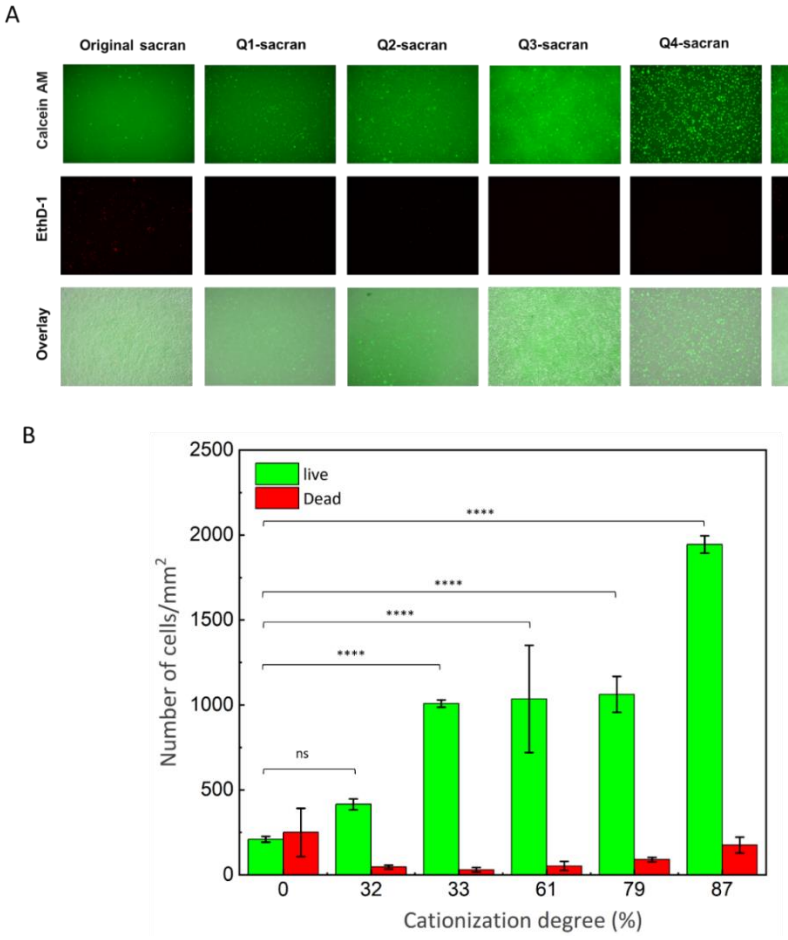

Figure 3.10 A) Image of live and dead staining after 3 days. Live cells green (calcein AM) while dead cells are red (EthD-1), and B) Quantification of cell live and dead/mm^2 from fluorescence microscopy images. Data are shown as a mean ±s.d., (n=3), ****p<0.0001, ***p<0.001, *p<0.05 and ns = not significant compare with original sacran, determined by one-way ANOVA followed by Tukey's test.

3.4 Conclusion

In conclusion, the sacran ampholyte hydrogels were fabricated using the solvent casting technique. The sacran ampholyte films underwent annealing at 140 °C for 4 hours before being

soaked in DI water for 24 hours at ambient temperature, after which the swelling characteristics of the sacran ampholyte hydrogels were analyzed. The swelling weight ratios, or q values, of the altered sacran labeled as Q1 and Q2 were lower compared to unmodified sacran, whereas Q3, Q4, and Q5-sacran exhibited higher values, though these differences were not statistically significant, with averages ranging from 5.9 to 9.3, escalating with an increased degree of cationization. To assess the anisotropic behavior of the Q-sacran hydrogels, the original sacran displayed an anisotropy of 62, whereas Q4 and Q5-sacran showed significantly elevated anisotropies exceeding 110, indicating that cationization enhances anisotropy. The cationized versions of sacran showed superior enhancement of hydrogel swelling anisotropy compared to the original sacran, suggesting that the carboxylic acids align perpendicularly to the thickness when cations are able to interact with anions. Consequently, ester linkages predominantly occurred along the plane. The water contact angle on the Q-sacran hydrogel films was recorded, with the angle measurement taken following water application at an annealing temperature of 140 °C. The initial contact angle for sacran was around 26.5°, which decreased progressively with increasing Q-sacran content, likely due to the presence of both positive and negative charges on the hydrogel surface, enhancing wetting and reducing the contact angle. MTT assay conducted on the fibroblast L-929 cell line showed that sacran had the lowest cytotoxicity, with a cell viability of 55% at a 0.5% sacran concentration. In comparison, Q-sacran, at a similar concentration of 0.625 wt.%, showed higher cytotoxicity with viability of 61 and 70% for Q4 and Q5-sacran, respectively. The study also explored how various levels of quaternary ammonium incorporation affected the properties of the hydrogel and their impact on cell viability, revealing significant differences in cell proliferation from day 1 to day 3. Cells exposed to Q5-sacran exhibited the highest proliferation rates over this period, while those exposed to the original sacran showed the lowest. This pattern is likely due to the presence of trimethyl ammonium ($+N(CH_3)_3$) groups, which enhance cell attachment and proliferation on

the modified hydrogels. SEM imaging was used to see the surface morphology, comparing cell adhesion on hydrogels made from original sacran and Q-sacran after a 3-day incubation. The cells kept their elongated fibroblast characteristics on all materials. The SEM images verified intercellular connections across all six compositions, although the number of cells adhering varied. More cells adhered to the Q-sacran surfaces, showing enhanced cell proliferation. Live and dead cells were quantified per square millimeter, with figures of 210±20 for the original sacran. As the degree of cationization in the sacran hydrogel increased, the number of living cells rose to 420±30, 1000±20, 1040±300, 1060±100, and 1950±50, respectively. So, the count of dead cells after 3 days of culture stood at 250±140, 50±10, 30±10, 50±30, 90±10, and 180±50, respectively.

3.5 Reference

71. Mahmood A, Patel D, Hickson B, DesRochers J, Hu X. Recent progress in biopolymer-based hydrogel materials for biomedical applications. International Journal of Molecular Sciences. 2022;23(3):1415.

72. Karoyo AH, Wilson LD. A review on the design and hydration properties of natural polymer-based hydrogels. Materials. 2021;14(5):1095.

73. Kesharwani P, Bisht A, Alexander A, Dave V, Sharma S. Biomedical applications of hydrogels in drug delivery system: An update. Journal of Drug Delivery Science and Technology. 2021;66:102914.

74. Bustamante-Torres M, Romero-Fierro D, Arcentales-Vera B, Palomino K, Magaña H, Bucio E. Hydrogels classification according to the physical or chemical interactions and as stimuli-sensitive materials. Gels. 2021;7(4):182.

75. Pita-López ML, Fletes-Vargas G, Espinosa-Andrews H, Rodríguez-Rodríguez R. Physically cross-linked chitosan-based hydrogels for tissue engineering applications: A state-of-the-art review. European Polymer Journal. 2021;145:110176.

76. Nahm D, Weigl F, Schaefer N, Sancho A, Frank A, Groll J, et al. A versatile biomaterial ink platform for the melt electrowriting of chemically-crosslinked hydrogels. Materials Horizons. 2020;7(3):928-33.

77. Dreiss CA. Hydrogel design strategies for drug delivery. Current opinion in colloid & interface science. 2020;48:1-17.

78. Liang Y, He J, Guo B. Functional hydrogels as wound dressing to enhance wound healing. ACS nano. 2021;15(8):12687-722.

79. Radulescu D-M, Neacsu IA, Grumezescu A-M, Andronescu E. New insights of scaffolds based on hydrogels in tissue engineering. Polymers. 2022;14(4):799.

80. Li Z, Cheng H, Ke L, Liu M, Wang CG, Jun Loh X, et al. Recent advances in new copolymer hydrogel-formed contact lenses for ophthalmic drug delivery. ChemNanoMat. 2021;7(6):564-79.

81. Watanabe T, Nishizawa Y, Minato H, Song C, Murata K, Suzuki D. Hydrophobic monomers recognize microenvironments in hydrogel microspheres during free-radical-seeded emulsion polymerization. Angewandte Chemie International Edition. 2020;59(23):8849-53.

82. Holz E, Rajagopal K. In situ-forming glucose-responsive hydrogel from hyaluronic acid modified with a boronic acid derivative. Macromolecular Chemistry and Physics. 2020;221(15):2000055.

83. Khuu N, Kheiri S, Kumacheva E. Structurally anisotropic hydrogels for tissue engineering. Trends in Chemistry. 2021;3(12):1002-26.

84. Kaushal N, Singh AK. Advancement in utilization of bio-based materials including cellulose, lignin, chitosan for bio-inspired surface coatings with special wetting behavior: A review on fabrication and applications. International Journal of Biological Macromolecules. 2023:125709.

85. Mayrhofer A, Kopacic S, Bauer W. Extensive Characterization of Alginate, Chitosan and Microfibrillated Cellulose Cast Films to Assess their Suitability as Barrier Coating for Paper and Board. Polymers. 2023;15(16):3336.

86. Wathoni N, Motoyama K, Higashi T, Okajima M, Kaneko T, Arima H. Physically crosslinked-sacran hydrogel films for wound dressing application. International Journal of Biological Macromolecules. 2016;89:465-70.

87. Sornkamnerd S, Okajima MK, Matsumura K, Kaneko T. Surface-Selective Control of Cell Orientation on Cyanobacterial Liquid Crystalline Gels. ACS Omega. 2018;3(6):6554.

88. Wei J, Yoshinari M, Takemoto S, Hattori M, Kawada E, Liu B, et al. Adhesion of mouse fibroblasts on hexamethyldisiloxane surfaces with wide range of wettability. Journal of Biomedical Materials Research Part B: Applied Biomaterials. 2007;81B(1):66-75.

CHAPTER IV

FRABICATION HYDROGEL OF SACRAN/POLY VINYL ALCOHOL MICRONEEDLE

4.1 Introduction

Microneedles are an innovative and emerging technology in the field of transdermal drug delivery systems. These tiny, needle-like structures, typically ranging from 50 to 900 micrometers in length (89, 90) , are designed to penetrate the stratum corneum, the outermost layer of the skin, to deliver therapeutic agents directly into the dermis. Unlike traditional hypodermic needles, microneedles offer a minimally invasive, pain-free alternative for drug administration (91), which can significantly improve patient compliance and comfort (92). There are various types of microneedles, each tailored for specific applications and drug delivery mechanisms (93). These include solid microneedles, which are used to create microchannels in the skin through which drugs can diffuse (94); hollow microneedles, designed to inject liquid formulations directly into the skin (95); coated microneedles, which are coated with drugs that dissolve upon skin insertion (96); and dissolving microneedles, made from biodegradable polymers that encapsulate drugs, releasing them as the microneedles dissolve in the skin (97). Additionally, hydrogel-forming microneedles can absorb interstitial fluid and swell, creating channels for sustained drug release (98). The versatility of microneedle technology extends beyond drug delivery to include applications in vaccine administration, cosmetic treatments, and diagnostics. Their small size and ease of use make them particularly suitable for mass vaccination programs, especially in resource-limited settings. Furthermore, advancements in materials science and fabrication techniques continue to enhance the efficacy, safety, and application range of microneedles, positioning them as a transformative tool in modern medicine. Microneedles represent a significant leap forward in the quest for efficient, patient-friendly drug delivery methods (99). By overcoming the limitations of traditional

needles and transdermal patches, they offer a promising solution for the controlled and targeted delivery of a wide variety of therapeutic agents.

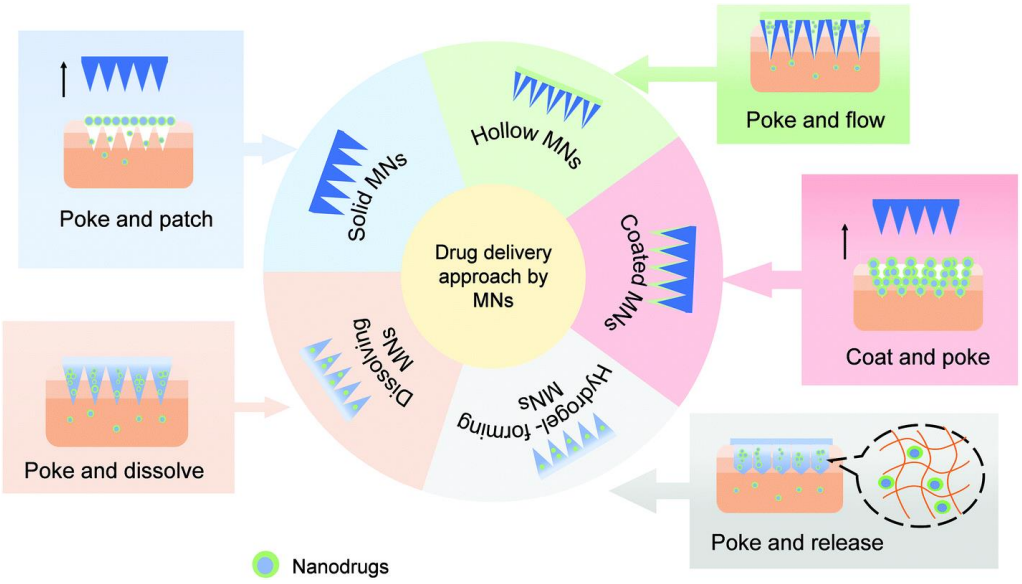

Figure 4.1 Type of microneedles patch (100)

The field of transdermal drug delivery has witnessed remarkable advancements with the advent of microneedle technology. Among the various types of microneedles, hydrogel microneedles have gained significant attention due to their biocompatibility, biodegradability, and ability to encapsulate and release therapeutic agents in a controlled manner (101). This study focuses on the fabrication of hydrogel microneedles composed of sacran and polyvinyl alcohol (PVA), aiming to leverage their unique properties for enhanced drug delivery applications.

Sacran, a high-molecular-weight polysaccharide derived from cyanobacteria, exhibits excellent water retention and gel-forming capabilities (27). These characteristics make it an ideal candidate for developing hydrogel microneedles that can effectively deliver drugs through the skin. Polyvinyl alcohol, a synthetic polymer known for its mechanical strength and flexibility, complements sacran by providing structural integrity to the hydrogel microneedles. The combination of sacran and PVA aims to create a robust yet flexible microneedle system capable of maintaining its form during insertion into the skin while ensuring a sustained release of

encapsulated drugs. The fabrication process involves the precise blending of sacran and PVA in optimal ratios to achieve the desired mechanical and drug delivery properties. This mixture is then subjected to micro molding techniques to form microneedles with uniform size and shape. Subsequent cross-linking and drying processes solidify the hydrogel structure, rendering the microneedles ready for use. The resulting sacran/PVA hydrogel microneedles are expected to exhibit superior performance in terms of drug encapsulation efficiency, insertion reliability, and sustained drug release profiles.

This innovative approach to microneedle fabrication not only enhances the potential of transdermal drug delivery systems but also opens new avenues for the application of natural polymers like sacran in biomedical engineering. The development of sacran/PVA hydrogel microneedles represents a significant step forward in creating more effective, patient-friendly, and versatile drug delivery platforms.

4.2 Materials and Methods

4.2.1 Materials

Sacran, a polysaccharide was extracted from the frozen biomaterials of *Aphanothece sacrum*. Quat-188 (N-(3-chloro-2-hydroxypropyl)-trimethylammonium chloride) was purchased Tokyo Chemical Industry Co., Ltd. Polyvinyl alcohol (PVA) was purchased from Japan VAM & POVAL Co., LTD. Sodium hydroxide (NaOH), Hydrochloric acid (HCl), Sodium chloride (NaCl), Citric acid and ethanol were purchased from Kanto Chemical, Japan. SnakeSkin ^{TM} Dialysis Tubing, 10K MWCO, 35 mm dry I.D., 35 feet were purchased from thermos scientific, USA. 3-(4,5-dimethylthiazol-2-yl)-2,5-diphenyltetrazolium bromide (MTT) dye were obtained from Sigma-Aldrich, USA. DMEM; sigma-Aldrich, St. Louis, MO, USA containing 10% fetal bovine serum (FBS).

4.2.2 Preparation of Hydrogel-Forming Films

Hydrogel films were fabricated from the aqueous polymer blend containing mainly a biocompatible polymer, PVA, Sacran and citric acid (as a crosslinking agent), dried at room temperature and heated at 130 °C. The blend compositions were achieved by investigating the effect of PVA concentration and adding other materials such as sacran and varying concentrations of Q-sacran on the swelling degree. The polymer blend was dried for 48 h at room temperature to form films. After drying, the films were cured at 130 °C for 60, 120 and 180 minutes to induce ester bonding crosslinking between PVA, sacran and citric acid. The crosslinking films were slowly cooled down at room temperature.

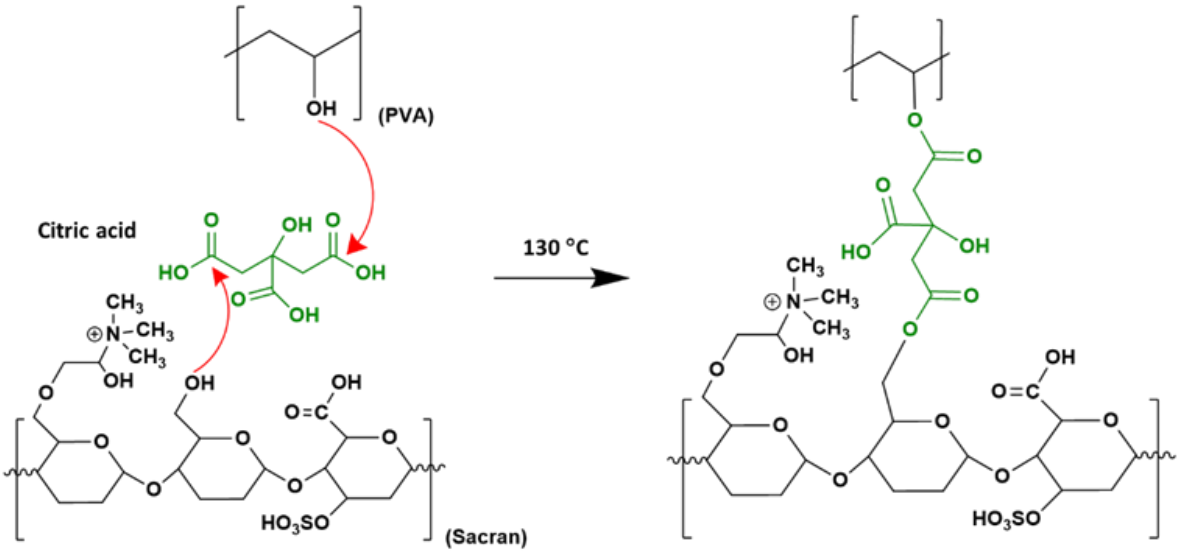

Figure 4.2. the esterification reaction between PVA, Q-scran and Citric acid.

4.2.3 Swelling Kinetic of The Hydrogel Films

The swelling properties of the hydrogels were investigated by directly immersing the hydrogel films sample in phosphate Buffer (PBS) 7.4 at room temperature. 10x10 mm^2 of the hydrogels were first weighted in the dry state and then placed into the PBS 7.4 at pre-determined time intervals, after finishing each time the hydrogel was wiped with paper to remove excess water and then weight again at each time point. To calculate the percentage of swelling degree at equilibrium (eq. 1)

$$\% \text{ swelling} = \frac{W\ gel - W\ film}{W\ film} \text{ x } 100 \qquad (1)$$

4.2.4 Attenuated Total Reflectance Fourier Transform Infrared Spectroscopy (ATR-FTIR).

Attenuated total reflectance (ATR) Fourier transform infrared (FTIR) spectroscopy was used to investigate the esterification crosslinking between PVA, sacran, Q-sacran and intermolecular interaction among the hydrogels film. The IR spectra of the original materials and hydrogels were performed using a Spectrum 100 FT-IR Spectrometer (Perkin Elmer). Spectra were recorded in transmittance mode across a range of 4000 to 400 cm^{-1}.

4.2.5 Thermogravimetric Analysis (TGA)

Thermogravimetric Analyses (TGA) of both Sacran and Q-sacran were conducted with a Rigaku TG 8121 instrument under a controlled nitrogen flow at a rate of 20 ml/min. Approximately 7 mg of the sample was placed in the platinum pan for analysis. Subsequently, the temperature parameters were programmed to increase at a rate of 20°C/min, ranging from an initial temperature of 50 °C to a final temperature of 850 °C.

4.2.6 Preparation of The Hydrogel-Forming Microneedles Arrays (HFM)

The sacran hydrogel formulation combined a 0.5% w/w of sacran, 0.5% and 1.0 % w/w of modified sacran in a 13% w/w of PVA solution. PVA stock solution was mixed for 3 hours with MilliQ-water at 90 ˚C to create solution then the sacran and modified sacran was mixed with PVA solution continuously for 6 hours at 90 ℃ to create the mixture of PVA and Sacran. Briefly, a 100 µL of mixture solution was poured into the microneedles silicon molds, needle density 6 x 6, 1000 µm height. Then use a high vacuum to crease the solution put into the needles shape until the bubbles disappear then dried at room temperature 48 hours. After drying, the hydrogel microneedles were cured in an oven 130 ˚C for 60, 120 and 180 minutes to induce the ester boned crosslinking between PVA and sacran. (Figure 4.2). After cooling, the hydrogel

microneedles were removed from the PDMS needle molds then stored in the silica gels until use.

4.2.7 Assessment of The Mechanical Properties of The Hydrogel-Forming Microneedles (HFM)

The mechanical integrity of microneedle patches is important for their effective application in transdermal drug delivery systems. To evaluate this, the maximum compressive mechanical load of PVA/Sacran, PVA/MSacran1, and PVA/MSacran2 microneedle patches was tested using a ZTA-1 Digital Force Gauge (IMADA, Inc., USA). The procedure involved sealing each microneedle patch to a lower substrate, with an array of 36 microneedles within a 1 cm x 1 cm area. The testing apparatus was configured to bring a force linker into contact with the microneedle array via a stepping motor, moving at a constant velocity of 20 μm/s. The compression test was designed to continue until the initial failure of a single microneedle was detected. The uniaxial facture force per one needle was follow from equation 2.

$$\text{Uniaxial Facture Force per one needle} = \frac{F_D}{36} \qquad (2)$$

4.2.8 Parafilm Insertion Study

Mechanical strength and penetration ability tests were conducted to detect the strength of the microneedles against the applied force. This evaluation involved measuring the microneedles ability to penetrate 8 layers of parafilm, which approximates the thickness of human skin. After penetration, the percentage of microneedle penetration ability was calculated using the following equation 3.

$$\%\ penetration\ of\ n\ layer = \frac{number\ of\ holes\ in\ n\ layer}{\text{total number of holes}}\ x\ 100\% \qquad (3)$$

4.2.9 Scanning Electron Microscope (SEM)

The morphology of the hydrogel microneedles was evaluated by using scanning electron microscopy (SEM). The microneedles shape was studied using scanning electron microscopy with energy dispersive spectroscopy (SEMEDS, Miniscope TM3030Plus) at an acceleration voltage of 15 kV under high chamber pressure with standard SEM carbon tape as background.

4.2.10 Cytotoxicity Test

The cytotoxicity of all samples has been evaluated using the 3-(4,5-dimethylthiazol-2-yl)-2,5-diphenyl tetrazolium bromide (MTT) method. Briefly, fibroblast cell lines (L-929) were introduced into a 96-well plate, with each well containing 0.1 mL of media and a cell concentration of 1.0 X 10^4 cells/mL. Following a 72-hour incubation period at 37 ˚C, the cells were subjected to the addition of 0.1 mL of medium containing all samples. Following that, the cells were incubated for a further 24 hours. Subsequently, the medium was put away, and the cells were subjected to three rinses using 0.2 mL of phosphate-buffered saline (PBS). Later, a volume of 0.1 mL of MTT solution with a concentration of 100 µg/mL was introduced. This MTT stock solution was made by dissolving 10 mg of MTT dye in DMEM, resulting in a final volume of 10 mL. Then, 2 mL of the stock MTT dye solution was mixed with 18 mL of DMEM without fetal bovine serum (FBS). The resulting mixture was added to the experimental, which was then subjected to incubation at a temperature of 37 ˚C for a duration of 4 hours. The insoluble formazan crystals generated by the reduction of MTT were dissolved in 0.1 mL of dimethyl sulfoxide (DMSO), and their absorbance at 540 nm was measured using a microplate reader (Versa Max, Molecular Device Japan K.K., Tokyo, Japan)

4.3 Results and Discussion

4.3.1 Swelling Kinetic of The Hydrogel Films

The swelling properties and the crosslinking density of hydrogel materials are important factors that influence their performance. The crosslinking materials should exhibit a high

swelling degree. When it comes to hydrogel microneedles, the ability to absorb skin interstitial fluid after insertion is of particular importance. This absorption facilitates the effective delivery of therapeutic agents encapsulated within the hydrogel matrix. The swelling behavior of the hydrogel can be affected by various factors, including the type, time to crosslinking, and concentration of the crosslinking agent. In this research, we studied the concentration of the crosslinking agent (citric acid) and the time to crosslinking. From these results (**Figures 4.3 – 4.6**), all materials without a crosslinking agent could not form hydrogels at optimization times of 60, 120, and 180 minutes. In **Figure 4.3**, the swelling degree at a curing time of 60 minutes, even with the addition of the crosslinking agent from 0.5 to 1.5%, did not result in hydrogel formation due to insufficient crosslinking time to create ester bonds between PVA. In contrast, under condition A5 (PVA with 0.5% w/w citric acid and a 120-minute crosslinking time), the swelling degree was higher than in other conditions as shown in Table 4.1.

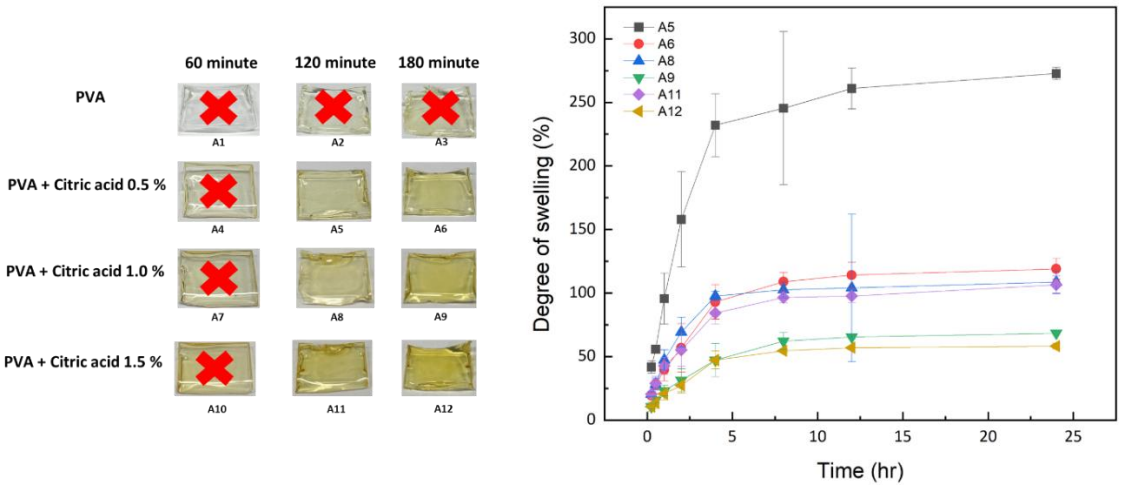

Figure 4.3 Swelling degree of PVA and varying concentration of citric acid.

In **Figures 4.4 - 4.6**, the condition involving PVA and sacran or Q-sacran with 1.0% w/w citric acid and a 60-minute crosslinking time showed hydrogel formation and a higher swelling degree compared to longer crosslinking times of 120 and 180 minutes. This phenomenon is due to sacran ability to form ester bonds with citric acid, similar to PVA with citric acid. Moreover, it also demonstrated the hydrogen bonding between PVA and sacran. In contrast, at

higher crosslinking times of 120 and 180 minutes, all conditions showed a higher crosslinking density than at 60 minutes. This effect resulted in a lower swelling degree with increasing crosslinking time.

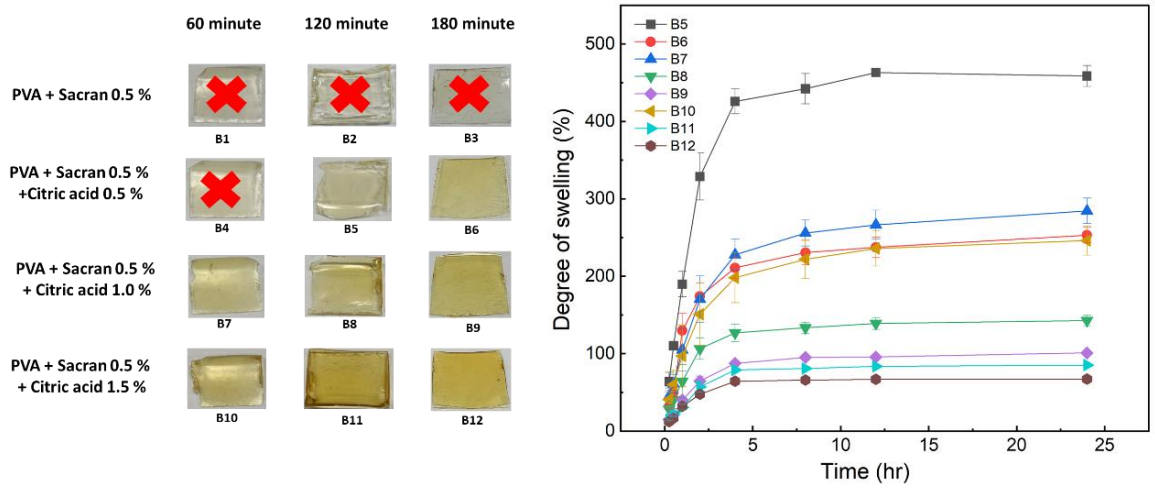

Figure 4.4 Swelling degree of PVA, sacran 0.5 % w/v and citric acid.

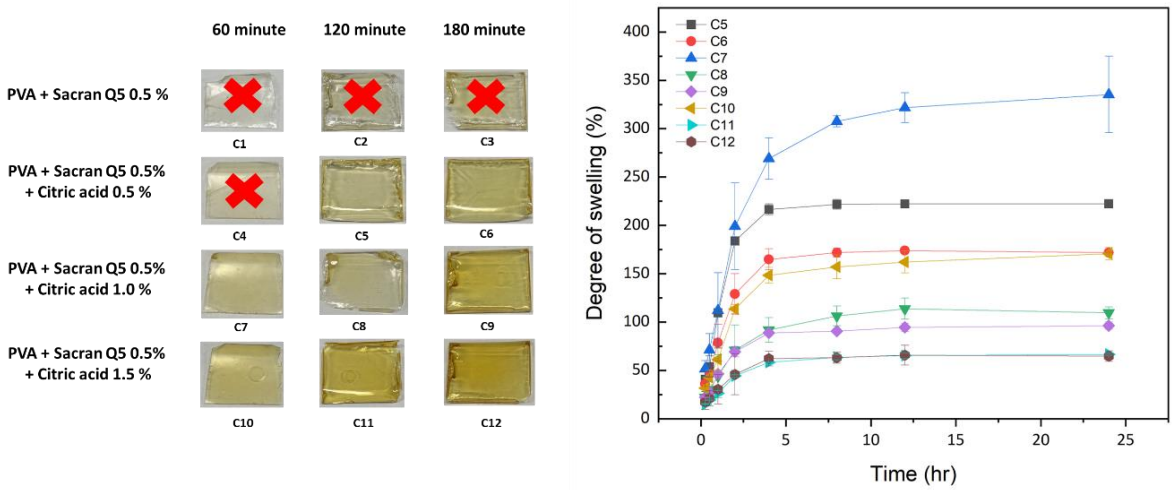

Figure 4.5 Swelling degree of PVA, Q-sacran 0.5 % w/v and citric acid.

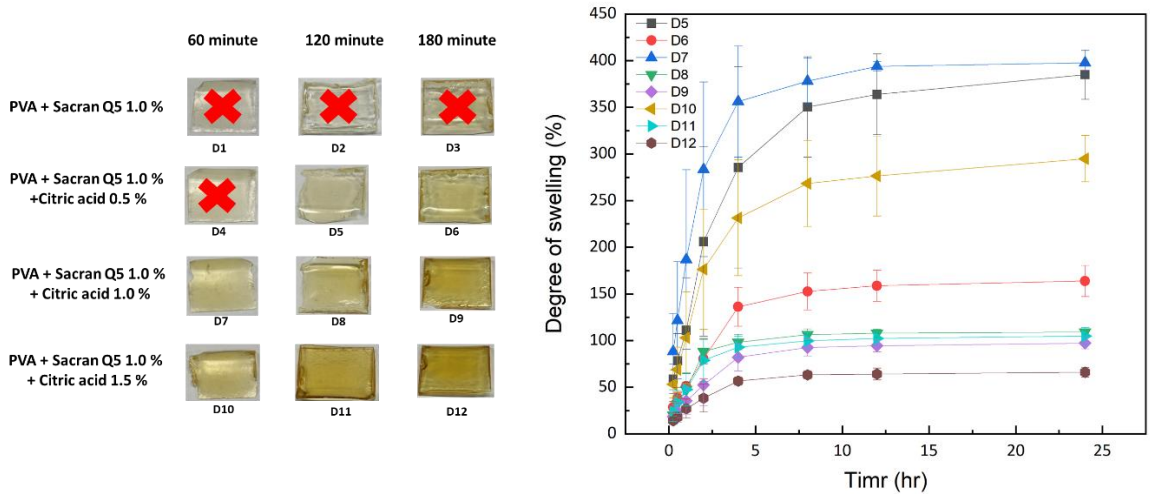

Figure 4.6 Swelling degree of PVA, Q-sacran 1.0 % w/v and citric acid.

The hydrogel formation with 1.0% w/w citric acid and a 60-minute crosslinking time generally results in a higher swelling degree compared to longer crosslinking times. This is attributed to the lower crosslinking density, which allows for more water uptake. Sacran has the ability to form ester bonds with citric acid and hydrogen bonds with PVA enhances the swelling capacity. To consider specific formulations, we want to select B7 which exhibits the highest swelling degree in the B-series, C7 which shows the highest swelling degree in the C-series and D7 which demonstrates a high swelling degree in the D-series.

Table 4.1 Present the formation which showed the highest swelling degree at the same concentration of citric acid 1% w/w at annelling time 60 minutes.

Formula	Conditions	Name
B7	PVA with Sacran at 0.5 %w/v	PVA/Sacran
C7	PVA with Modified sacran at 0.5 %w/v	PVA/M1-Sacran
D7	PVA with Modified sacran at 1.0 %w/v	PVA/M2-Sacran

4.3.2 Attenuated Total Reflectance Fourier Transform Infrared Spectroscopy (ATR-FTIR).

FTIR spectroscopy was used to investigate the chemical structures of various individual materials and their composites in hydrogel films. The materials analyzed included polyvinyl alcohol (PVA), PVA crosslinked with citric acid (CA), sacran, quaternized sacran (Q-sacran),

and the resultant hydrogel films. The FTIR spectrum of PVA displayed a broad band at 3200-3400 cm^{-1}, which is indicative of the presence of hydroxyl (OH) groups. This broad absorption band confirms the extensive hydrogen bonding typically associated with the hydroxyl groups in PVA. When PVA was crosslinked with CA, the FTIR spectrum showed a broad absorption band in the region between 3000-3500 cm^{-1}. This band is attributed to the stretching vibrations of the hydroxyl groups from the carboxylic acids in CA. Additionally, a band observed between 1600-1700 cm^{-1} corresponds to the carbonyl (C=O) stretching vibrations, a characteristic absorption band of the carboxylic group. The sacran spectrum presented characteristic peaks, notably the C-O ester linkage observed around 1200-1300 cm^{-1}, and the C-O-C linkage of polysaccharides at approximately 1000 cm^{-1}. These bands are typical of sacran complex polysaccharide structure. The Q-sacran spectrum shows the characteristic spectrum new peak at 1466 cm-1, which was attributed to C-H asymmetric stretching of methyl group ($+N(CH_3)_3$) of Quat188. The hydrogel films, which incorporate PVA, Q-sacran and citric acid, exhibited all the characteristic peaks of their individual components. The presence of the broad hydroxyl band at 3200-3400 cm^{-1}, the carbonyl absorption at 1600-1700 cm^{-1}, the ester linkage at 1200-1300 cm^{-1}, and the C-H asymmetric stretching peak 1466 cm^{-1} confirm the successful integration of these materials into the hydrogel matrix.

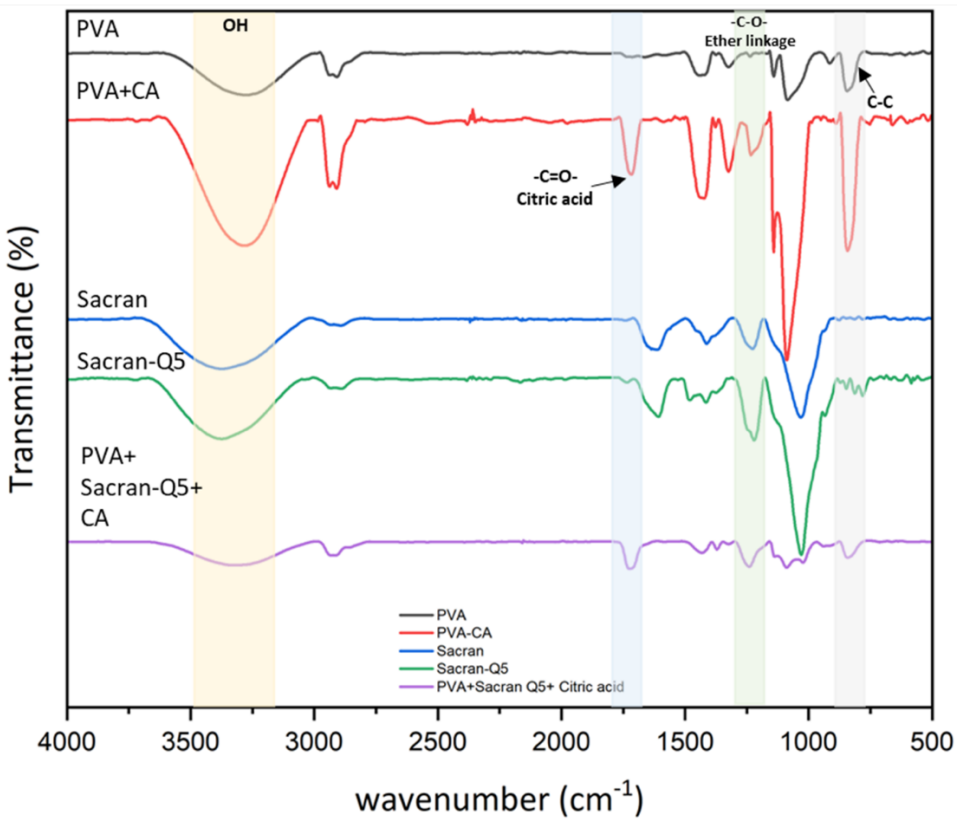

Figure 4.7 FTIR spectra of PVA, citric acid (CA), sacran and Q-sacran.

4.3.3 Thermogravimetric Analysis (TGA)

The provided thermogravimetric analysis (TGA) and derivative thermogravimetric (DTG) curves detail the thermal degradation behavior of hydrogel films made from blends of PVA, Sacran, Citric Acid, and Q5-Sacran as shown in Figure 4.8. From the TGA results PVA, Sacran, Sacran-Q5 and Hydrogel films had shown the initial degradation begins around 200 °C, PVA exhibits initial degradation at 200°C, with significant weight loss between 200°C and 450°C, and stabilization after 450°C. Citric Acid degrades rapidly starting at 150°C, with complete degradation by 300°C and no significant residual weight. Sacran begins degrading at 200°C, with major weight loss between 200°C and 500°C, continuing to decrease gradually up to 800°C. SacranQ5 follows a similar pattern to Sacran, with initial degradation at 200°C, significant weight loss between 200°C and 450°C, and continued decrease up to 800°C. Hydrogel Films start degrading at 200°C, with major weight loss between 200°C and 450°C,

stabilizing after 450°C. following the TGA results was shown that hydrogel films demonstrate improved thermal stability due to crosslinking, with degradation extending beyond 450°C due to the hydrogel films combine the thermal degradation behaviors of PVA, Sacran, and Citric Acid, showing complex degradation patterns due to crosslinking, which enhances their thermal stability and broadens the degradation temperature range. The results from the TGA and DTG analyses demonstrate that the hydrogel films have improved thermal stability due to the crosslinking between PVA, Sacran, and Citric Acid. This crosslinked structure ensures gradual and extended degradation

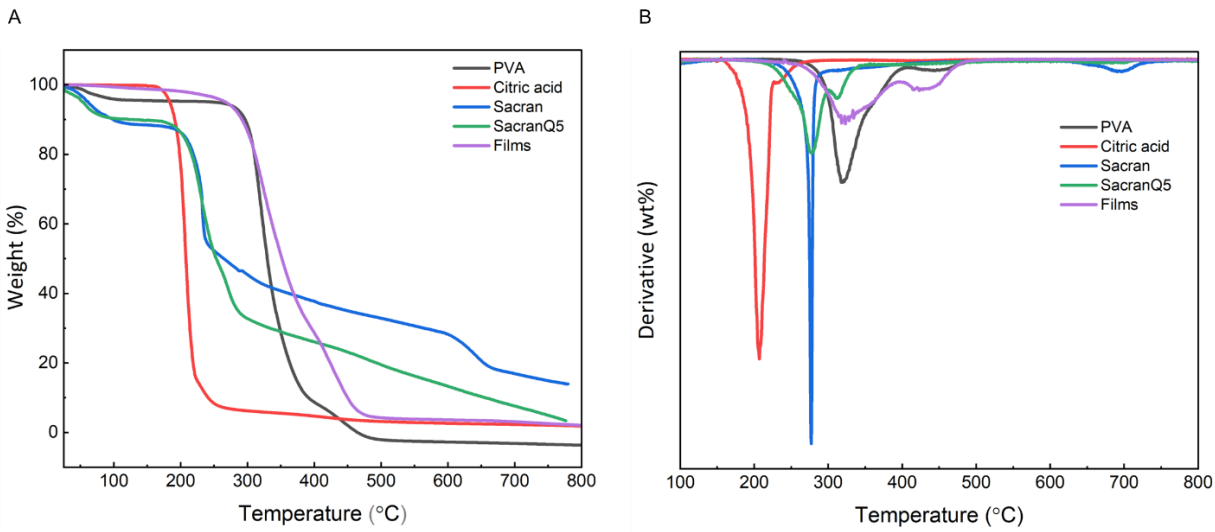

Figure 4.8 A) Presents the thermogram obtained from the thermogravimetric analysis (TGA) of PVA, Citric acid, Sacran, SacranQ5 and Films settings and B) displays the temperature composition obtained from the derivative thermogravimetry (DTG) analysis.

4.3.4 Mechanical Test

The results of the compressive mechanical load tests are shown in **Figure 4.9**. The force (N) is plotted against displacement (mm) for each type of microneedle patch. A minimum force of 0.058 N/needle was required to penetrate the stratum corneum, the outermost layer of our skin. The testing apparatus was configured to bring a force linker into contact with the microneedle

array via a stepping motor moving at a constant velocity of 20 µm/s. The compression test continued until the initial failure of a single microneedle was detected. Once failure was detected, the sensor advanced an additional 1 mm to ensure complete recording of the failure event. PVA/Sacran microneedles exhibited the highest mechanical strength, with a maximum force approaching 39.18 N before initial failure. Compared to PVA/Msacran1 and PVA/Msacran2, Msacran1 showed the lowest mechanical strength among the three types, with a maximum force around 25.57 N, while PVA/Msacran2 showed a mechanical strength of 32.05 N, higher than that of PVA/Msacran1 (Table 4.2). From this behavior, it could be concluded that Msacran has more hydrophilicity than sacran, which can lead to swelling and reduced structural integrity. Increased water uptake can weaken the interactions between polymer chains, making the microneedles less rigid.

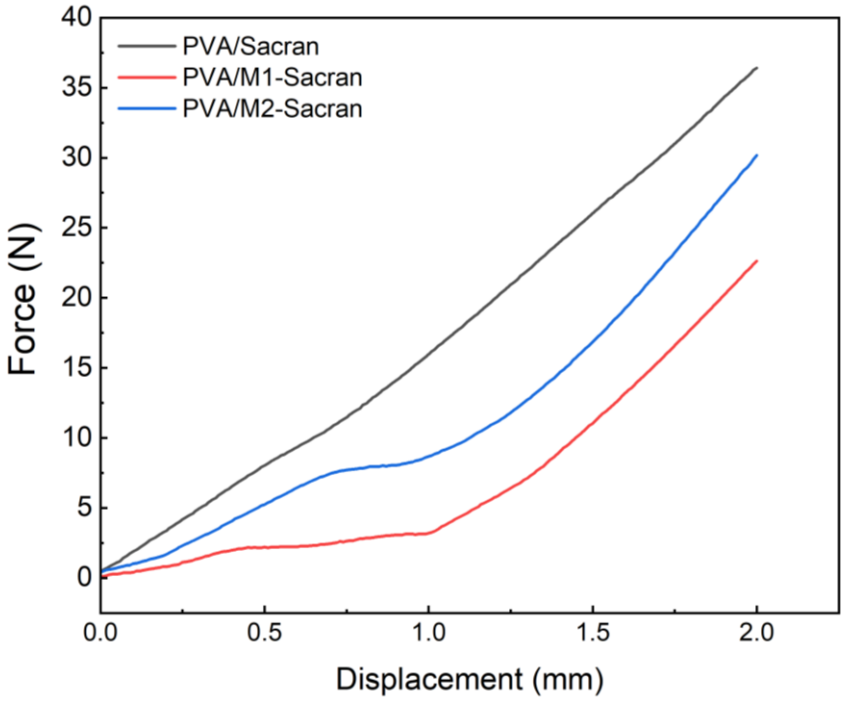

Figure 4.9 Facture force of the microneedles patch in a uniaxial fracture force test.

Table 4.2 The summary of the mechanical strength of various microneedle patches.

Formula	Total Force (*N*)	Force/needle (*N*)
PVA/Sacran	39.18±3.9	1.08±0.10
PVA/M1-Sacran	25.57±3.5	0.71±0.09
PVA/M2-Sacran	32.05±2.4	0.89±0.06

4.3.5 Penetration Test

The results provided summarize the mechanical strength and penetration ability of microneedles made from PVA/Sacran, PVA/M1-Sacran, and PVA/M2-Sacran, tested against eight layers of parafilm to simulate human skin thickness (Table 4.3). As a PVA/Sacran microneedles Shows excellent penetration ability up to the 3rd layer (100%) and the penetration ability starts to drop significantly after the 4th layer, with only 67% penetration. PVA/M1-Sacranm was shown good penetration in the 1st layer (94%) but decreases sharply in subsequent layers, By the 3rd layer, penetration drops to 53%, and by the 4th layer, it is 33% and PVA/M2-Sacran Maintains 100% penetration ability up to the 2nd layer shows a significant reduction in penetration ability in the 3rd layer (85%).

Table 4.3 The percentage of penetration test

Layer	PVA/Sacran	PVA/M1-Sacran	PVA/M2-Sacran
1	100	94	100
2	100	75	100
3	100	53	85
4	67	33	68
5	3	0	6
6	0	0	0
7	0	0	0
8	0	0	0

These results indicate that the mechanical strength and penetration ability of microneedles vary significantly based on their composition**.** Each Parafilm® layer has an average thickness of about 126 μm. Consequently, stacking 8 layers of Parafilm® results in a total thickness of 1008 μm, which matches the thickness of the skin layer from the stratum corneum to the upper dermis.

4.3.6 Scanning Electron Microscopy

The SEM images in Figure 4.8 illustrate the morphology of hydrogel-forming microneedles prepared with various formulations of sacran and modified sacran in a polyvinyl alcohol (PVA) matrix. The detailed preparation method ensures that the microneedles are formed correctly and crosslinked to achieve the desired mechanical properties. The following discussion evaluates the results and provides insights into the differences observed between the various formulations. **Figure 4.10A** shown PVA/Sacran microneedles exhibit a well-defined, uniform conical structure with smooth surfaces and sharp tips. The use of unmodified sacran in the hydrogel matrix contributes to the formation of robust microneedles with high mechanical strength. The uniformity and structural integrity are essential for consistent skin penetration and effective drug delivery. The microneedles in **Figure 4.10B** also display a conical shape but with slightly less uniformity compared to those in Figure 4.8A. The surface appears to have more irregularities, and the tips are not as sharp. The presence of 0.5% w/w modified sacran (M1-Sacran) increases the hydrophilicity of the hydrogel, leading to potential swelling and reduced structural integrity. This could result in decreased mechanical strength and less efficient skin penetration. **Figure 4.10C** shown the microneedles shape of 1.0% w/w modified sacran (M2-Sacran). The microneedles in Figure 4.8C show similar morphological characteristics to those in Figure 4.8B, with conical shapes and some surface irregularities. However, these microneedles appear slightly more robust than those in Figure 4.8B. The use of 1.0% w/w modified sacran (M2-Sacran) further increases hydrophilicity. While this

formulation shows improved robustness compared to MSacran1, it still does not achieve the same mechanical strength as the PVA/Sacran microneedles. The increased hydrophilicity may contribute to swelling, affecting the overall mechanical properties.

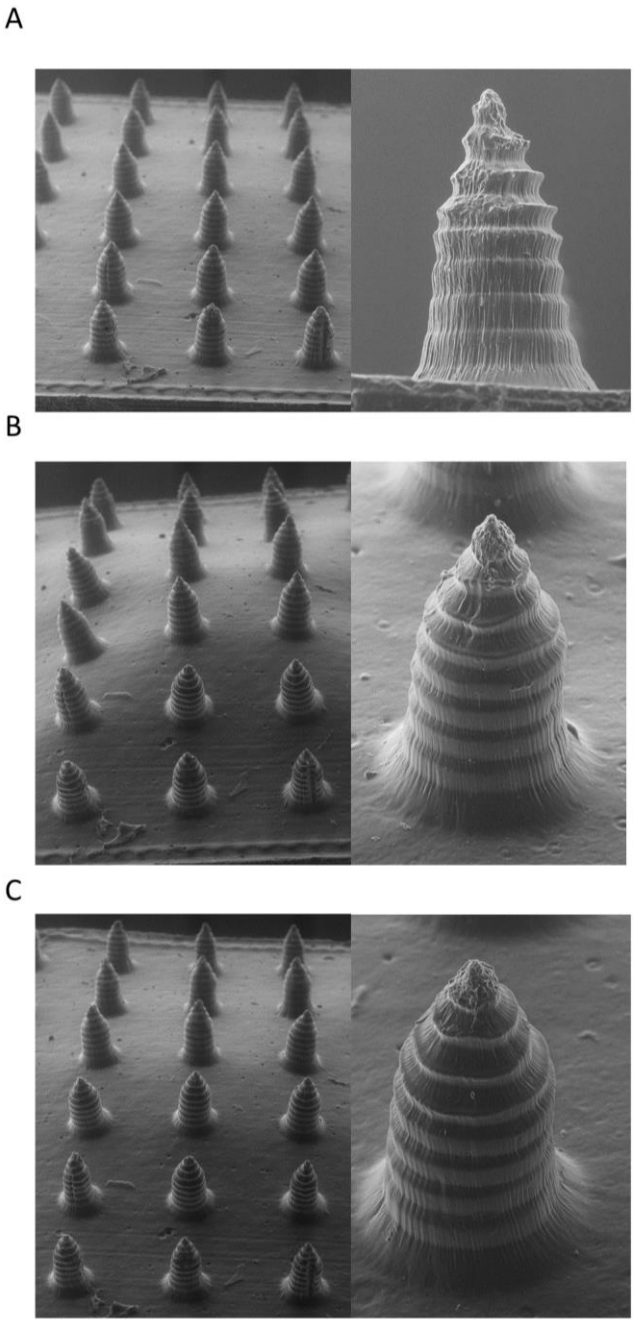

Figure 4.10 SEM image of hydrogel microneedles A) PVA/Sacran B) PVA/M1-Sacran and C) PVA/M2-Sacran.

4.3.7 Cytotoxicity Test

The image displays the results of a cytotoxicity test conducted on fibroblast cell lines (L-929) using the MTT method was shown in Figure 4.11. The test evaluates the cell viability after exposure to various concentrations of different samples, specifically PVA, PVA/Sacran, PVA/M1-Sacran, and PVA/M2-Sacran. At low concentration PVA and PVA/Sacran maintain high cell viability, close to 100%. PVA/M1-Sacran and PVA/M2-Sacran show slightly viability, but still above 80%. As the concentration increases, PVA and PVA/Sacran consistently show minimal cytotoxicity, with cell viability near or above 80%. However, PVA/M1-Sacran and PVA/M2-Sacran exhibit a dose-dependent reduction in cell viability,

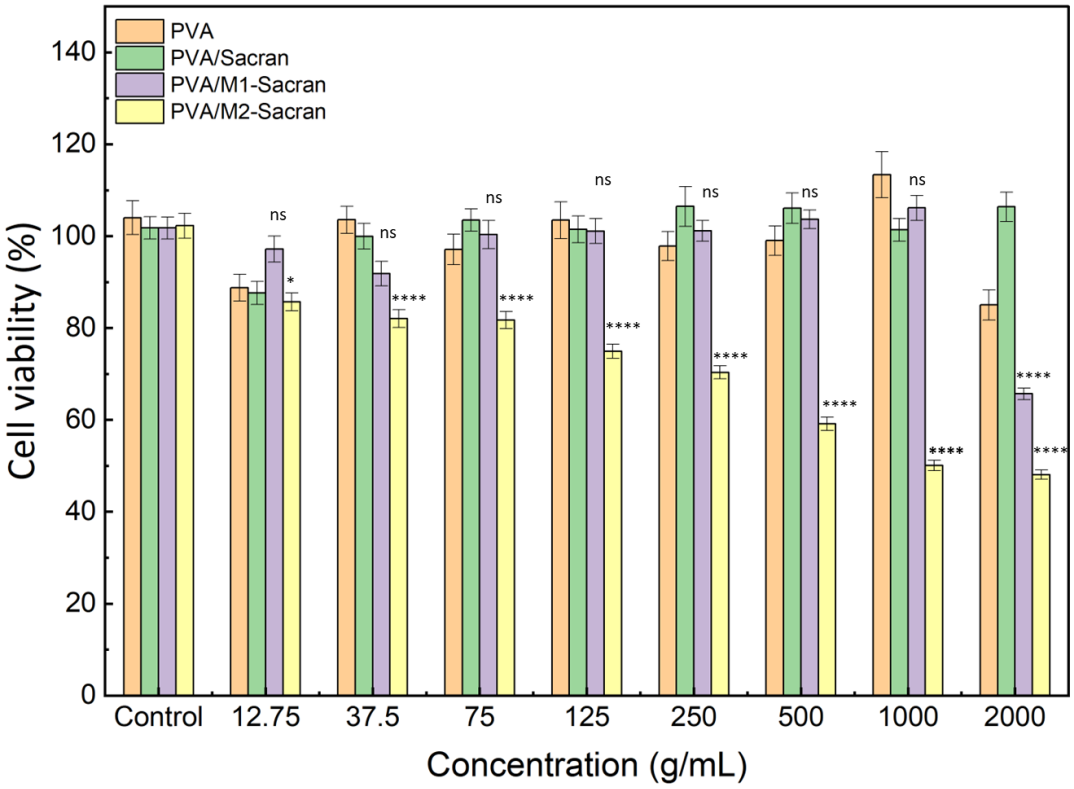

Figure 4.11 The cell viability of PVA, PVA/Sacran, PVA/M1-sacran and PVA/M2-sacran, Data are shown as a mean ±s.d., (n=8), ****p<0.0001, ***p<0.001, *p<0.05 and ns = not significant compare with original sacran, determined by one-way ANOVA followed by Tukey's test.

4.4 Conclusion

The study successfully demonstrates the fabrication and evaluation of hydrogel-forming films and microneedles using polyvinyl alcohol (PVA), sacran, modified sacran (Q-sacran), and citric acid as a crosslinking agent. The results reveal key insights into the swelling behavior, thermal stability, mechanical properties, and cytotoxicity of the hydrogel formulations. Hydrogel films with 1.0% w/w citric acid and a 60-minute crosslinking time exhibit the highest swelling degree compared to those with longer crosslinking times of 120 and 180 minutes. This is attributed to the lower crosslinking density, which allows for greater water uptake. The selected formulations B7 (PVA/Sacran), C7 (PVA/M1-Sacran), and D7 (PVA/M2-Sacran) show optimal swelling properties, demonstrating the ability of sacran to form ester bonds with citric acid and hydrogen bonds with PVA, enhancing swelling capacity. The thermogravimetric analysis (TGA) and derivative thermogravimetric (DTG) curves indicate that hydrogel films exhibit improved thermal stability due to crosslinking. PVA, sacran, and Q-sacran start degrading at around 200°C, with significant weight loss occurring between 200°C and 450°C. Hydrogel films combine the thermal degradation behaviors of PVA, sacran, and citric acid, showing complex degradation patterns and extended thermal stability beyond 450°C due to the crosslinked structure. Mechanical testing of the microneedles reveals that PVA/Sacran microneedles possess the highest mechanical strength, with a maximum force of approximately 39.18 N before initial failure. In contrast, PVA/M1-Sacran microneedles show the lowest mechanical strength at 25.57 N, while PVA/M2-Sacran microneedles exhibit intermediate strength at 32.05 N. The increased hydrophilicity of modified sacran formulations (M1-Sacran and M2-Sacran) leads to swelling and reduced structural integrity, affecting mechanical performance. Penetration tests using parafilm layers show that PVA/Sacran microneedles maintain excellent penetration ability up to

the 3rd layer, with significant drops in penetration after the 4th layer. PVA/M1-Sacran microneedles demonstrate good initial penetration but rapidly decrease in subsequent layers. PVA/M2-Sacran microneedles maintain 100% penetration up to the 2nd layer, with a notable reduction thereafter. The cytotoxicity evaluation using the MTT method indicates that at low concentrations, PVA and PVA/Sacran maintain high cell viability close to 100%. PVA/M1-Sacran and PVA/M2-Sacran show slightly reduced viability but remain above 80%. At higher concentrations, PVA and PVA/Sacran exhibit minimal cytotoxicity with cell viability near or above 80%, whereas PVA/M1-Sacran and PVA/M2-Sacran display a dose-dependent reduction in cell viability. The study highlights that hydrogel formulations with 1.0% w/w citric acid and a 60-minute crosslinking time are optimal for achieving high swelling degrees. The crosslinked hydrogel films demonstrate improved thermal stability and mechanical properties suitable for biomedical applications. Among the microneedle formulations, PVA/Sacran shows the best mechanical strength and penetration ability, making it a promising candidate for transdermal drug delivery systems. The cytotoxicity results confirm the biocompatibility of the hydrogel formulations, supporting their potential for safe and effective medical use.

4.5 Reference

89. Donnelly RF, Majithiya R, Singh TRR, Morrow DI, Garland MJ, Demir YK, et al. Design, optimization and characterisation of polymeric microneedle arrays prepared by a novel laser-based micromoulding technique. Pharmaceutical research. 2011;28:41-57.

90. Vučen SR, Vuleta G, Crean AM, Moore AC, Ignjatović N, Uskoković D. Improved percutaneous delivery of ketoprofen using combined application of nanocarriers and silicon microneedles. Journal of Pharmacy and Pharmacology. 2013;65(10):1451-62.

91. Aldawood FK, Andar A, Desai S. A comprehensive review of microneedles: Types, materials, processes, characterizations and applications. Polymers. 2021;13(16):2815.

92. Ganeson K, Alias AH, Murugaiyah V, Amirul A-AA, Ramakrishna S, Vigneswari S. Microneedles for efficient and precise drug delivery in cancer therapy. Pharmaceutics. 2023;15(3):744.

93. Bilal M, Mehmood S, Raza A, Hayat U, Rasheed T, Iqbal HM. Microneedles in smart drug delivery. Advances in wound care. 2021;10(4):204-19.

94. Tariq N, Ashraf MW, Tayyaba S. A review on solid microneedles for biomedical applications. Journal of Pharmaceutical Innovation. 2022;17(4):1464-83.

95. Cárcamo-Martínez Á, Mallon B, Anjani QK, Domínguez-Robles J, Utomo E, Vora LK, et al. Enhancing intradermal delivery of tofacitinib citrate: Comparison between powder-loaded hollow microneedle arrays and dissolving microneedle arrays. International Journal of Pharmaceutics. 2021;593:120152.

96. Jin M, Jeon W-J, Lee H, Jung M, Kim H-E, Yoo H, et al. Preparation and evaluation of rapid disintegrating formulation from coated microneedle. Drug Delivery and Translational Research. 2021:1-11.

97. Ali M, Namjoshi S, Benson HA, Mohammed Y, Kumeria T. Dissolvable polymer microneedles for drug delivery and diagnostics. Journal of Controlled Release. 2022;347:561-89.

98. Shriky B, Babenko M, Whiteside BR. Dissolving and Swelling Hydrogel-Based Microneedles: An Overview of Their Materials, Fabrication, Characterization Methods, and Challenges. Gels. 2023;9(10):806.

99. Yadav PR, Munni MN, Campbell L, Mostofa G, Dobson L, Shittu M, et al. Translation of polymeric microneedles for treatment of human diseases: Recent trends, Progress, and Challenges. Pharmaceutics. 2021;13(8):1132.

100. Ruan S, Zhang Y, Feng N. Microneedle-mediated transdermal nanodelivery systems: a review. Biomaterials Science. 2021;9(24):8065-89.

101. Liu T, Luo G, Xing M. Biomedical applications of polymeric microneedles for transdermal therapeutic delivery and diagnosis: Current status and future perspectives. Advanced Therapeutics. 2020;3(9):1900140.

CHAPTER V

GENERAL CONCLUSION

The aim of this study is to modify sacran into ampholytic materials for use in biological applications. Additionally, the research aims to examine various properties of the modified sacran, such as molecular weight, solubility, hydrodynamic radius, and zeta potential. Subsequently, hydrogel sheet materials were prepared from the modified sacran, and investigations were conducted on cell adhesion and cell viability.

Chapter 2. In this study, we investigated the impact of quaternary ammonium (Q-188) on sacran, a supergiant polysaccharide. A modified version of Sacran was successfully synthesized. The degree of quaternization of sacran was range around 32 % to 87 % of sugar residues. The modification of sacran can result in two structural changes: 1) improved ampholytic properties, showing a better balance between negative and positive charges, and 2) conversion of hydroxyl groups into cationic groups to enhance the overall charge. The hydrodynamic radius (R_h) of sacran particles in water was found to be decreased with the cationization degree increase. These findings show that the cationization of sacran reduces its R_h. Despite the presence of densely substituted anionic groups, sacran naturally forms supercoiled assemblies, most likely due to hydrogen bonding and hydrophobic interactions. Sacran, while having extensively substituted anionic groups, spontaneously forms supercoiled assemblies, most likely as a result of hydrogen bonding and hydrophobic interactions. The value of the Zeta potential of sacran and modified sacran was also increased from – 54.8 to -41.9 mV This can be considered as indication of cationization. The rate of increase was calculated to be 19 millivolts per cationization unit. It is important to mention that the zeta-potential still is negative even in samples with high levels of cationization. The assembly

properties of sacran can be related to the presence of both positive charges ($+N(CH_3)_3$) and original negative charges ($-COO^-$ and $-SO_4^-$), as well as their interactions with each other. We have investigated the screening effect in polysaccharides in NaCl environment, The ratio of the zeta-potential difference to the initial zeta-potential of sacran was utilized to calculate the NaCl screening effects, which were then plotted against the cationization degree. The screening effects exhibited a slight rise as the cationization degree raised from 0% to 60%, but a substantial increase above 60%. If the effects of NaCl are merely an ionic strength-based screening of surface potential for sacran assembly, then the screening effects should be virtually constant without regard to the degree of cationization. The phenomenon of the screening effect increasing may be ascribed to a structural alteration of amphoteric sacran chains, such as the appearance of a part of the cation on the upper surface of aggregates. This modification could potentially promote interactions both within and between molecules.

Chapter 3. In this study, we investigated the crosslinking of the hydrogel sacran sheet through physical crosslinking at 140 °C. After immersing the film sheet, it was seen that the sheet swelled and exhibited anisotropic properties. The swelling degree increased as the degree of cationization increased, with the values ranging from 5.9 to 9.3. in order to investigate the anisotropic behavior of modified sacran gels, Original sacran shows the anisotropy of 62 but the modified sacran was showed the valve over 110, from these results means the cationization degree has an effect in anisotropic properties. The hydrogel sheet showed hydrophilicity and wettability. The water contact angle of sacran was seen to be approximately 26.5° while the value gradually decreased when the Q-sacran composition increased. To assess the safety of Q-sacran, we conducted the MTT assay using the fibroblast cell line L-929. The cell viability of Q-sacran was shown that sacran exhibited the least cytotoxicity, with viability of 55 %. In contrast, the results show that Q-sacran, at a concentration of 0.625 wt.%, showed cytotoxicity with viability of 61% and 70% for Q4 and Q5-sacran, respectively. From these results showed

that modified sacran did not show Q-sacran has been found to cause significant cytotoxicity in fibroblast cell lines, showing its potential for use in biological applications. The cells adhesion of cell lines was creased from the original sacran and modified sacran, the results presented that the cells keep their elongated fibroblast properties on all materials and presence of intercellular connections on all six material compositions, but the number of cells adhered to the surface varies. The original sacran surface has a negative charge that is compatible with the negative charge of the cell lines. However, there are certain cells that are still able to adhere to the sacran surface. In contrast, Q-sacran has a positive charge due to its strong hydrophilic properties and the presence of quaternary ammonium. Q-sacran seems to enhance the adhesion of cell lines to the surface of the material. After conducting thorough investigations, we are interested in applying the modified sacran in the field of biology.

Chapter 4. In this study demonstrates the successful fabrication and evaluation of hydrogel-forming films and microneedles using PVA, sacran, modified sacran (Q-sacran), and citric acid as a crosslinking agent. Key findings include, Swelling Behavior, hydrogel films with 1.0% w/w citric acid and a 60-minute crosslinking time exhibit the highest swelling degree. Formulations B7 (PVA/Sacran), C7 (PVA/M1-Sacran), and D7 (PVA/M2-Sacran) show optimal swelling due to lower crosslinking density, facilitating greater water uptake. The thermal stability at the results TGA and DTG analyses reveal improved thermal stability of hydrogel films due to crosslinking. PVA, sacran, and Q-sacran start degrading at around 200°C, with significant weight loss between 200°C and 450°C. Crosslinked hydrogel films exhibit extended thermal stability beyond 450°C. Mechanical testing shows PVA/Sacran microneedles possess the highest mechanical strength (39.18 N). PVA/M1-Sacran microneedles have the lowest strength (25.57 N), while PVA/M2-Sacran microneedles exhibit intermediate strength (32.05 N). Increased hydrophilicity in modified sacran formulations leads to swelling and reduced structural integrity. PVA/Sacran microneedles maintain

excellent penetration up to the 3rd parafilm layer, with significant drops after the 4th layer. PVA/M1-Sacran shows good initial penetration but decreases rapidly in subsequent layers. PVA/M2-Sacran maintains 100% penetration up to the 2nd layer, with a notable reduction thereafter. At low concentrations, PVA and PVA/Sacran maintain high cell viability close to 100%. PVA/M1-Sacran and PVA/M2-Sacran show slightly reduced viability but remain above 80%. At higher concentrations, PVA and PVA/Sacran exhibit minimal cytotoxicity, while PVA/M1-Sacran and PVA/M2-Sacran show a dose-dependent reduction in cell viability. hydrogel formulations with 1.0% w/w citric acid and a 60-minute crosslinking time are optimal for achieving high swelling degrees. These crosslinked hydrogel films exhibit enhanced thermal stability and mechanical properties, making them suitable for biomedical applications. Among the microneedle formulations, PVA/Sacran stands out for its superior mechanical strength and penetration ability, indicating its potential for transdermal drug delivery systems. Cytotoxicity results confirm the biocompatibility of these hydrogel formulations, ensuring their safe and effective use in medical applications.

LIST OF PUBLICATIONS

Journal:

First author:

- C. Supachettapun, M. Asif Ali, N. Muangsin, K. Takada, K. Matsumura, M. Okajima, T. Kaneko. *Biomacromolecules* 2024.

Co-author:

- J. Kobayashi, M. Kaneko, C. Supachettapun, K. Takada, T. Kaneko, Joon Yang Kim, M. Ishida, M. Kawai, and T. Mitsumata. *Polymers* **2024**, 16, 80.

CONFERENCE:

1. Poster “Fabrication of Microneedle Using Hydrogels from Cross-Linked Sacran” Chamaiporn Supachettapun, Kenji Takada, Maiko Okajima, and Tatsuo Kaneko. The 13th SPSJ International Polymer Conference (IPC 2023), Sapporo, Japan. July 18-21, 2023.

2. Poster “Quaternized sulfated polysaccharides with a super high molecular weight sacran” Chamaiporn Supachettapun, Kazuaki Matsumura, Maiko Okajima, and Tatsuo Kaneko. The 13th Suizenji Nori sacran conference, Kumamoto, Japan. March 9, 2024.